Thermal Analysis of Lanthanide Complexes for Nuclear Security

A Dissertation Presented for the
Doctor of Philosophy
Degree
The University of Tennessee, Knoxville

Shayan Shahbazi
August 2018

Acknowledgments

I would like to thank my parents for instilling in me the importance of education and the pursuit of knowledge, while allowing me the opportunity to make decisions on my own. The sacrifices they have made are no doubt motivation that I carry with me, and my growth as a student or otherwise would not have been possible without their unconditional love and support.

I would like to thank Dr. Howard L. Hall for giving me this research opportunity, and the continued teaching in the field of nuclear science and chemistry. I would like to thank Dr. John D. Auxier II for his advising to my sometimes unceasing questioning. I would like to thank the other members of my doctoral committee, Dr. G. Ivan Maldonado and Dr. Robert M. Counce. I would also like to thank Dr. J. Wesley Hines and the other faculty of the Nuclear Engineering department at the University of Tennessee that have had an impact in my education, notably Dr. Steven E. Skutnik for his educating in the topics of nuclear fuel cycle and waste management. I would like to thank Dr. George K. Schweitzer and members of his research group for their assistance in research. Additionally, I would like to thank Katrina Pangilinan, Brad Miller and other members of the Polymer Characterization Lab at the University of Tennessee for assistance in running samples in thermal analysis. Finally, I would like to thank all the members of our research group that I was fortunate enough to work with over the years, specifically Adam Stratz, CJ Oldham, Austin Mullen and Ashlyn Jones.

This work was funded by the Stewardship Science Academic Alliances Program of the National Nuclear Security Administration under the U.S. Department of Energy, and based on work supported by the U.S. Department of Homeland Security. I wish to gratefully thank all those who made this work possible, especially the U.S. Department of Energy National Nuclear Security Administration DE-NA-0001983.

Abstract

In an effort to meet the growing demand for more rapid separation methods, this work reports the vaporization and thermodynamic characterization of lanthanide complexes as vehicles for the rapid separation of volatile nuclear fission products. Volatile lanthanide β-diketonate complexes can be synthesized and rapidly separated from each other via gas phase chromatographic separations due to differences in adsorption enthalpy. Because adsorption and sublimation thermodynamics are linearly correlated, there is considerable motivation to determine sublimation enthalpies to improve the ability to predict separations effectiveness. A method of thermogravimetric analysis (TGA) was employed in this study on up to four lanthanide β-diketonate complexes to compare volatility and stability across the series and for each chelate. Sublimation enthalpies were determined using the Langmuir method involving isothermal jump heating. Thermogravimetric analysis coupled with a mass spectrometer (TGA-MS) and melting point analysis was used to confirm the occurrence of sublimation as well as confirm the stability of the chelate through the sublimation region. Elemental analysis, mass spectroscopy and infrared spectroscopy were also used to characterize additional ligands in the coordinating sphere and better understand the decomposition ranges of the complexes. Thermal analysis was carried out on lanthanide chlorides and oxychlorides in order to determine the potential for chromatographic separations of these ionic compounds.

Table of Contents

List of Tables

List of Figures

List of Abbreviations

TGA	Thermogravimetric analysis
MS	Mass spectroscopy or spectrometer
FTIR	Fourier transform infrared [spectroscopy]
NMR	Nuclear magnetic resonance [spectroscopy]
acac	2,4-Pentanedione (or Acetylacetone)
hfac	1,1,1,5,5,5-Hexafluoro-2,4-pentanedione (or Hexafluoroacetyleacetone)
tfac	1,1,1-Trifluoro-2,4-pentanedione (or Trifluoroacetylacetone)
dpm	2,2,6,6-Tetramethyl-3,5-heptanedione (or Dipivaloylmethane) [also abbreviated as thd]
fod	6,6,7,7,8,8,8-Heptafluoro-2,2-dimethyl-3,5-octanedione
thd	See dpm
RE	Rare earth element

Chapter 1: Introduction

The goal of this work is the synthesis and thermal characterization of volatile lanthanide complexes as they relate to fission product separations within the field of nuclear forensics. Nuclear forensics has become very important to the field of nuclear security, where there is considerable interest in developing rapid separations of radionuclides and isotopes. In the event of detonation of a nuclear device, the fallout debris should be analyzed for signature isotopes that may provide evidence on the origin and type of nuclear materials used as well as other clues to the device design [1,2]. Lanthanides cover a portion of the fission product curve with varying yields dependent on a number of variables (e.g. neutron energy, fissile parent, etc), motivating the quantitative separation of these elements. One method of analysis is separation via ion exchange, although the procedure is strongly dependent on the resin particle size, the column temperature and flow parameters such as eluent flow rate [1]. Additionally, this method requires longer sample processing times, which can be detrimental to analyses of samples with short half-lives such as fission products. Therefore, there is considerable motivation to investigate other methods of chemical separation of the rare earths. The rapid gas phase separation of rare earth metals from other components of the debris via isothermal thermochromatography has been investigated and is a promising method [3]. Early studies have shown the utility of volatile β-diketone ligands as separating agents for rare earth metals [4–6]. 1,1,1,5,5,5-hexafluoro-2,4-pentanedione (hfac) has been shown to produce volatile complexes with lanthanides, although there are many other ligands that readily form volatile chelates with the rare earth metals and warrant further investigation and thermodynamic characterization [7].

Thermochromatography is a gas phase separation method that utilizes either temperature gradients on a chromatographic column to vary adsorption location or uses constant column temperatures to vary retention time. The adsorption time of a compound on a column, i.e. retention time, is dependent on the thermodynamics of that compound, most notably the adsorption enthalpy for that state. There are several models used in predicting the retention time of a compound through a chromatographic column. These models include a Monte Carlo simulation of single atom chemistry of the compound on a

column, as well as a thermodynamic equation dependent on column and compound parameters. Both of these require knowledge of the adsorption enthalpy of each compound, or, more specifically, knowledge of the relative differences in adsorption enthalpy. Studies of heavy metals have generated empirical correlations between adsorption enthalpy on a quartz column and sublimation enthalpy of the solid material [8–11]. Because of this relationship, there is considerable motivation to investigate the relative volatilities, and thus the sublimation enthalpy of lanthanide chelates.

Thermogravimetric analysis (TGA) is useful in the characterization of a compound's thermodynamics, especially the sublimation enthalpy. Many methods analyze weight loss curves as a function of a constant heating rate [12–16]. Ashcroft introduced a method based on Langmuir's work for vapor pressure determination and the Clausius-Clapeyron relation [17]. This method analyzes weight loss rates over multiple isothermal heating curves within a temperature region where sublimation is occurring [17–20]. This method is utilized in this study for the sublimation enthalpy determination of lanthanide chelates for up to four different ligands to better understand variations across the lanthanide series.

The ligands studied here are 1,1,1,5,5,5-hexafluoro-2,4-pentanedione or hexafluoroacetyleacetone (hfac), 1,1,1-trifluoro-2,4-pentanedione or trifluoroacetylacetone (tfac), 2,2,6,6-tetramethyl-3,5-heptanedione or dipivaloylmethane (dpm), and 6,6,7,7,8,8,8-heptafluoro-2,2-dimethyl-3,5-octanedione (fod). These four ligands and the 14 stable lanthanides make up 56 unique compounds, and are studied here for thermodynamic characterization. The syntheses for each homologous chelate are slightly different, but all follow the basic approach of deprotonating the ligand to form a salt and adding to a solution of the metal salt. These four ligands were chosen because they have been shown to volatilize the lanthanides at relatively lower temperatures while maintaining thermal stability. They also cover the spectrum of ligands for both sterics and fluorination. For example, fod and dpm are much larger than the other two ligands, and dpm is the only of the four ligands that is not fluorinated; similarly, tfac offers intermediate fluorination between dpm and hfac. Fluorination of the ligand increases volatility of the chelate, which is shown later.

There is additional motivation to develop a method to rapidly separate lanthanide chlorides from a solid mixture. Because nuclear melt glass is often more easily converted to its chloride form, this would save steps in the sample preparation stage and allow for quicker

elucidation of the material. Although not as volatile, metal chlorides have been shown to separate in the gas phase, motivating their thermodynamic characterization. Although only volatile at much higher temperatures, the lanthanide chlorides are still investigated with TGA as a vehicle for chemical separations.

Chapter 2: Technical Background

2.1 Separations of Fission Product Chelates

In the unfortunate event of a nuclear explosion, the analysis of the fallout debris is especially important information. Because conventional separation techniques may require long counting times and considerable sample preparation [2], there is much interest in developing rapid separations of gas phase fission products, specifically using a gas chromatography (GC) apparatus [3,21,22]. Starting with the dissolution of nuclear fallout debris, fission products in ionic form may be afforded, such as that of a metal chloride. Such metal chlorides may be used as precursor in the synthesis of a more volatile and more easily separated chelate. A chelate is a complex formed by the presence of coordinated ligands around a single central atom, and is often organometallic. Because lanthanide isotopes comprise a portion of the fission product curve, the gas phase chromatographic separation of lanthanide chelates can be an important topic to the field of nuclear forensics.

A mixture of lanthanide chelates formed from fallout debris can be representative of the starting nuclear material used in the nuclear weapon, therefore the chromatographic separation of such a unique mixture, as well as the quantification of the concentration of each isotope, are both important. Using mass spectrometry (MS) in conjunction with a GC can be helpful in analyzing the concentrations of the various mass numbers detected, but some mass spectrometers often have mass limits. Additionally, the lack of elemental information on a detected nuclide is a drawback of relying solely on MS data. Knowledge of the concentration of a certain mass number does not necessarily correlate with an isotopic breakdown. Understanding exactly how much of each isotope of each fission product is the information most desired, therefore it is desirable to utilize chemical separations.

Although there are various methods of nondestructive assay of nuclear materials, such as radiation detection, the chromatographic separation allows for the detection of stable nuclides also. In order to separate nuclides of the same mass, knowledge of the thermodynamic properties, and thus the chemical or electronic structure, is required. Some have studied theoretical predictions of thermodynamic properties of similar compounds

[23], while many have detailed experimental methods [9,24–26]. Understanding the chemical properties of compounds allows one to predict the separations, i.e. retention times or adsorption location, on a gas phase chromatographic column. Understanding retention times and elution order is essential to quantifying the composition of the lanthanide mixture.

2.2 Predicting the Separations

Chromatographic separation techniques can often be modified, such as in thermochromatography which utilizes temperature gradients across a column, or isothermal gas chromatography, which may utilize pressure gradients. In any case, there are several parameters necessary in order to predict the separation of a compound in a mixture of compounds. Temperature gradient or isothermal are the most important factors, as well as the introduction of a pressure gradient, a vacuum or an isobaric flow. The column material should be carefully chosen, so as to encourage varying adsorption times for each compound type, yet not so slow that experiment times are unnecessarily long. The carrier gas should be ideally inert, yet the introduction of a reactive gas such as the uncoordinated ligand may also be necessary for some heavy metal chelates to maintain volatility [27]. Finally, the length and size of the column will be very important in deciding the retention time of the compounds. Assuming constant column parameters, the separation of different compounds in a uniquely chosen environment is mostly dependent on the differences in adsorption enthalpy of the specific molecule.

The adsorption enthalpy can be used in several models to predict retention time. Zvara introduced a Monte Carlo simulation based on single atom chemistry as a molecule travels down the length of a column [25]. They report that the probability and estimation of time spent in the reversible adsorbed state versus the free flowing vapor state ultimately predict the retention time on the column, where surface adsorption is governed by equation 1 below.

$$\bar{\tau}_a = \tau_0 \, e^{\left(\frac{-\Delta H_{ads}}{RT}\right)} \qquad (1)$$

The equation estimates time spent adsorbed to the surface as a function of τ_0, the period of oscillations of the molecule in adsorbed state perpendicular to the surface, which is often

taken as a surface constant based on column type. Additionally, the time spent adsorbed is dependent on the enthalpy of adsorption, ΔH_a and the absolute temperature, T. Various other parameters are used to estimate time spent in each state in this simulation, yet the greatest weight in affecting the results lies with the value of adsorption enthalpy of the compound and its relationship with temperature.

Schadel summarizes research on the separations of superheavy elements, and while lanthanide chelates may behave slightly different, these models have proven relevant to this research [9]. Zvara summarizes other techniques in estimating radiochemical separations, such as theoretical predictions for retention time based on column parameters and thermodynamics [24]. One such prediction for ideal isothermal chromatography is shown in equation 2.

$$t_R = \frac{ZA}{Q} e^{\left(\frac{\Delta S_a T_0 - \Delta H_a}{RT_0}\right)} \qquad (2)$$

The retention time is dependent on column parameters including the length of column, Z, area per unit length of column, A, flow rate, Q, and isothermal temperature of the column, T_0. Also required are the enthalpy and entropy of adsorption for the compound. While there are many forms of this equation, most share the same form and depend on the extent of knowledge of the column's specific characteristics such as free surface area or free volume. Differences in retention time of various compounds on the same column ultimately depend on differences in the adsorption thermodynamics.

Regardless of the method used to estimate retention time, it is necessary to know the enthalpy of adsorption of the compound. In characterizing the surface and thermodynamic properties of solid compounds, some have shown the utility of inverse gas chromatography [28]. Due to the higher volatility of these chelates, thermal methods in analyzing and characterizing the thermodynamics are studied here out of preference.

2.2.1 Monte Carlo Thermochromatography Model

Henceforth referred to as the MCTC model, Monte Carlo Thermochromatography simulations based on single atom chemistry are a great example of how retention time is related to adsorption enthalpy of a compound. Our group is allocating research efforts to the

development of a model that expands on that introduced by Zvara [24–26]. For an isothermal column of known length, the characteristic equations involve mean adsorption sojourn time (equation 1), mean number of collisions with surface (equation 3), ratio of time spent in adsorbed and non-adsorbed state (equation 4), and mean jump length (equation 5). The time spent in adsorbed state (equation 6) and time spent in gas phase (equation 7) are randomized based on an exponential distribution, where *rand* is a randomly chosen number between 0 and 1. The retention time is calculated as the sum of these two times for every jump, and the molecule is "jumped" as many times until the length of the column is reached. A large number of molecular histories is completed for desirable results and a smooth distribution.

$$\nu_1 = \frac{r}{Q}\sqrt{\frac{2\pi RT}{M_{w,1}}} \qquad (3)$$

$$\phi = \frac{\frac{1}{u}}{\frac{1}{u}+\nu_1\bar{\tau}_a} \qquad (4)$$

$$\bar{\eta} = \frac{\pi r^2 D}{Q} + (11 - 16\phi + 6\phi^2)\left(\frac{Q}{48\pi D}\right) + \frac{1}{2\nu_1} \qquad (5)$$

$$\tau_\mu = \bar{\tau}_a\,\nu_1\,\bar{\eta} \quad \rightarrow \quad \tau_a = -\tau_\mu * \ln(rand) \qquad (6)$$

$$\eta = -\,\bar{\eta} * \ln(rand) \quad \rightarrow \quad \tau_g = {}^{\eta}/_{u} \qquad (7)$$

The variables *r* (column radius), *Q* (volumetric flowrate) and *u* (linear flow velocity) are column parameters. *D* is the mutual diffusion coefficient between the complex and carrier gas, and can be calculated in several ways. One method that proves reliable is Gilliland's semi-empirical correlation (equation 8). As mentioned previously, τ_0, the oscillatory period, is a column material parameter. *P* is the carrier gas pressure and M_i are the molar masses of the diffusing complex and the carrier gas.

$$D = \frac{0.0044\,T^{3/2}}{P\,[\left({}^{M_1}/_{\rho_1}\right)^{1/3} + \left({}^{M_2}/_{\rho_2}\right)^{1/3}]^2}\left(\frac{1}{M_1} + \frac{1}{M_2}\right)^{1/2} \qquad [{}^{cm^2}/_{s}] \qquad (8)$$

2.2.2 Estimating Adsorption Enthalpy

It has been shown that the value of adsorption enthalpy is important in predicting the separations of these compounds on a column. Unfortunately, at present, the adsorption enthalpy values of these compounds has yet to be found. Nonetheless, several methods which may be utilized in the future to estimate adsorption thermodynamics are summarized here. Pershina et al. have shown that the electronic properties and adsorption thermodynamics of heavy metal oxychlorides and oxides can be elucidated via "fully relativistic density-functional calculations" [29,30]. Members of this group are utilizing density functional theory (DFT) to elucidate the most thermodynamically favorable structures of these compounds, as well as enthalpic values of interest. Due to intense computing demands, this method may be undesirable.

As mentioned previously, the adsorption enthalpy is a parameter in several different methods in solving for retention time. Therefore, one method that has been explored and will continue to be explored by this group is to inject the compounds on a chromatography column of known characteristics and find each compounds retention time. Solving backwards using either the MCTC model or the thermodynamic model outlined above will yield values of adsorption enthalpy, although the accuracy of these methods can be called into question. At present, there are ongoing efforts in solving for these retention times.

2.2.3 Correlating Adsorption Enthalpy and Sublimation Enthalpy

Eichler et al. have shown that the adsorption enthalpy of a heavy metal oxide or chloride on a quartz column under certain conditions can be empirically correlated to the sublimation enthalpy of the compound [8–11]. Although no correlation exists for lanthanide chelates, this remains a goal of this work. But assuming the validity of this correlation motivates the investigation of the sublimation enthalpy of these compounds. An example correlation for material with similar volatility is that for metal chlorides or oxychlorides on a quartz column (equation 9) [9].

$$-\Delta H_{ads} = (21.5 \pm 5.2) + (0.600 \pm 0.025)\, \Delta H_{sub} \qquad (9)$$

Therefore, the focus of the research presented here is the thermal characterization of several types of lanthanide β-diketonates, and the elucidation of the sublimation enthalpic values.

2.3 Thermal Methods of Analysis

Many have used thermogravimetric analysis (TGA) and differential scanning calorimetry (DSC) to analyze the thermal stability and volatility of compounds. There have also been various studies of TGA and DSC on similar rare earth chelates on the stability and structure [31–34]. The use of thermal methods of analysis are very important to understanding the volatility of the compounds, as well as the ability of the chelate to maintain the same chemical form throughout volatilization. Due to the relatively weak bond characteristics of ligand complexes, some chelates may decompose shortly after or even during vaporization.

TGA is typically used to note the onset and end set of a weight loss event. A weight loss event of a compound constitutes the thermodynamic and kinetic processes of a compound's transfer to a vapor state. Dependent on the reaction taking place, and thus reaction order, a TGA curve may take on several shapes. The curve is also dependent on heating rate, as faster heating rates tend to shift chemical reaction weight loss events to higher temperatures, as they are typically overshot and take longer to develop than physical transitions. To overcome some of the issues with shifted peaks, there are various types of advanced TGA and proprietary heating programs in instruments designed to finish a weight loss event before raising the temperature [35].

Standard TGA coupled with MS can be used to characterize the coordination and purity of pure chelate compounds. For example, a weight loss event that occurs simultaneous with a peak in detected water or carbon dioxide mass may indicate a possible oxidation of the compound at high temperatures. Similarly, a reduction in the mass of oxygen would occur prior to this chemical reaction. Likewise, an increase in the masses of water or nitrogen during weight loss may indicate de-coordination of the chelate with those compounds.

A very important use of TGA is the determination of the sublimation thermodynamics of a compound. Many have shown that with standard heating programs as described above, the sublimation enthalpy can be found [12–16,36–39]. Previous work of this group has

shown the ability to do so, although the precision and accuracy of such methods may be in question for such highly volatile compounds [7]. Additionally, melting point analysis coupled with TGA is necessary to decide if sublimation of the solid compound is occurring as opposed to melting then vaporization. If the latter is occurring, then the value of enthalpy is indicative of the enthalpy of vaporization rather than the enthalpy of sublimation. This value is less useful to this study due to a higher tendency for some compounds to decompose as they melt. Such calculated values of vaporization enthalpy would account for the energy involved in decomposing the compound and/or the enthalpic values associated with vaporizing the decomposed product.

Ashcroft showed [17] that combining Langmuir's method for vapor pressure determination [20] with the Clausius-Clapeyron relation for phase transition affords an isothermal method of determining the adsorption enthalpy. This method has been used extensively on many types of compounds [40–43], as well as several studies on similar metal chelates [18,19,44] and by the present author [45]. This technique has shown a higher level of precision than other methods in determining sublimation enthalpy. Sublimation temperature and vapor pressure can be found using a calibration standard, or under ideal conditions. Ideal conditions include TGA in vacuum and constant sample surface area.

2.3.1 Langmuir Method

Sublimation and other phase changes follow zero-order kinetics, therefore the rate of mass loss by sublimation (m_{sub}) is constant at a given temperature with change in time (Δt) per unit surface area of sample.

$$m_{sub} = \frac{\Delta[mass\ of\ sample]}{\Delta t \times SA} \qquad (10)$$

Langmuir related the vapor pressure of a solid, p, with its sublimation rate, m_{sub}, where T is the temperature, R is the gas constant and M_W is the molecular weight of the compound [20]. The parameter α is the vaporization coefficient, usually assumed to be 1 for samples in a vacuum.

$$p = \left[\frac{2\pi RT}{M_W}\right]^{0.5} \frac{m_{sub}}{\alpha} \quad (11)$$

The Clausius-Clapeyron relation may be written as equation 12, where ΔH_{sub} is the enthalpy of sublimation.

$$\frac{d(\ln p)}{dT} = \frac{\Delta H_{sub}}{RT^2} \quad (12)$$

Ashcroft showed [17] that combining equations 11 and 12 yields a correlation between the mass loss rate and the enthalpy of sublimation. The resulting equation 13 can be written in a linear form. A plot of the left hand side of this equation versus *1/T* provides a linear trend line with a slope used to find the enthalpy of sublimation. The slope and y-intercept of such line can also be used to determine the vapor pressure, *p*.

$$\ln\left(m_{sub}\sqrt{\frac{2\pi RT}{\alpha^2 M_W}}\right) = \frac{\Delta H_{sub}}{RT_{sub}} - \frac{\Delta H_{sub}}{RT} \quad (13)$$

It is important to note that while the enthalpy is solely dependent on the slope of the trend line, the vapor pressure is dependent on both slope and y-intercept, and variations in the y-intercept can be attributed to the parameter, α, described above. A TGA instrument not used under vacuum requires calibration to a standard of known vapor pressure. The nitrogen gas flow of the instrument will have an effect on the value of α, which is dependent on experimental setup and independent of the substance, assuming the vapor is not associating with the sample. This means that α is part of the y-intercept of equation 13 and has no effect on the slope, and therefore no effect on the enthalpy value. The best way to solve for this is using the original Langmuir equation for vapor pressure.

This method can be used to calculate sublimation enthalpy values for lanthanide chelates by measuring the mass loss rate for each isotherm via TGA data. Figure 1 displays example mass loss data for each isotherm of a sample and Figure 2 displays isothermal jumps between temperatures, and its effect on weight loss percent and the time derivative.

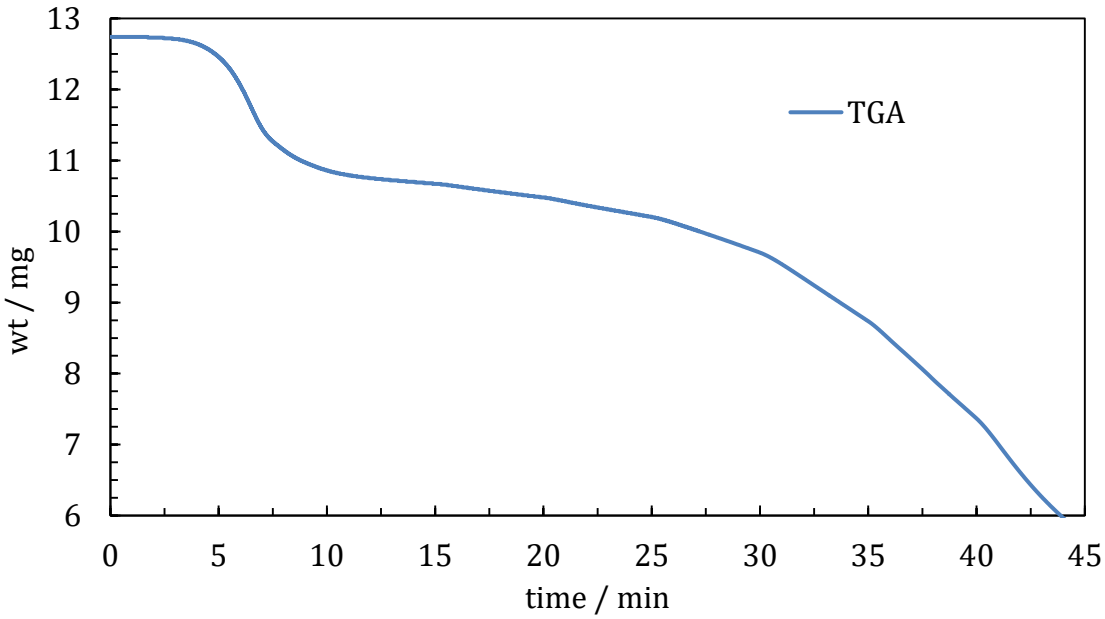

Figure 1: Example of consecutive jump isotherms shown as mass loss curves.

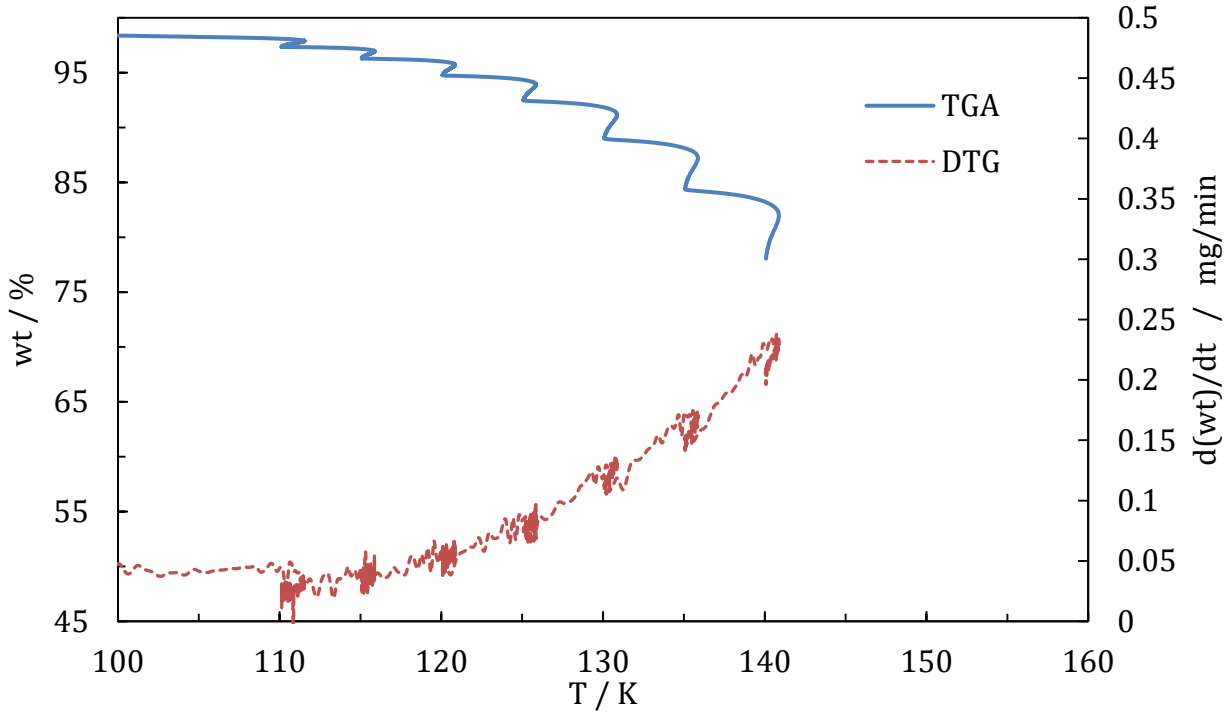

Figure 2: Example of an isothermal jump TGA-DTG spectrum.

2.3.2 TGA-MS and Melting Point Analysis

Thermogravimetric analysis of each sample can be carried out using a TGA connected to a mass spectrometer at constant heating rate until completion of the mass loss events. The vaporized compound is analyzed by the MS and curves can be overlaid on the TGA/DTG plots. The melting point of each of the samples is taken to verify the phase change of the sample at increasing temperatures. An example analysis using TGA-MS is shown in Figure 3. A major loss event of about 94% is seen from 143-163 °C. The sample's melting point range of 200-208 °C confirms this event is most likely sublimation. A small peak of 1% weight lost occurs between 71-89 °C and corresponds to a peak of mass 18, indicating possible hydration or aquo ion coordination of the compound.

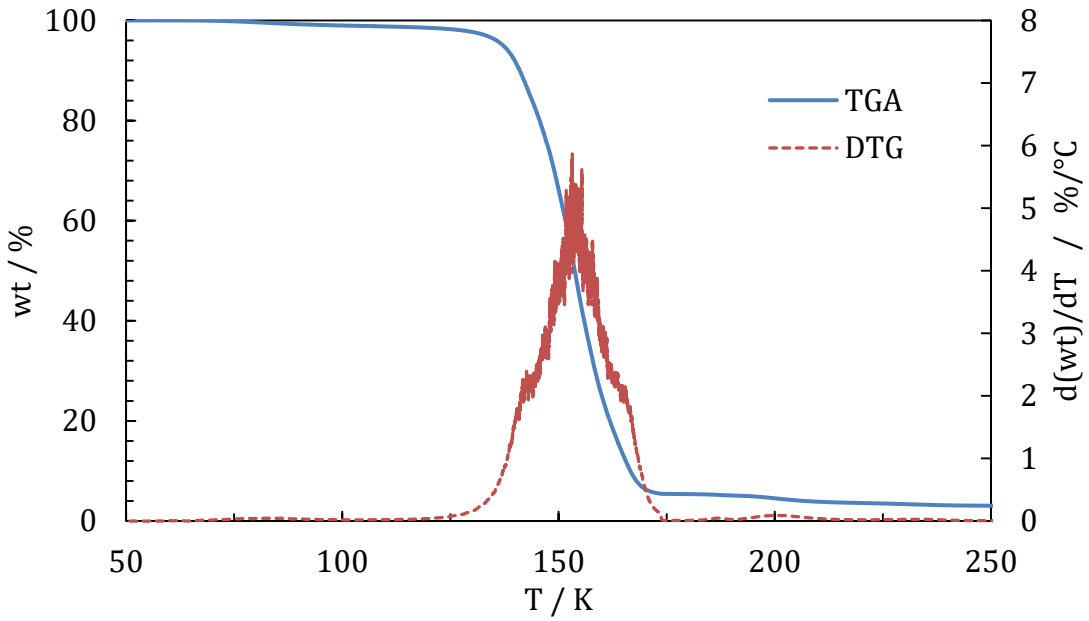

Figure 3: Example of a TGA-DTG spectrum.

2.4 The Lanthanide Series

Thermal analysis of lanthanides cannot be complete without an understanding of the chemical and physical trends and characteristics of the lanthanide series. Featuring a wide range of coordination numbers, lanthanides contain 4f orbitals which are well shielded by the 5s and 5p orbitals. They penetrate the xenon core configuration somewhat, and thus do

not covalently bond. This allows for similar spectroscopic and magnetic properties for lanthanide complexes of different ligands. Compared to the transition metals, the reactivity of the lanthanides is greater. As seen in this study, they prefer anionic ligands with donor atoms of high electronegativity such as O and F, and readily form hydrated complexes. Oxophillic lanthanide complexes lacking O-donor ligands are very oxygen and moisture sensitive and must be handled anaerobically [46]. Although there is a smooth trend seen in decrease of ionic radii across the series, the decrease in atomic radii across the series is disjointed with two spikes in radii, by Eu and Yb, due to their tendency to adopt the +2 state. Johnson notes, "The lanthanide elements behave similarly in reactions in which the 4f electrons are conserved, and very differently in reactions in which the number of 4f electrons change" [47].

2.4.1 The Lanthanide Contraction

The lanthanide series exhibits what is called the lanthanide contraction across the series, which is a decrease in radius of 3+ ions from La to Lu, despite an increase in weight. This is believed to be caused by the poor screening of the 4f electrons. Because of this, Lu resembles Sc and Y in terms of size and other physical and chemical properties more so than La does [48]. Some arguments have been made whether to group Sc and Y with the end of the lanthanide and actinide series (Lu and Lr) rather than the beginning (La and Ac). The exact placement and grouping of the lanthanide series among the periodic table has been discussed, yet more research into characterizing and understanding trends among the series is needed to support one side or another. The lanthanide contraction is nonetheless an important example of why more research into comparing lanthanides against each other is relevant.

2.4.2 Additional Characteristics of the Lanthanide Series

A pattern seen in the ionization energies of the series motivates the often cyclical nature of chemical properties of lanthanides. The first and second ionization energies exhibit a mostly increasing trend across the series because of the similar removal of the 6s electrons for each lanthanide. But when removing the third and fourth electron, the ionization energies

show evidence towards the stabilizing effects of a half filled or fully filled f sub shell. The cumulative energies when including the third ionization energy values better show the relationship between those lanthanide neighbors with different valence sub shells. For example, Gd and Lu have a 5d electron that Eu and Yb respectively do not. The removal of this third electron corresponds to that 5d electron for Gd and Lu, but not for most of the other lanthanides, whereas it might be a 4f electron. The trend is magnified when including the fourth ionization energy, as well as trends seen related to the differing stabilities of different oxidation states of various lanthanide neighbors [48].

Similarly, Ce behaves uniquely in the series, having both a 4f and 5d electron. Because it is at the beginning of the series, having only one 4f electron, its valence electron is more easily removed to leave a stable closed shell. Because of this, Ce has a common +4 oxidation state, unlike most lanthanides. As a result, Ce forms more types of oxides and some forms of chemical separation from the other lanthanides is more easily achieved with redox reactions. Special care is needed to ensure the correct oxidation state of the cerium complex, and thus ensure the chemical form and phase purity of the cerium in solution.

Hydration enthalpies have been found for the +3 lanthanides, where there is a smooth increase in magnitude of enthalpy of hydration across the series as smaller ions show an increased attraction for water molecules. Additionally, the hydration energy increases for higher charge ions, simply as charge density increases, electrostatic attraction increases [48]. The enthalpy of formation values of lanthanide trichlorides show similar trends, where there is mostly a decrease in magnitude of value across the series, but straying from the pattern are again the Eu/Gd/Tb neighbors and the Tm/Yb/Lu neighbors. The trichlorides become less stable with increase in atomic number up to Tb, with an almost linear decrease in melting point, but from Dy to Lu, the melting point increases [46]. The redox potentials of the series are consistent across the series, again with irregularities at Eu and Yb, similar to the ionization energy. Worth noting is the large negative value of enthalpy of this reduction, which is expected for reactive metals. This is also more proof of the difficulty in isolating the lanthanides, motivating the underlying project of this research.

2.5 Lanthanide Complexes Investigated

In addition to trends across the lanthanide series, it is of considerable interest to understand the chemical behaviors of varying complex types. Different chelates or compounds will sublime and adsorb based on different kinetics and thermodynamics. The relative differences in enthalpic values among homologues may be larger for one ligand versus another. Oppositely, one ligand may form a chelate where the homologous lanthanides do not show much appreciable difference in chemical behavior. If this is the case, a mixture of lanthanides in this chelated form will not separate very easily. A goal is to compare several different ligand types based on O-donors and sterics, to find a series of homologues where separation can be most easily exploited.

In the case of nuclear fallout debris, or melt glass, the material is easily converted to the stable chloride chemical form. Although chelated lanthanides are more volatile, more easily sublimed and are handled at lower temperatures, they require additional chemistry steps to arrive at this form. While the process is not always difficult, this can be time consuming and difficult to achieve in the field. There is thus motivation to chemically separate the chloride or oxychloride form. Although higher temperatures and lower pressures are most likely required to achieve this vaporization, the lanthanide chlorides and oxychlorides should still be studied for their ability to enter and stay in the gas phase. Unfortunately, there is no evidence that they will sublime at atmospheric pressure under nitrogen flow.

2.5.1 Lanthanide β-diketonates

There is considerable research showing the increased volatility of lanthanide chelates, specifically those using β-diketone (BDK) ligands [4–6,18,27,31,34,36,44,49,50]. As highlighted earlier, previous work has shown the utility of hfac as a ligand in subliming lanthanides. The present work is proposing the use of three additional BDK ligands for comparison of the efficacy in sublimation and stability of lanthanide ions. While all may sublime similarly, comparisons can be made as to the ease of hydration, differences in thermodynamics and kinetics, the stability in phase changes and the onset of decomposition.

Additional information about the chemistry of lanthanides may be hypothesized regarding inconsistencies in trends across the series for different chelates.

The β-diketonate complexes analyzed will be produced at the Radiochemistry Center of Excellence within the Institute for Nuclear Security at the University of Tennessee (Knoxville, TN, USA). Synthesis is outlined in the next chapter and will follow that done by Hanson et al [21] and other literature reports [49–54]. The four ligands used which are common in metal volatilization experiments are shown in Figure 4, Figure 5, Figure 6 and Figure 7.

Comparing other ligands to hfac, 1,1,1-trifluoro-2,4-pentanedione (tfac) will be used to confirm the reduction in volatility when replacing the fluorinated methyl group. Adding steric qualities to the chelate, the ligand 2,2,6,6-tetramethyl-3,5-heptanedione (dpm [or thd]) will be used. And finally, adding both steric qualities and fluorine atoms to the chelate, 6,6,7,7,8,8,8-heptafluoro-2,2-dimethyl-3,5-octanedione (fod) will be used. These ligands are expected to coordinate around the lanthanide ion similar to that of the hfac ligand. Despite many metals having coordination number of 6, and the lanthanides having +3 charge, previous work has elucidated the octacoordination of these metals with hfac [21]. For some of these complexes, tris chelation is more likely but octacoordination is still found by coordinating two water molecules on the inner shell with three ligands. Hydration is also possible given the metal ionic radius and size of the ligand. Steric crowding of the shell leads to the conclusion that larger, bulkier ligands will more likely produce anhydrous complexes [55]. Tetrakis chelation or octacoordination may not hold true for these new ligands chosen, especially considering the multitude of research which supports hexacoordination of lanthanide acac and dpm, but elucidating this information will be another goal of this work. Nonetheless, the general structure of the chelate should follow that seen in Figure 8.

2.5.2 Lanthanide Chlorides & Oxychlorides

The halides and oxyhalides of lanthanides have been well studied, but there is still uncertainty as to the rapid, chromatographic separations of such compounds [56–64]. Separation of lanthanide chlorides would be preferred if possible, but due to lanthanide oxychloride formation upon heating, it is difficult to predict which chemical form the metal

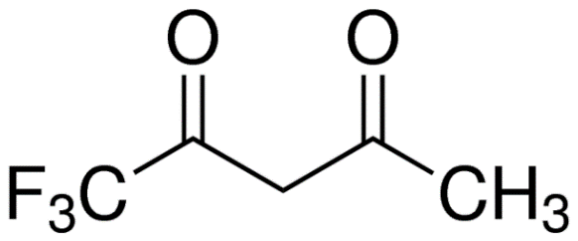

Figure 4: 1,1,1-trifluoro-2,4-pentanedione (tfac)

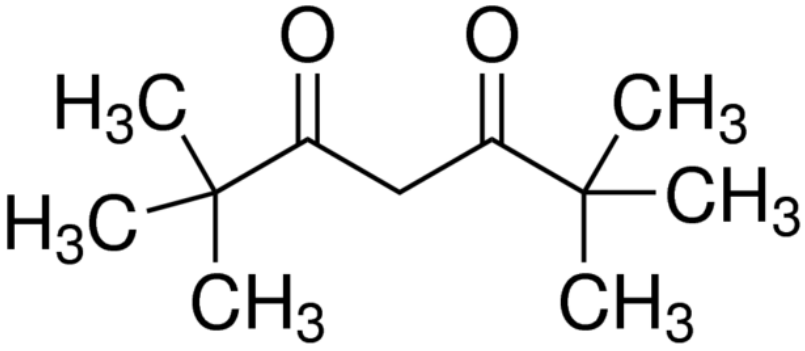

Figure 5: 2,2,6,6-tetramethyl-3,5-heptanedione (dpm)

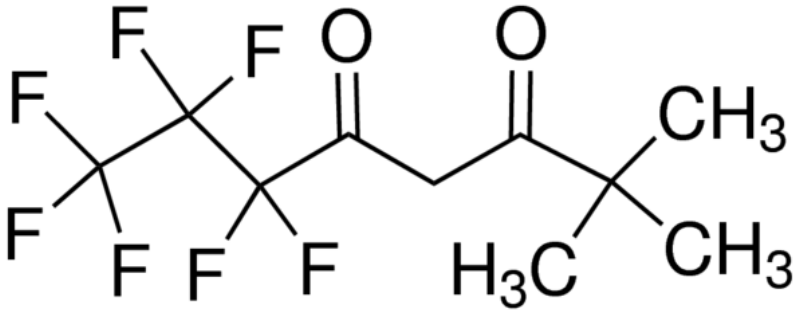

Figure 6: 6,6,7,7,8,8,8-heptafluoro-2,2-dimethyl-3,5-octanedione (fod)

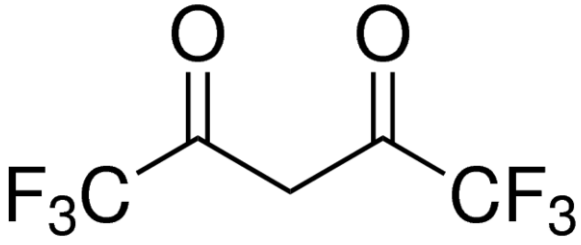

Figure 7: 1,1,1,5,5,5-hexafluoro-2,4-pentanedione (hfac)

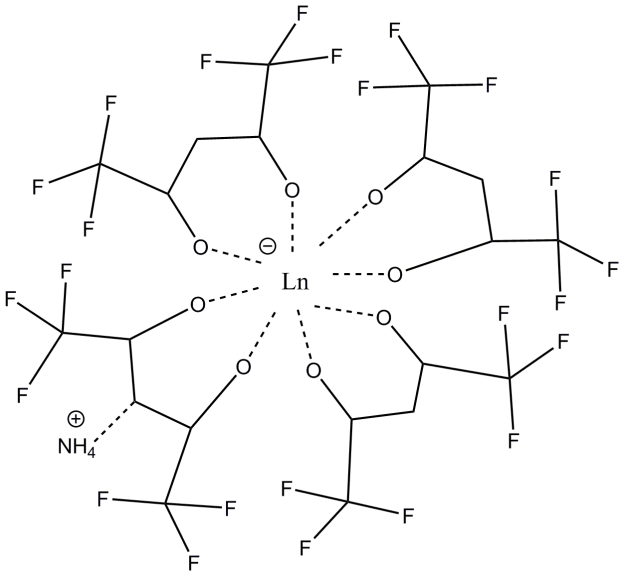

Figure 8: NH_4•Ln[hfac]$_4$, where Ln is a lanthanide ion.

will be in. Uncertainty in product formation translates to uncertainty in vaporization behavior, and thus separation ability. Synthesis of lanthanide trichlorides will be done to characterize both compound types [65,66]. Trichlorides have the hexagonal UCl_3-type crystal structure for La-Gd and the monoclinic $AlCl_3$-type structure for Ho-Lu. Tb and Dy are both dimorphic, where Tb has the orthorhombic $PuBr_3$-type structure most commonly, and Dy has the monoclinic $AlCl_3$-type structure most commonly.

If vaporization of the trichlorides is not possible, lanthanide chlorides have been shown to vaporize at lower temperatures by forming a complex with aluminum trichloride [67–71]. The LnCl-AlCl complex requires more chemical preparation, but in the case of no chloride sublimation, this pathway represents a possible solution. Vaporization of some of these complexes has been shown near the range 325-625 °C, which is considerably lower than the literature boiling points of the lanthanide trichlorides, which are well over 1000 °C. This provides a second avenue to explore given little success in subliming lanthanide chlorides or oxychlorides.

Oxychlorides have higher melting points, which complicates separations. For La to Ho, oxychlorides crystallize in the tetragonal PbFCl-type structure, which can be visualized as distinct layers of Ln, O and Cl, where each Ln is coordinated to four O and five Cl. As the size of Ln decreases, the deformation of Cl ions increases and the complex becomes unstable.

For Tm to Lu, compounds have the SmSI-type rhombohedral structure, where Ln is coordinated to four O and four Cl. ErOCl is dimorphic, which is different than the trichlorides, where the dimorphic Ln in the series is seen for the larger sized Tb and Dy ions. Thermodynamic data is scarce for the oxychlorides, given for at least four Ln ions [72]. Methods to avoid oxychloride formation upon heating of trichlorides may involve heating under reactive chlorine gas, strictly dry and anaerobic conditions and at heating rates as low as 0.5 °C/min [73].

Chapter 3: Materials and Methods

3.1 Synthesis and Characterization

3.1.1 Lanthanide Hexafluoroacetylacetonates

The 1,1,1,5,5,5–hexafluoroacetylacetonate (hfac) chelates of the lanthanides were synthesized according to that done by Halverson et al [6,7,21,27,45,52,53,55,74]. The β-diketonate complexes were produced at the Radiochemistry Center of Excellence within the Institute for Nuclear Security at the University of Tennessee (Knoxville, TN, USA). The complexes synthesized were NH_4•Ln[hfac]$_4$, where Ln is the following: La, Pr, Nd, Sm, Eu, Gd, Tb, Dy, Ho, Er, Tm, Yb or Lu. Hfac complexes of Ce or Pm were not available. All reagents and solvents were used from commercial sources and used without further purification. The lanthanide oxides (Sigma Aldrich, 99.99%) were combined with hot, concentrated HCl (Fisher, ACS Reagent Grade) to yield the chloride salt. The solution was allowed to cool. 1,1,1,5,5,5–hexafluoroacetylacetone (H[hfac], Acros, 99.9%) was obtained and combined with equimolar amounts of concentrated NH_4OH (Fisher, ACS Reagent Grade) at 0°C. The two liquids reacted vigorously producing a white solid (NH_4[hfac]) that was stirred to fully react the reagents. The solid was then placed in a desiccator for storage. The NH_4[hfac] was dissolved in 5 mL of diethyl ether (ACS Reagent Grade, Fisher) to which the aqueous lanthanide chloride was added in a ratio of 4:1. The mixture was shaken vigorously for 30 seconds, and then set for 5 minutes, repeating 3 times. At the conclusion of the last agitation, the organic phase was drawn off and placed in a vacuum desiccator to dry the sample and remove the ether.

Characterization Methods

The melting point of each of the thirteen samples is taken to verify the phase change of the sample at increasing temperatures. Four capillary tube samples of each compound were run simultaneously using a MP50 Melting Point System (Mettler Toledo, USA). The samples were run at 10 °C min^{-1} and with video recording of the samples. Qualitative assessment of the melting point was completed with 0.5 °C margin of uncertainty at the temperature where each sample begins and completes melting.

Elemental analysis was performed by Atlantic Microlab in Norcross, GA. Infrared spectra were recorded using a Perkin Elmer FT-attenuated total reflectance – infrared spectrometer (FT-ATR-IR) spectrum 100 instrument in the range from 4000-550 cm^{-1}. Mass spectra were recorded using a GBC 9000 Opti-mass inductively coupled plasma time-of-flight mass spectrometer (ICP-TOF-MS) for detection of the RE ions. Mass fragments were analyzed using a HP 5973 inert Mass Selective Detector (EI-MS). NMR data for H and F were obtained using a Varian NMR system at 500 MHz, using 1,4-dioxane-99% (Cambridge Isotopes) as a solvent. Single Crystal X-Ray Diffraction data was collected on a Bruker SMART APEXII three circle diffractometer equipped with a CCD area detector and operated at 1,800 W power (45 kV, 40 mA) to generate Mo K_α radiation (λ = 0.71073 Å). The incident X-ray beam was focused and monochromated using Bruker Excalibur focusing optics. Single crystals were mounted on nylon CryoLoops (Hampton Research) with Paratone-N (Hampton Research) and frozen at -100 °C and -173 °C, respectively. Initial scans of each specimen were taken to obtain preliminary unit cell parameters and to assess the mosaicity (i.e. breadth of spots between frames) of the crystal to select the required frame width for data collection. For all cases frame widths of 0.5° were judged to be appropriate and full hemispheres of data were collected using the Bruker APEX2 software suite to carry out overlapping φ and ω scans at detector setting of 2θ = 28°.

SC-XRD

Determination of crystal structure was only achieved for $Gd[hfac]_4$, and was done by Dr. David Jenkins in the Department of Chemistry at the University of Tennessee. Following data collection, reflections were sampled from all regions of the Ewald sphere to re-determine unit cell parameters for data integration. Following exhaustive review of collected frames the resolution of the dataset was judged, and, if necessary, regions of the frames where no coherent scattering was observed were removed from consideration for data integration using the Bruker SAINTplus program. Data was integrated using a narrow frame algorithm and was subsequently corrected for absorption. Absorption corrections were performed for both samples using the SADABS program. Space group determination and tests for merohedral twinning were carried out using XPREP. The highest possible space

group was chosen. The final model was refined anisotropically (with the exception of H atoms). Hydrogen atoms were not placed on solvent molecules due to disorder. The structure was examined using the Addsym subroutine of PLATON4 to assure that no additional symmetry could be applied to the models. The structure arrived at is shown in the Figure 9 below.

Elemental Analysis

For 1. Formula: Sm[hfac]$_4$. Yield: 35.68%. Elemental analysis calc'd (%): C 24.37, H 1.75 N 4.06, F 45.80. Found: C 24.3, H 1.87, N 4.06, F N/A. For 2. Formula: Gd[hfac]$_4$. Yield: 65.34%. Elemental analysis calc'd: C 24.84, H 1.04 N 2.90, F 47.15. Found: C 24.35, H 0.96, N 2.20, F 42.74. For 3. Formula: Dy[hfac]$_4$. Yield: 73.77%. Elemental analysis calc'd: C 23.71, H 1.93, N 3.95, F 45.00. Found: C 24.45, H 2.08, N 3.87, F 46.10. For 4. Formula: Tm[hfac]$_4$. Yield: 58.17%. Elemental analysis calc'd: C 23.42, H 1.18, N 2.43, F 44.46. Found: C 24.18, H 1.18, N 2.50, F N/A.

FTIR

For 1. (ATR cm^{-1}): 3184 (br), 1644 (w), 1563 (w), 1538 (w), 1440 (m), 1252 (m), 1194 (m), 1179 (m), 1130 (br, s), 805 (w), 744 (m). For 2. (ATR cm^{-1}): 3127 (br), 3040 (br), 1645 (s), 1611 (w), 1563 (w), 1537 (m), 1502 (w), 1472 (w), 1405 (m), 1349 (w), 1253 (s), 1201

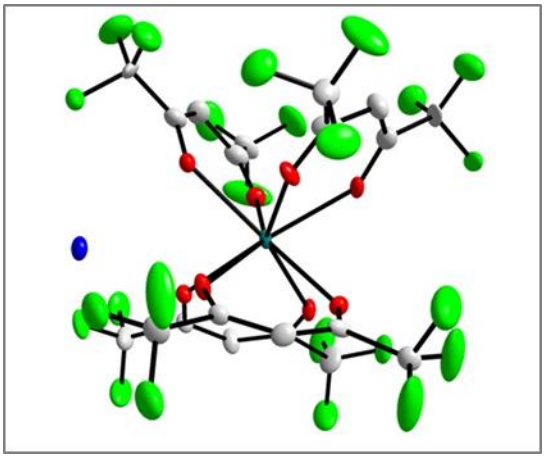

Figure 9: Crystal Structure of NH_3^+(Gd[hfac]$_4^-$)

(s), 1136 (s), 1096 (s), 804 (s), 768 (w), 744 (s), 752 (w), 661 (s). For 3. (ATR cm^{-1}) 3211 (br), 1645 (w), 1564 (w), 1535 (w), 1459 (m), 1253 (m), 1196 (s), 1177 (s), 1123 (s), 800 (m), 738 (m). For 4. (ATR cm^{-1}) 3149 (br), 1649 (w), 1564 (w), 1537 (w), 1473 (m), 1251 (m), 1203 (s), 1177 (s), 1132 (s), 804 (m), 744 (m).

NMR

For 1: 1H NMR (500 MHz, 1,4-Dioxane-d8) δ 7.26 (s, 1H), 5.34 (s, 1H), 2.64 (s, 2H). 19F NMR (470 MHz, dioxane) δ -76.50, -76.98, -77.41. For 2: 1H NMR (500 MHz, dioxane) δ 6.91, 2.37. 19F NMR (470 MHz, dioxane) δ -78.02, -79.70, -80.93. For 3: 1H NMR (500 MHz, dioxane) δ 1.03, 0.97. 19F NMR (470 MHz, dioxane) δ -71.83, -75.13, -76.22, -77.42, -78.24. For 4: 1H NMR (500 MHz, 1,4-Dioxane-d8) δ 4.72 (s, 1H). 19F NMR (470 MHz, dioxane) δ -77.49, -108.66, -109.94.

3.1.2 Lanthanide Dipivaloylmethanates

2,2,6,6-tetramethyl-3,5-heptanedione (thd), also known as dipivaloylmethane (dpm), commonly forms a tris chelate with the lanthanides, although lanthanum and cerium are believed to form tetrakis chelates with the deprotonated ligand. The synthesis of 14 lanthanide dipivaloylmethanates follows closely that according to Berg and Acosta [51] and others [4,27,31,75]. The β-diketonate complexes were produced at the Radiochemistry Center of Excellence within the Institute for Nuclear Security at the University of Tennessee (Knoxville, TN, USA). The complexes synthesized were $Ln[dpm]_3$, where Ln is the following: Pr, Nd, Sm, Eu, Gd, Tb, Dy, Ho, Er, Tm, Yb or Lu. The $Ln[dpm]_4$ complexes are presumed for: La and Ce. Pm was not available. All reagents and solvents were used from commercial sources and used without further purification. The lanthanide oxides (Sigma Aldrich, 99.99%) were combined with hot, concentrated HCl (Fisher, ACS Reagent Grade) to yield the chloride salt for all RE except La, Ce and Lu; the solution was allowed to cool. The syntheses started with lanthanum (III) chloride (ACROS 99.9%), cerium(III) chloride heptahydrate (SigmaAldrich, 99.999% trace metals basis) for Ce, and lutetium(III) chloride (ACROS Organics, 99.9%) for Lu, instead of the oxide. The trichlorides were dissolved in 50% ethanol in water. A 4:4:1 ratio of ligand:base:metal was used for all compounds. The ligand was first

added to 50 ml of 50% ethanol, then NaOH was added to deprotonate the ligand. After stirring, the ligand solution was mixed with the metal chloride solution. The solution was mixed on a stirplate for minimum 2 hours, and as long as 24 hours. The precipitate was suction filtered, dried on a watch glass in open air for 24-48 hours, and weighed. Yields range from 60% to essentially quantitative.

Adjusting Experimental Methods

Various parameters of the synthesis were tested for effect on the product. For example, 5 of the 14 syntheses involved adding the ligand solution to the metal solution, instead of the opposite. There is no evidence in yield or melting point analysis that this had any effect, as the kinetics of reaction were much slower than the rate at which the solution was poured. Additionally, the order of adding NaOH to the ligand was tested. In 3 of the 14 syntheses, the NaOH was added to the ligand before adding to the solvent. This did not have a negative impact on the yield or melting point results. One parameter that does show good results in product formation is longer mixing times. For the 7 samples allowed to mix overnight, all show melting points within literature ranges and good yields. Once again, the slower kinetics of chelate formation may require longer than previously believed mixing times. Finally, the form of sodium hydroxide used was tested. Half of the first batch of samples were synthesized with solid, dry pebbles of sodium hydroxide added to the ligand solution, while the other half involved the addition of 1 M NaOH to the ligand solution. The melting point data points to the conclusion that the use of 1 M NaOH might not allow for the full deprotonation of the ligand and produces a complex with much lower melting point and a softening range around 100 °C. One possibility is the formation of lanthanide aquo ion complexes, due to a potential lack of basic potency in the 1 M NaOH solution that was made and left open to air over the span of a week. This much lower melting point is seen in at least 4 of the 14 complexes in the first batch.

Nearly half of the lanthanide dpm compounds resulted in melting points too low. For some, recrystallization in hexanes one time produced new melting point values near literature. For others, the synthesis was redone with the following adjustments: overnight mixing as opposed to 2 hours only; solid NaOH was added to the ligand instead of basic NaOH

solution to ensure deprotonation before contact with water; the metal chloride solution was added to the ligand solution while stirring, as opposed to the opposite. All 14 samples were produced with melting points near literature and were further characterized by elemental analysis, FTIR, and ICP-MS.

Characterization Methods

The melting point of each of the fourteen samples is taken to verify the phase change of the sample at increasing temperatures. Two capillary tube samples of each compound were run simultaneously using a MP50 Melting Point System (Mettler Toledo, USA). The samples are run at 5 °C min^{-1} up to 300 °C and with video recording of the samples. Qualitative assessment of the melting point is completed with 0.5 °C margin of uncertainty at the temperature where each sample begins and completes melting.

Table 1. Results from melting point and elemental analyses for $Ln[dpm]_n$ complexes

		mp/°C		Found		Calculated	
	Color	Found	Literature[a]	%C	%H	%C	%H
$La[dpm]_4$	white	224-230	239-245	55.15	8.13	59.05	8.56
$Ce[dpm]_4$	reddish brown	275-283	276-278[b]	54.06	7.86	58.97	8.55
$Pr[dpm]_3$	light green	214-220	222-224	50.63	7.39	57.38	8.32
$Nd[dpm]_3$	reddish blue	205-209	215-218	52.10	7.57	57.11	8.28
$Sm[dpm]_3$	yellowish white	197-202	200-201	54.86	8.02	56.61	8.21
$Eu[dpm]_3$	yellow	186-191	190-191	49.95	7.46	56.48	8.19
$Gd[dpm]_3$	white	181-183	183-184	53.56	7.91	56.06	8.13
$Tb[dpm]_3$	white	177-179	177-180[c]	49.97	7.25	55.92	8.11
$Dy[dpm]_3$	yellowish white	177-182	182-183	53.69	7.78	55.64	8.07
$Ho[dpm]_3$	light red	181-185	178-180	55.25	7.93	55.46	8.04
$Er[dpm]_3$	pink	168-176	179-181	54.21	8.12	55.28	8.01
$Tm[dpm]_3$	yellowish white	169-172	170-173	53.62	7.80	55.15	7.99
$Yb[dpm]_3$	white	166-170	165-167	54.73	8.10	54.83	7.95
$Lu[dpm]_3$	white	174-178	173-174	54.13	7.96	54.69	7.93

[a]Berg [51], except otherwise stated

[b]Hubert-Pfalzgraf [76]

[c]Eisentraut [55]

Table 2. Infrared spectral results for $Ln[dpm]_n$ complexes[a]

cm^{-1}	peak	cm^{-1}	peak	cm^{-1}	peak
2950	m, sh	1380	s, sh	1135	m
2860	w	1350	s	868	s
1570	m, sh	1285	w	793	m, sh
1540	m	1250	w	760	w
1495	s, sh	1220	w, sh	735	w
1450	w	1180	w	600	m

[a]Spectral notations: s, strong intensity; m, medium intensity; w, weak intensity; b, broad; sh, shoulder

Elemental analysis was performed by Atlantic Microlab in Norcross, GA. For these compounds, only weight percentages of C, H and N were analyzed by EA. The samples were ran as is and also after being dried under vacuum for 5 min at 105 °C. The results differed by less than 1%, which is the margin of uncertainty, confirming the compound's lack of affinity for atmospheric water. Infrared spectra were recorded using a Thermo Scientific Nicolet iS10 FT-IR Spectrometer in the range from 4000-500 cm^{-1}. All infrared spectra can be seen in Figure 10. Mass spectra were recorded using a GBC OptiMass 9500 inductively coupled plasma time-of-flight mass spectrometer (ICP-TOF-MS) for detection of the RE ions. Mass fragments were analyzed using a HP 5973 inert Mass Selective Detector (EI-MS). All samples were confirmed as containing the expected rare earth metal, although some contained trace amounts of one or two other lanthanides.

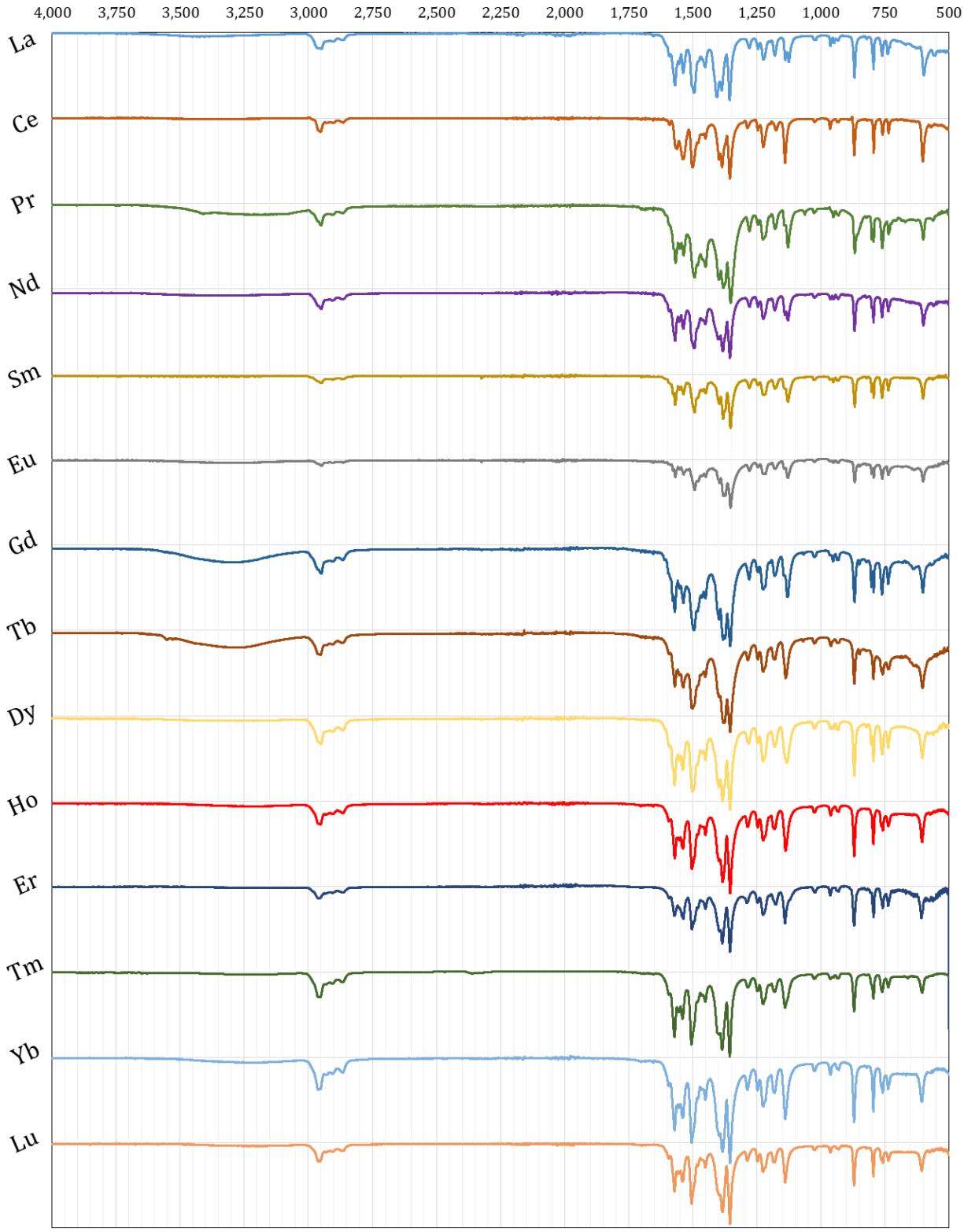

Figure 10: FT-IR spectra for the lanthanide dipivaloylmethanates

3.1.3 Lanthanide Trifluoroacetylacetonates

1,1,1-trifluoro-2,4-pentanedione also known as trifluoroacetylacetone (tfac), commonly forms a tris chelate with the lanthanides as a deprotonated ligand. The synthesis of 14 lanthanide trifluoroacetylacetonates follows closely that according to Berg and Acosta [51] and others [77,78]. The β-diketonate complexes were produced at the Radiochemistry Center of Excellence within the Institute for Nuclear Security at the University of Tennessee (Knoxville, TN, USA). The complexes synthesized were $Ln[tfac]_3$, where Ln is the following: La, Ce, Pr, Nd, Sm, Eu, Gd, Tb, Dy, Ho, Er, Tm, Yb or Lu. Pm was not available. All reagents and solvents were used from commercial sources and used without further purification. The lanthanide oxides (Sigma Aldrich, 99.99%) were combined with hot, concentrated HCl (Fisher, ACS Reagent Grade) to yield the chloride salt for all RE except La, Ce, Er and Lu; the solution was allowed to cool. The other four syntheses started with lanthanum (III) chloride (ACROS 99.9%) for La, cerium (III) chloride heptahydrate (SigmaAldrich, 99.999% trace metals basis) for Ce, erbium (III) chloride hexahydrate (Aldrich 99.9%) for Er, and lutetium (III) chloride (ACROS Organics, 99.9%) for Lu, instead of the oxide. The trichlorides were dissolved easily in 50 ml water. A roughly 4:4:1 ratio of ligand:base:metal was used for all compounds. The base solution (ammonium hydroxide aka concentrated aqueuous ammonia) was first added to a dry beaker, then the ligand was added to deprotonate the ligand. Instant vapor products formed, and the solution turned to a wet solid. After stirring and setting for 5 minutes, the ligand solution was added to 50 ml of water and mixed until dissolved. The ligand solution was added slowly to the aqueous metal solution and mixed on a stirplate for 24 hours. The mixture did turn cloudy within 30 minutes of mixing. The precipitate was suction filtered, dried on a watch glass in open air for 48 hours, and weighed. Yields range from as low as 20% to essentially quantitative, although were typically around 50%.

Similar to the syntheses of the LnDpm compounds, it was found that adjustments and trial runs were necessary to ensure sufficient yields and the synthesis of the correct compounds. It was found that addition of ligand-base solution to the metal solution only produced good results when the deprotonated ligand was in dissolved aqueous form, and not as a solid ligand salt. Therefore the ligand salt was always dissolved in water before

added to the metal solution. It was also found that overnight mixing still yielded good results, so solutions were not mixed for less time, although it is assumed that several hours of mixing is sufficient. The ligand solution was always added to the metal solution except for one sample, which was added in opposite order and provided good results, therefore this does not seem to be an issue. All 14 samples were further characterized by elemental analysis, FTIR, and ICP-MS.

Characterization Methods

The melting point of each of the fourteen samples is taken to verify the phase change of the sample at increasing temperatures. Two capillary tube samples of each compound were run simultaneously using a MP50 Melting Point System (Mettler Toledo, USA). The samples are run at 5 °C min^{-1} up to 300 °C and with video recording of the samples. Qualitative assessment of the melting point is completed with 0.5 °C margin of uncertainty at the temperature where each sample begins and completes melting. All samples that did not produce melting points near the literature values were recrystallized in hot benzene. The benzene was boiled off and the samples were left in hood overnight for residual benzene to evaporate. La, Ce, Pr, Nd, Sm, and Gd did not require recrystallization, although Gd was recrystallized and maintained similar melting point range. Eu, Tb, Dy, Ho, Tm, Yb were all recrystallized, although for each the melting point range did not shift closer to the literature values. Drying the samples for a week in a desiccator with phosphorus pentoxide did not appreciably shift the melting point range closer to literature values, and in some cases shifted it lower (farther away).

Elemental analysis was performed by Atlantic Microlab in Norcross, GA. For these compounds, only weight percentages of C, H, N and F were analyzed by EA. The samples were run after being dried under vacuum for 5 min at 105 °C. Analysis of the data confirms tris chelation of tfac ligand with all lanthanides, and proposes hypothesis of hydration or coordination of one or two water molecule per chelate. Infrared spectra were recorded using a Thermo Scientific Nicolet iS10 FT-IR Spectrometer in the range from 4000-500 cm^{-1}. All infrared spectra can be seen in Figure 11 below. Mass spectra were recorded using a GBC OptiMass 9500 inductively coupled plasma time-of-flight mass spectrometer (ICP-TOF-MS)

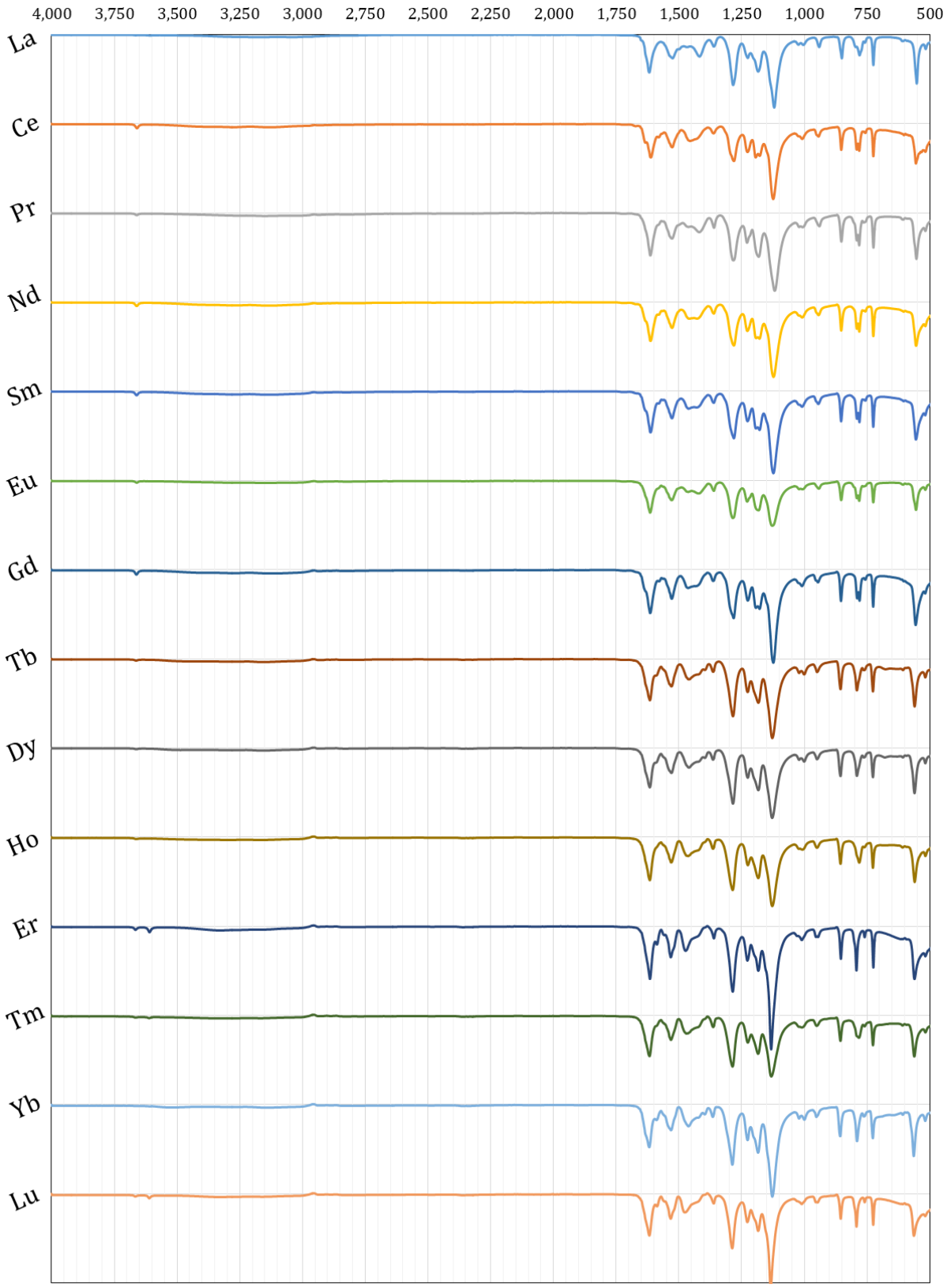

Figure 11: FT-IR spectra for the lanthanide trifluoroacetylacetonates

for detection of the RE ions. Mass fragments were analyzed using a HP 5973 inert Mass Selective Detector (EI-MS). All samples were confirmed as containing the expected rare earth metal, although some contained trace amounts of one or two other lanthanides. The results are outlined in Table 3 and Table 4.

Ammine Formation

Through elemental analysis, it was found that when a large ratio of moles base to moles metal was used, the compound synthesized was an ammine of the tfac diketonate. In other words, if an excess of ammonia was present in solution, it was found that ammonia molecules will coordinate with the metal ion or on the outer coordination sphere, along with the ligand ions. This has been previously reported in literature [79]. There is a direct correlation for samples where a large excess of base was used with higher than literature melting points; additionally nitrogen was found for these samples via elemental analysis. TGA-MS data indicates higher percent sublimation of the compound for these ammines, while the non-ammine compounds do not appear to sublime an appreciable amount. Berg and Acosta report difficulty in subliming the tfac hydrates, and this is also seen here, but it is important to note that the tfac ammines sublime sometimes up to 30 wt% prior to melting [51]. Table 5 outlines major differences found between the ammine and non-ammine forms of the tfac diketonate, and Table 6 compares the six synthesized ammines to each other. Note that the ammines sublime between 10-30 wt%, which is still not ideal for the Langmuir method, and more importantly is not ideal for this project, namely the gas phase separations of lanthanides. Partial sublimation of these compounds in different amounts does not allow for quantitative analysis of the composition of an unknown mixture of lanthanides. Additionally, there isn't enough separation in the sublimation range of temperatures.

Comparing the ammine and non-ammine compounds of La and Lu may shed some light on the ease with which ammonia coordinates to the lanthanide. Even with low amounts of excess base, lanthanum forms a partial ammine, according to EA and TGA-MS data. Oppositely, even with large amounts of excess base, lutetium does not seem to coordinate with ammonia in as high of a ratio, forming ammines partially, noted by the low nitrogen content. This may be explained by the lack of 4f electrons in La and the filled 4f shell in Lu. Although f-block electrons do no participate in bonding, the electronegativity of Lu is greater

Table 3. Results from melting point and elemental analysis for Ln[tfac]$_3$ complexes

		mp/°C		Found			Calculated		
	Color	Found	Literature[b]	%C	%H	%F	%C	%H	%F
La[tfac]$_3$-2H$_2$O[a]	white	137-143	142-144	28.51	2.17	26.73	29.24	2.29	27.75
Ce[tfac]$_3$-2H$_2$O	brown	132-138	127-129	26.82	1.95	25.05	29.18	2.29	27.70
Pr[tfac]$_3$-2H$_2$O[a]	light green	139-151	136-138	28.71	2.22	27.76	29.15	2.28	27.66
Nd[tfac]$_3$-2H$_2$O	reddish blue	144-147	147-149	25.47	1.98	26.94	28.99	2.27	27.51
Sm[tfac]$_3$-2H$_2$O	yellowish white	147-150	147-149	26.41	2.00	25.40	28.71	2.25	27.24
Eu[tfac]$_3$-2H$_2$O[a]	yellowish white	159-169	144-146	29.86	2.36	27.48	28.63	2.24	27.17
Gd[tfac]$_3$-2H$_2$O	white	149-151	145-147	26.38	1.97	24.95	28.39	2.22	26.95
Tb[tfac]$_3$-2H$_2$O	white	141-148	154-156	27.32	2.01	25.63	28.32	2.22	26.88
Dy[tfac]$_3$-2H$_2$O	yellow	133-140	152-154	26.53	1.89	25.91	28.16	2.21	26.73
Ho[tfac]$_3$-2H$_2$O	light red	127-134	154-156	26.32	1.89	25.69	28.06	2.20	26.63
Er[tfac]$_3$-2H$_2$O	pink	129-135	148-150	26.99	2.01	22.52	27.95	2.19	26.53
Tm[tfac]$_3$-2H$_2$O	white	124-128	156-158	25.82	1.90	23.98	27.88	2.18	26.46
Yb[tfac]$_3$-2H$_2$O	yellowish white	110-114	140-142	26.18	1.91	24.48	27.70	2.17	26.29
Lu[tfac]$_3$-2H$_2$O	white	123-128	188-190	26.73	1.92	24.99	27.62	2.16	26.22

[a]Nitrogen found in sample; potential partial ammine complex

[b]Melting point data from Berg [51]

Table 4. Infrared spectral results for Ln[tfac]$_3$ complexes[a]

cm-1	peak	cm-1	peak	cm-1	peak
3660	w	1230	m	790	m
1620	s, sh	1180	s, sh	780	m
1530	m, sh	1120	s	760	w
1420	w, b	1010	w, sh	725	m
1360	w	940	w	553	s
1280	s, sh	850	m	517	w

[a]Spectral notations: s, strong intensity; m, medium intensity; w, weak intensity; b, broad; sh, shoulder

Table 5. Comparing Ln[tfac]$_3$ complexes to Ln[tfac]$_3$ ammines

	mp/°C		Molar ratios in synthesis			Elemental analysis found				Sublimation data	
	Found	Literature[a]	ligand:Ln	NH_4OH:Ln	Excess base	% C	% H	% N	% F	wt%	Peak Temp
La[tfac]$_3$-2H_2O	137-143	142-144	5.56	7.69	2.13	28.51	2.17	0.90	26.73	7.2	113
La[tfac]$_3$-NH_3-H_2O	166-169	-	4.08	8.64	4.55	31.27	2.54	1.77	26.49	19.6	121
Ce[tfac]$_3$-2H_2O	132-138	127-129	6.02	5.83	-0.18	26.82	1.95	0.00	25.05	4	-
Ce[tfac]$_3$-NH_3-H_2O	167-171	-	4.03	43.43	39.40	23.77	1.86	1.31	22.73	20.6	128
Er[tfac]$_3$-2H_2O	129-135	148-150	4.28	6.98	2.70	26.99	2.01	0.00	22.52	2	-
Er[tfac]$_3$-NH_3-H_2O	176-178	-	5.19	27.27	22.08	29.83	2.42	1.61	28.17	29.8	132
Lu[tfac]$_3$-2H_2O	123-128	188-190	4.56	6.67	2.11	26.73	1.92	0.00	24.99	3.5	-
Lu[tfac]$_3$-NH_3-H_2O	144-160	-	2.95	28.46	25.50	25.57	1.96	0.42	23.98	10.4	142

Table 6. Comparing Ln[tfac]$_3$ ammines

	mp/°C		Molar ratio	% Nitrogen		Sublimation data		
	Found	Literature[a]	NH_4OH:Ln	Found	Calculated	wt%	Beg Temp	Peak Temp
La[tfac]$_3$-NH_3-H_2O	166-169	142-144	8.64	1.77	2.21	19.6	81	121
Ce[tfac]$_3$-NH_3-H_2O	167-171	127-129	43.43	1.31	2.21	20.6	92	128
Pr[tfac]$_3$-NH_3-H_2O	139-151	136-138	10.20	0.92	2.21	14.7	104	130
Eu[tfac]$_3$-NH_3-H_2O	159-169	144-146	11.52	1.59	2.17	22.2	100	136
Er[tfac]$_3$-NH_3-H_2O	176-178	148-150	27.27	1.61	2.12	29.8	102	132
Lu[tfac]$_3$-NH_3-H_2O	144-160	188-190	28.46	0.42	2.09	10.4	128	142

[a]Berg [51]

than that of La, possibly due in part to the lanthanide contraction, or the 4f subshell's poor shielding of the greater nuclear charge. This might explain the lower likelihood of ammonia displacing water on the outer coordination sphere for more electronegative lanthanides, because of water's greater dipole moment.

The TGA-MS curves for the $Ln[tfac]_3$ ammines are discussed later, but Figure 12 is a comparison of the curves for the ammine and hydrate forms of the $Ce[tfac]_3$ chelate. Note the larger percentage of water for the hydrate, which evaporates around 75 °C, and the sublimation of around 20 wt% of the ammine around 125 °C, well below the compound's melting point range. The hydrate has a large, broad weight loss event around 225 °C, well above the compound's melting point range, indicating melting followed by vaporization. The ammine also has a potential vaporization stage, indicating either partial sublimation of the ammine complex, or just partial formation of the ammine in synthesis. Both compounds oxidize or decompose around 225-250 °C, confirming the lack of total sublimation for the tfac chelates.

The FTIR spectra comparing the ammine and hydrate forms of the four tfac chelates is shown in Figure 13. Note there isn't a large difference in peak location or intensity, although there are some small differences. For example, around 1400 cm^{-1}, the ammines display a slightly stronger peak intensity, while the hydrates have that peak shifted to a larger wavenumber or do not contain it at all. Overall, both complexes cannot be quantitatively differentiated by FTIR.

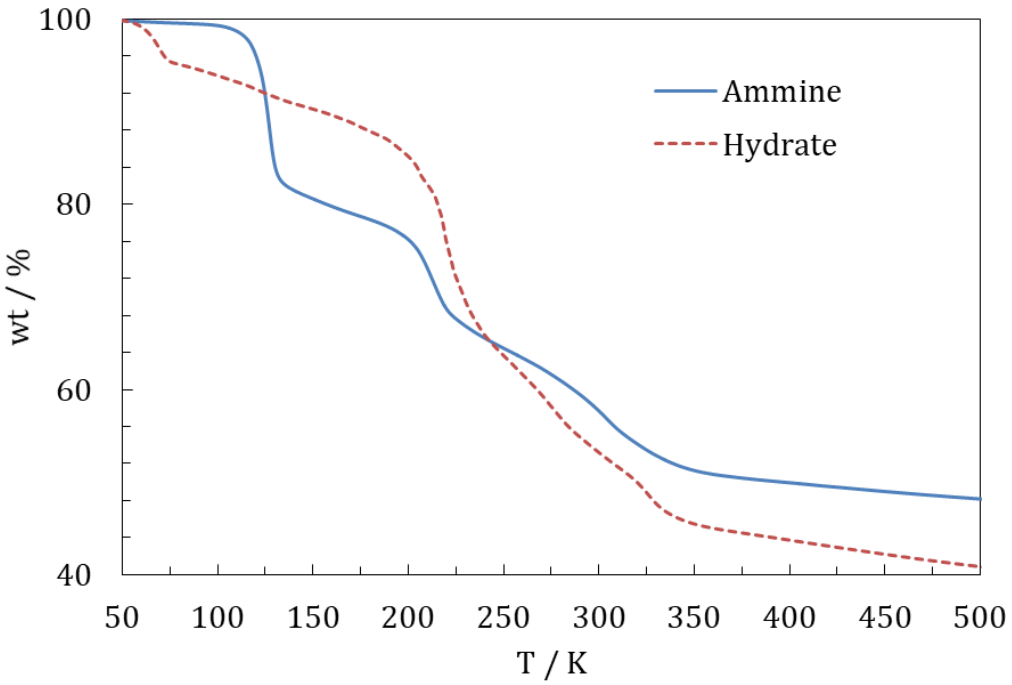

Figure 12: Comparison of TGA curves for the ammine and hydrate forms of Ce[tfac]$_3$.

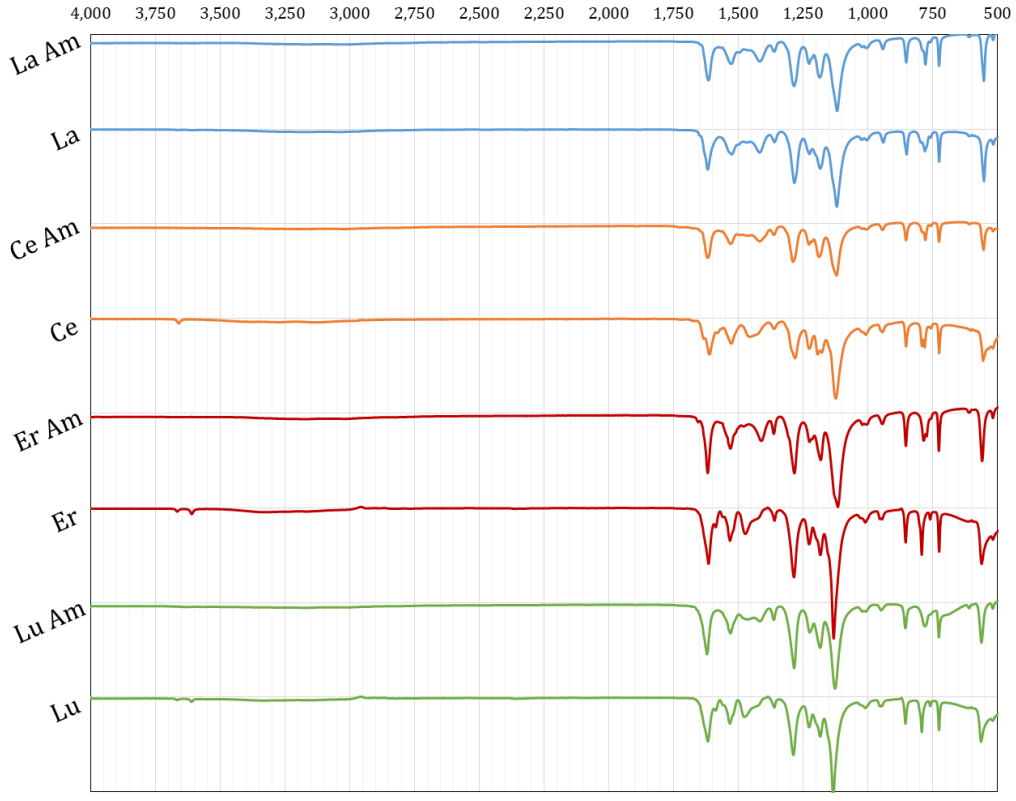

Figure 13: Comparison of FTIR curves for the ammines ("Ln Am") and hydrates ("Ln") of Ln[tfac]$_3$.

3.1.4 Lanthanide Heptafluorodimethyloctanedionates

6,6,7,7,8,8,8-heptafluoro-2,2-dimethyl-3,5-octanedione (fod), commonly forms a tris chelate with the lanthanides. The synthesis of 14 lanthanide heptafluorodimethyloctanedionates follows closely that according to Springer [6] and others [55,80], although some compounds were also made according to Johnson [81]. The β-diketonate complexes were produced at the Radiochemistry Center of Excellence within the Institute for Nuclear Security at the University of Tennessee (Knoxville, TN, USA). The complexes synthesized were $Ln[fod]_3$, where Ln is the following: La, Ce, Pr, Nd, Sm, Eu, Gd, Tb, Dy, Ho, Er, Tm, Yb or Lu. Pm was not available. All reagents and solvents were used from commercial sources and used without further purification.

The chelates of La, Ce, Pr, and Nd were made by the following method described by Johnson [81] due to difficulties in synthesizing the early lanthanides following Springer's synthesis route. The lanthanide chlorides (ACROS, 99.9%) were dissolved in 5 mL methanol (approximately 0.2 M). A 3:1 ratio of the ligand to the metal was added to a beaker to which 5 mL methanol was added. The metal solution was added slowly to the ligand solution and was allowed to mix for 10 min to fully incorporate. 6.25 M NaOH was added dropwise to the solution; precipitates were seen after each drop briefly before dissolving back into solution. The pH was monitored so not to exceed 8, and the solution was allowed to mix for up to 30 min. The chelate was extracted into hexanes and the solvent was boiled off, leaving an amorphous powder or a viscous oil. The product was dried in a desiccator with phosphorus pentoxide for a week. The chloride of La and Nd were anhydrous while the chloride of Ce (III) and Pr were the heptahydrate.

The chelates of Sm, Eu, Gd, Tb, Dy, Ho, Er, Tm, Yb and Lu were synthesized by the following method, which follows Springer. The lanthanide oxides (Sigma Aldrich, 99.99%) were combined with concentrated nitric acid (Fisher, ACS Reagent Grade) to yield the nitrate salt; the solution was heated to promote dissolution and boil off water, then allowed to cool, forming a sticky nitrate salt. The rare earth nitrates were dissolved in 10 mL methanol. A 3:3:1 ratio of ligand to base to metal was used; the ligand was added to 10 mL methanol in a separatory funnel, and the molar equivalent of 4.12 M NaOH was added to that. After mixing for 5 min, the metal solution was added and the funnel was shaken for 5 min. The solution

was added slowly over 15 min to 400 mL water stirring. The precipitate was suction filtered, dried on a watch glass in a desiccator for 48 hours with phosphorus pentoxide, and weighed. Yields range from 25% to 90%, but average approximately 70%.

Characterization Methods

The melting point of each of the fourteen samples is taken to verify the phase change. Two capillary tube samples of each compound were run simultaneously using a MP50 Melting Point System (Mettler Toledo, USA). The samples are run at 5 °C min^{-1} up to 300 °C and with video recording of the samples. Qualitative assessment of the melting point is completed with 0.5 °C margin of uncertainty at the temperature where each sample begins and completes melting. All fod chelates exhibit softening followed by melting in an often wide range.

Elemental analysis was performed by Atlantic Microlab in Norcross, GA. For these compounds, only weight percentages of C, H, N and F were analyzed by EA. The samples were run without being dried prior. Infrared spectra were recorded using a Thermo Scientific Nicolet iS10 FT-IR Spectrometer in the range from 4000-500 cm^{-1}. Results from elemental analysis and the tabulated FTIR data can be seen in Table 7 and Table 8, respectively. All infrared spectra can be seen in Figure 14. FTIR data shows a very close match in spectra, although some samples have certain peaks with lower or higher intensity than previously reported by Springer, also shifted in wavenumber. For example, two strong peaks were previously reported at 1500 cm^{-1} and 1480 cm^{-1}, yet in this study, one strong peak was found at 1510 cm^{-1} with a medium peak found at 1465 cm^{-1}. Among the early lanthanides, which are some of the samples synthesized by a different route, a medium shoulder peak can also be seen at 1480 cm^{-1}, indicating that this route may be better. This shoulder does not appear in the spectra of the later lanthanides.

All elemental analysis data appears very close to calculated based on the formula for tris fod monohydrate chelates. Comparing data for the first four lanthanides to that of the remaining lanthanides, there does not seem to be any large variation in elemental percentages, beyond the margin of error. Both synthesis routes seem to be acceptable.

Table 7. Results from melting point and elemental analyses for LnFod complexes

		mp/°C		Found			Calculated		
	Color	Found	Literature[a]	%C	%H	%F	%C	%H	%F
La[fod]$_3$-H_2O	yellowish white	95-105	215-230[b]	34.71	2.90	37.98	34.57	3.09	38.27
Ce[fod]$_3$-H_2O	reddish brown	88-94	149-150	34.40	2.97	37.93	34.53	3.09	38.23
Pr[fod]$_3$-H_2O	green	80-90	218-225[b]	34.55	2.89	37.94	34.50	3.09	38.20
Nd[fod]$_3$-H_2O	light purple	110-114	210-215[b]	34.59	3.09	38.22	34.39	3.08	38.08
Sm[fod]$_3$-H_2O	yellowish white	122-129	63-67	34.98	2.93	37.70	34.19	3.06	37.86
Eu[fod]$_3$-H_2O	yellowish white	82-98	59-67	34.41	2.95	37.59	34.14	3.06	37.80
Gd[fod]$_3$-H_2O	white	85-103	60-65	34.04	3.17	37.47	33.97	3.04	37.61
Tb[fod]$_3$-H_2O	white	80-103	92-97	33.81	3.09	37.28	33.91	3.04	37.55
Dy[fod]$_3$-H_2O	yellowish white	112-120	103-107	34.10	3.01	37.14	33.80	3.03	37.42
Ho[fod]$_3$-H_2O	yellow	98-128	103-111	33.63	3.04	37.47	33.72	3.02	37.34
Er[fod]$_3$-H_2O	pink	57-62	104-112	34.81	2.97	38.07	33.65	3.01	37.26
Tm[fod]$_3$-H_2O	white	107-112	110-115	33.26	2.82	37.22	33.60	3.01	37.20
Yb[fod]$_3$-H_2O	yellowish white	85-108	112-115	33.42	2.92	37.33	33.47	3.00	37.06
Lu[fod]$_3$-H_2O	white	54-72	111-115	34.09	2.93	37.07	33.41	2.99	36.99

[a]Melting point data from Springer 1967, except for Ce[fod]$_3$ from McAleese 1996

[b]Springer reports that the sample melted with decomposition

Table 8. Infrared spectral results for LnFod complexes[a]

cm-1	peak	cm-1	peak	cm-1	peak
3600	w, b	1225	s, b	835	m
2950	w	1195	s, sh	795	m
1620	s	1180	s	755	m, sh
1595	m, sh	1150	s, sh	740	m
1530	m, sh	1115	s	695	m, sh
1510	s	1105	s, sh	690	m
1465	m	1070	m	625	w
1395	m	1020	w	590	w
1370	m, sh	965	m	575	w
1345	s	940	w	540	w
1275	m	910	m	525	w

[a]Spectral notations: s, strong intensity; m, medium intensity; w, weak intensity; b, broad; sh, shoulder

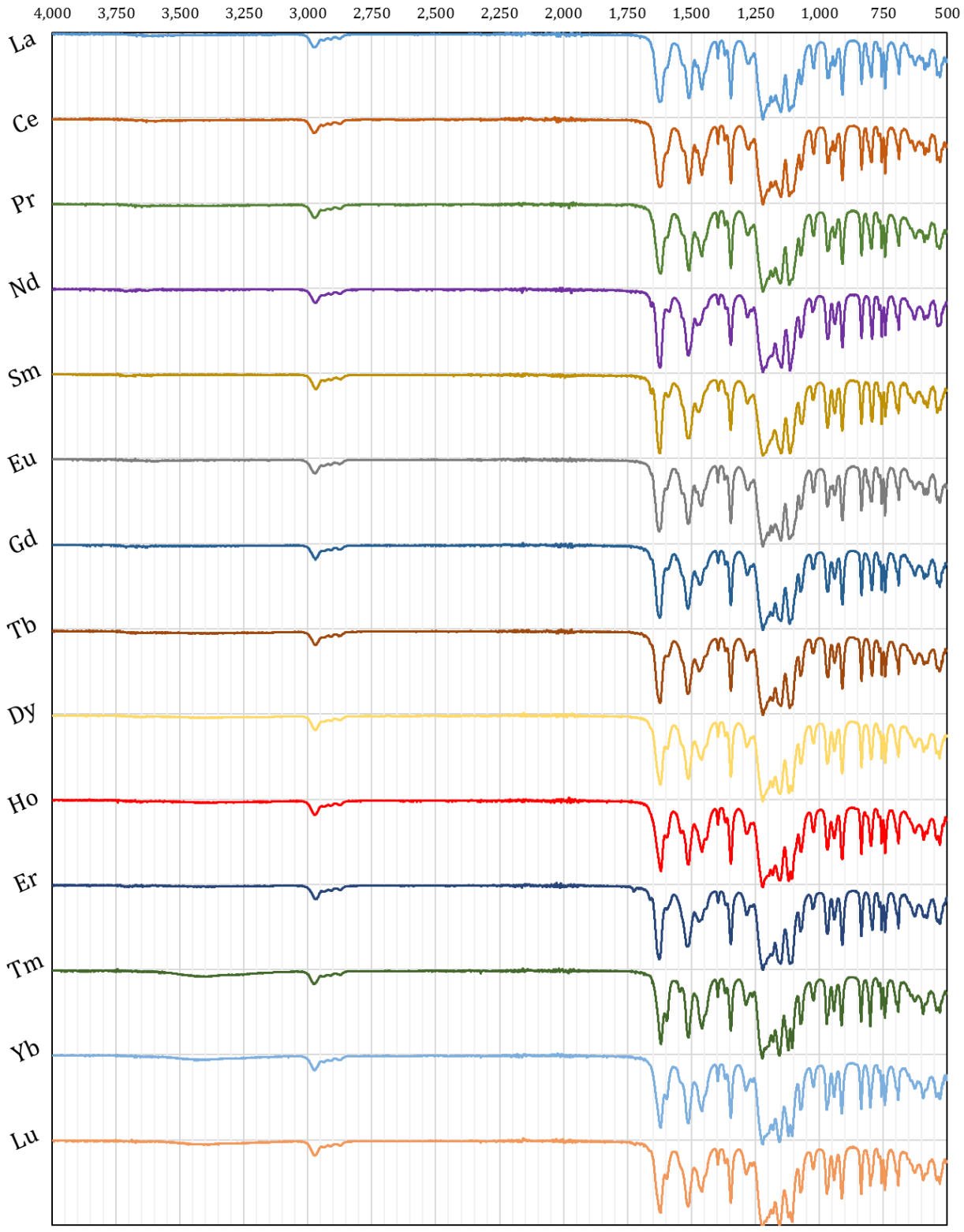

Figure 14: FT-IR spectra for the lanthanide heptafluorodimethyloctanedionates

3.2 Experimental Methods of Thermal Analysis

3.2.1 TGA-MS

For all TGA-MS spectra, the samples were analyzed using a Discovery TGA-MS (TA Instruments, USA) and open faced High Temperature Platinum (HT Pt) pans. A balance purge rate of 10 mL min^{-1} and sample purge rate of 25 mL min^{-1} were used for all samples in a non-pressurized furnace under nitrogen gas. The TGA pans were loaded with an arbitrary amount of compound between 1-4 mg. The instrument requires small sample sizes due to the sensitive thermal ionization filament. Because of the small amounts used and the varying crystal sizes, the samples did not always maintain consistent geometries, although many runs have indicated a very good level of precision with nanogram-level uncertainty. Pans were reused after each sample by washing with mild HCl solution and torching in an open flame, and tared before sample addition.

The TRIOS software was used to analyze differential TGA curves. The sample was heated at 20°C min^{-1} up to 600°C in the proprietary Hi-Res™ TGA programming. The program heats at a constant rate until a weight loss event greater than the desired sensitivity begins. The "Hi Resolution Sensitivity" parameter was set to 1.00 and the "Res" parameter was set to 4. With these very sensitive parameters, the curves appear almost isothermal at the major weight loss events. The differential TG curve is taken with respect to temperature due to the varying heating rates of the program. The peak height temperature of the DTG curve was found, as well as the onset and end set temperatures, by using the respective TRIOS software analysis functions.

The Discovery TGA-MS is coupled to a thermal ionization filament with mass spectrometry capabilities up to 300 amu. Mass spectrometry data is provided for each mass up to 300 amu for the hfac compounds, and up to 50 amu for all others. Masses of 18, 32 and 44 are especially important, corresponding to water, oxygen and carbon dioxide, respectively.

A major result of the project is the calculation of the sublimation enthalpy of the lanthanide compounds previously described. As mentioned, methods employed by Ashcroft, based on Langmuir's work on vapor pressure determination, were used to solve for sublimation enthalpy.

3.2.2 Langmuir Method

The experimental data collected consisted of running isothermal TGA for 5 min per isotherm, typically for 7 different temperatures in a range 30 °C wide, although the range width depends on the width of the weight loss event for the compound. For example, the dpm complexes were run over a 24 °C range, with isotherms every 4 °C. This gives 7 different mass loss rates for 7 different temperatures. Figure 15 shows an example of the 7 isotherms along with the corresponding differential TGA curve with respect to time. By plotting equation 13 with these mass loss rates and corresponding temperatures, the 7 data points would ideally form a linear trend. The slope and y-intercept of the trendline are used to solve for desired variables such as sublimation enthalpy. Figure 16 shows an example of plotting the left hand side of equation 13 vs inverse temperature.

The hfac and fod samples were run on TA Instruments (USA) TGA Q50 with nitrogen gas (balance purge 40 mL/min, sample purge 60 mL/min) and the dpm samples were run on TA Instruments (USA) TGA Q500 with nitrogen gas (balance purge 40 mL/min, sample purge 60 mL/min). The data from each TGA instrument is calibrated by running the Langmuir method on industrial standards of transition metal β-diketonates which have vapor pressure values reported in literature. It is worth repeating that the enthalpy value calculated is not dependent on the different furnace atmospheres. It is only dependent on the mass loss rates and corresponding temperatures, and the different instruments produced data for the same compound that confirmed this.

For most of the hfac complexes and all of the dpm complexes, sublimation is confirmed by the melting point which is much higher than the weight loss range seen in the TGA data. For the fod complexes, melting point ranges that are much lower than the major weight loss events found via TGA confirm that the compound is not subliming, but rather melting as it heats, and vaporizing in the respective temperature ranges. Although the Langmuir method was first used to represent the thermodynamics of sublimation, the enthalpy value found can also represent the vaporization enthalpy and any decomposition of the compound that occurs with it. For all fod samples, decomposition is found to occur at temperatures higher than the range of vaporization. Therefore, it is fair to assume the enthalpy value calculated is the vaporization enthalpy of the complex.

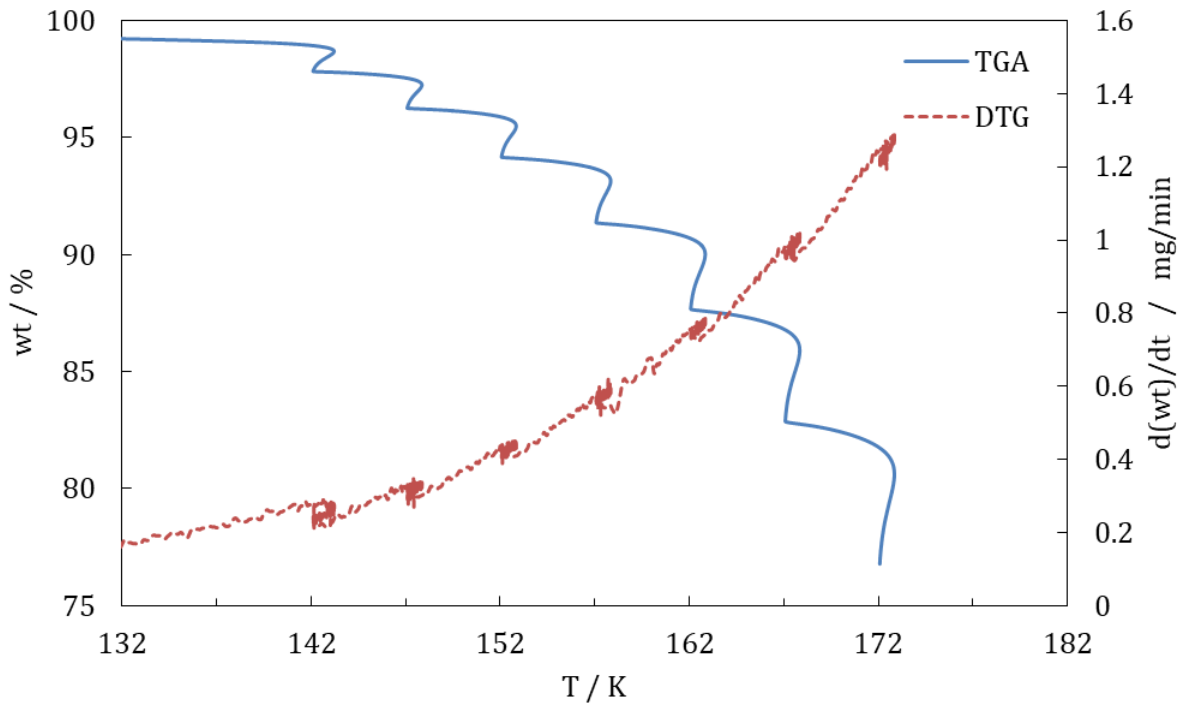

Figure 15: Isotherms of the Langmuir method and corresponding mass loss rates for Tb[fod]$_3$.

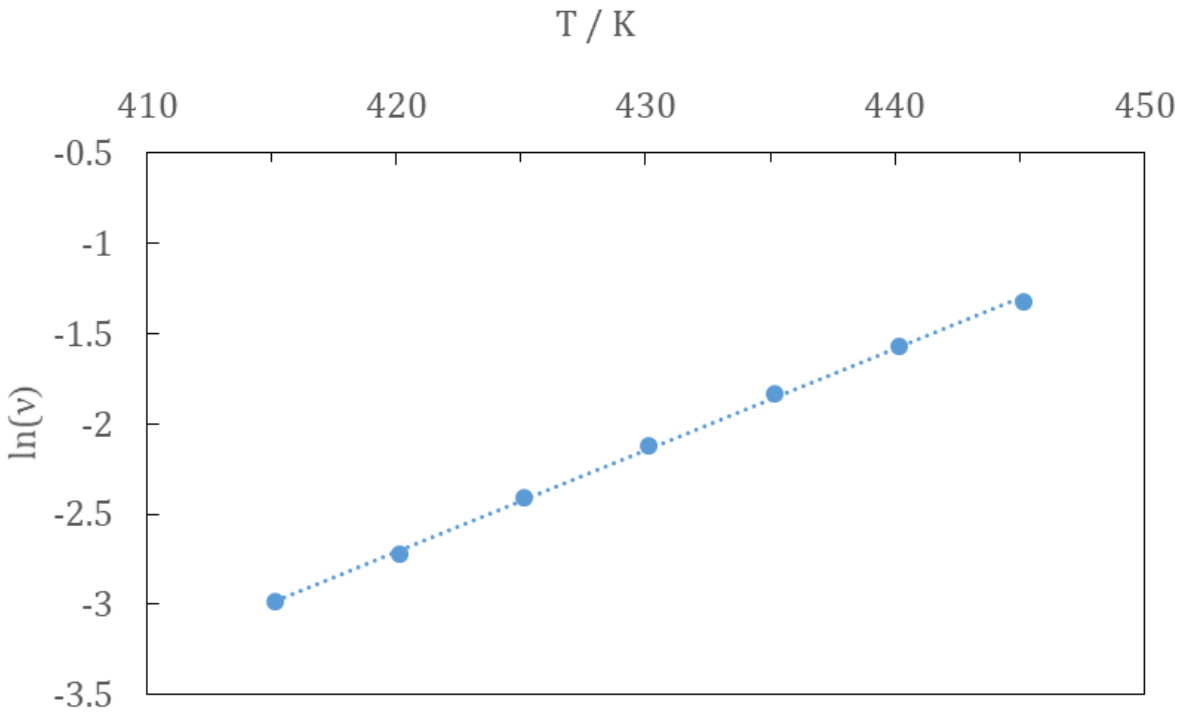

Figure 16: Plotting the left hand side of equation 13 vs 1/T for the Langmuir method for Tb[fod]$_3$.

Chapter 4: Results and Discussion of Thermal Analysis

4.1 TGA-MS

The TGA and DTG spectra for each of the chelates are shown in this section. Each spectrum is analyzed for weight loss events which are characterized by percent weight lost during the event, as well as the onset and end set temperature of the event. Most compounds exhibited one major event, and typically accompanied by smaller peaks before and after, typically corresponding to loss of coordinated water molecules and decomposition, respectively. Sublimation is confirmed (as opposed to melting and subsequent evaporation) by comparing melting point analysis to TGA-MS curves. In some cases, stepwise sublimation occurs, where a compound will sublime in multiple large steps at different temperatures.

It is especially important to note that no significant mass peaks are detected during the major weight loss event in any of the spectra for the hfac compounds. This is noteworthy because it indicates that no mass below 300 amu is detected, and because some compound must clearly be vaporizing in the furnace during this event, it can be concluded that the mass of the compound vaporizing is most likely above the mass 300 amu. This would support the understanding that the compound is vaporizing as an intact chelate, and not as individual components, which is very crucial to the chromatographic separation of the compounds.

Confirming sublimation of the chelate within these various ranges of temperatures and confirming that the compound is maintain its chelating bond during sublimation are two important conclusions. Special cases exist for some of the chelates and all the characteristics are noted below. One result of importance is the low melting point of lanthanum hfac, which indicates that sublimation is not occurring during the heating range. This is the only hfac compound that does not sublime, and therefore the enthalpy calculated corresponds to the enthalpy of vaporization, and not the enthalpy of sublimation. This should not be compared to the other results of the series, as the enthalpy of vaporization can represent different thermodynamics. Additionally, some chelates degrade as they melt, and therefore the enthalpy of vaporization may not be representative of the energy required for a vapor phase

change. Similarly, all of the lanthanide fod chelates synthesized here have melting points well below their major weight loss events, indicating these do not sublime either.

Analysis via TGA-MS was carried out under nitrogen gas, although in the future it may be recommended to complete under different inert gas flows. For example, running under argon allows for the detection of mass 28 via MS, whereas running under nitrogen does not. Moreover, a purge of the furnace can be accomplished by allowing at least 10 minutes to pass before data collection. This will reduce the atmosphere contributed impurities in the furnace. For these runs, the furnace was purged for at least 5 minutes. Additionally, improvements to this system include allowing the mass spectrometer to detect fewer mass numbers per run, which will improve the resolution of the MS data.

4.1.1 Lanthanide Hexafluoroacetylacetonates

The TGA-MS curves for the lanthanide hexafluoroacetylacetonates can be seen in the Appendix.

Lanthanum

The TGA-DTG-MS spectra indicate a major weight loss event starting at 153 °C with over 60% weight lost over a 10 °C range. The melting point range was found to be below this, and the compound maintained a liquid phase up to this point, therefore this event is attributed to vaporization, and not sublimation. This is followed by a loss of 10.2% between 194-204 °C and because no significant mass peaks are found here, this is potentially a continuation of the stepwise vaporization. The second largest weight loss event occurs from 67-82 °C with 13.6% lost, and because this is below the onset of melting, this could be attributed to sublimation, but because this coincides with a strong peak of mass 18, it is likely either dehydration or loss of coordinated water molecules. A weight loss of 7.8% occurs between 237-317°C. This range of two peaks also coincides with an increase of masses 18 and 44, indicating possible oxidation of the organic ligands, also in two steps. Weight loss levels off by 350 °C and remains around 4.7 wt% up to 600 °C, indicating possible oxidation.

Praseodymium

The spectrum shows major weight loss between 146-153 °C, with about 91% lost. No significant mass peaks are detected up to 300 amu during this event, indicating the compound vaporized is above this mass limit. Because of the melting range between 172-180 °C, this major event is believed to be sublimation of the amorphous solid to the gas phase. A small event of 1.7% weight lost occurs between 61-83 °C and coincides with an increase in mass 18, indicating dehydration. Weight loss of 4.3% occurs from 220-280 °C, and coincides with peak increases in mass 18 and 44, indicating a chemical reaction such as oxidation. About 3% weight remains after 330 °C up to the final temperature of 600 °C. Increases in mass 44 indicate more oxidation, although increases in mass 32 until completion indicate some chemical reaction releasing oxygen.

Neodymium

A major weight loss event occurs at 148-160 °C with over 90% weight lost. The melting range of 188-197 °C indicates this major event to be sublimation. Two smaller peaks occurring at 76-90 °C and 105-120 °C correspond to weight loss events of each about 2%. The first peak coincides with an increase in mass 18 and the second peak coincides with a slight increase in mass 44, indicating possible removal of coordinated water and carbon dioxide, respectively. A weight loss event of about 3% weight lost between 224-273 °C consists of two small peaks. This event coincides with strong increases in mass 18, 32 and 44. The same mass peaks are seen again after weight loss discontinues around 360 °C.

Samarium

Similar to $Pr[hfac]_4$, the TGA spectrum shows major weight loss of 92% between 142-162 °C. The melting point analysis resulted in a melting range of 180-193 °C, indicating sublimation of the majority of the compound prior to melting. A small peak between 67-84 °C corresponds to a weight loss of 1.5%, and coincides with a peak in mass 18. A final weight loss event of 4.1% occurs between 171-187 °C and does not correspond to any significant mass peaks, leading to the conclusion of post-sublimation melting and eventual evaporation

of the liquid. Peaks of mass 18, 32 and 44 are all seen above 200 °C, with no weight loss events, indicating one or more chemical reactions.

Europium

A major loss event of about 94% is seen from 143-163 °C. The melting point range of 200-208 confirms this event is most likely sublimation. A small peak of 1% weight lost occurs between 71-89 °C and corresponds to a peak of mass 18, similar to the spectra of other compounds. Similarly, peaks of mass 18 and 44 occur above 220 °C, where there is no further weight lost, and staying constant at 3.5% weight remaining. This is accompanied by a loss in mass 32, although mass 32 eventually increases until completion.

Gadolinium

Similar to other compounds, a major weight loss event of 95% is seen with an onset of 150 °C and ending around 175 °C. This is well below the melting range of 217-220 °C, confirming the occurrence of sublimation. A small peak of less than 0.5% weight lost coincides with a peak of mass 18 around 79-99 °C, indicating possible dehydration or de-coordination of water molecules. Only 0.3% weight remains after the final weight loss event around 210 °C and is followed by a strong decrease in mass 32 and increases in masses 18 and 44, indicating oxidation of any remaining ligand.

Terbium

A major weight loss event is seen between 145-170 °C and corresponds to 94.5%, which is believed to be sublimation because it well below the melting range of 214-218 °C. A small loss of 0.5% occurs between 94-124 °C, and is accompanied by an increase in mass 18. Above 205 °C, the weight remains constant at 1% remaining, although peaks of mass 18, 32 and 44 are all detected between 200-600 °C.

Dysprosium

The TGA spectra indicates a unique stepwise sublimation process, which occurs first between 127-136 °C with a loss of about 21% and then a second weight loss event occurs

with an onset at 150 °C and concludes by 166 °C after about 74% of weight is lost. The melting range of 196-205 °C indicates these are both sublimation events. Occurring consecutively, the two peaks are probably due to a complex formation of two different dysprosium chelates. Each chelate could consist of a unique coordination of hfac, and possibly with other molecules introduced in synthesis. Dysprosium appears to uniquely form two chelate formations, each in considerable concentration. Additionally, a small peak of 1.5% weight loss occurs between 67-86 °C. A weight loss event of 2.7% between 180-186 °C is also seen after sublimation, potentially corresponding to melting and evaporation. Above 200 °C, the remaining weight of 0.75% is probably an oxide residue formed due to decomposition.

Holmium

Similar to the dysprosium analog, the holmium hfac chelate appears to sublime in two steps, indicating two formations of the complex. The first event occurs at 132-142 °C and corresponds to about 47% of the initial weight. The second occurs at 158-169 °C and corresponds to about 42%. Both of these are below the melting range of 170-180 °C, and sublimation is assumed for each event. A weight loss event of about 9% occurs between 66-81 °C and coincides with a peak of mass 18, indicating a loss of water. The final weight loss event concludes by 210 °C and about 1.5% weight remains as residue. Above this temperature, a strong peak of mass 32 is seen, coinciding with peaks of mass 18 and 44. Similar to the other compounds, all three of these masses also increase again above 400 °C until completion.

Erbium

The spectra shows similar characteristics as the others, with a major weight loss event between 145-162 °C, corresponding to 92% lost. This is well below the melting range of 218-226 °C, therefore sublimation of the sample is assumed. A peak of 1.5% weight lost is seen between 83-100 °C and coincides with a peak of mass 18. Between 174-185 °C, a peak corresponding to 5% weight loss occurs, and is potentially additional sublimation of the compound. At temperatures above 205 °C, weight loss subsides and the residue of 0.5% maintains a constant value. An increase in all masses 18, 32 and 44 are seen.

Thulium

Unlike most of the compounds, the thulium chelate does not have a small peak prior to sublimation. Between 145-165 °C, over 95% of the sample's weight is lost. Well below the melting range of 214-217 °C, this is due to sublimation. A small weight loss event of 3.5% occurs between 180-187 °C and is probably a second step of sublimation. An increase in masses of 18, 32 and 44 are seen after the final event above 200 °C, and is indicative of a chemical reaction such as oxidation.

Ytterbium

The spectra of the ytterbium chelate is similar to that of thulium except a peak corresponding to loss of water is seen at 61-71 °C with a loss of about 5%. The onset of the major event is at 141 °C and concludes by 161 °C with an overall loss of about 90% weight. A small peak is seen at 180-185 °C and corresponds to a small loss of 3.3%. Above 200 °C, no weight loss is observed until completion at 600 °C. Additionally, an increase in masses 18, 32 and 44 are all observed.

Lutetium

Very similar to the previous compound, the major event occurs at 135-155 °C and corresponds to a loss of 91.6% weight, which is below the melting range of 194-198 °C. The small peak at the low temperature range of 84-101 °C is observed with a loss of 2.1% and coincides with a peak of mass 18. A final third peak is observed between 170-179 °C and corresponds to a 4.7% weight loss. Above 195 °C, the sample does not experience weight loss and an increase in masses 18, 32 and 44 are all observed up to completion at 600 °C.

4.1.2 Lanthanide Dipivaloylmethanates

The TGA-MS curves for the lanthanide dipivaloylmethanates can be seen in the Appendix.

Lanthanum

The major weight loss event occurs at 217-239 °C with about 93.6% sample lost. With a melting point range of 224-230 °C, most sample lost is believed to be due to sublimation, not boiling following melting. A second event after this occurring up until the final temperature of 600 °C results in a total loss of 4 wt%, which coincides with an increase in masses 18 and 44 detected starting around 300 °C. This could be potential oxidation or degradation of the compound. There is around 1 wt% lost around 100 °C, although MS data is inconclusive.

Cerium

The major weight loss event occurs at 199-229 °C with about 89.7% sample lost. With a melting point range of 275-283 °C, most sample lost is believed to be due to sublimation, not boiling following melting. A second event after this occurring up until the final temperature of 600 °C results in a total loss of 5 wt%, which coincides with an increase in masses 18 and 44 detected starting around 300 °C. This could be potential oxidation or degradation of the compound. There is around 1 wt% lost between 100-160 °C, although MS data is inconclusive.

Praseodymium

The major weight loss event occurs at 203-221 °C with about 83.7% sample lost. With a melting point range of 214-220 °C, most sample lost is believed to be due to sublimation, not boiling following melting. A second event after this occurring up until the final temperature of 600 °C results in a total loss of 5.4 wt%, which coincides with an increase in masses 18 and 44 detected starting around 300 °C. This could be potential oxidation or degradation of the compound. There is around 1 wt% lost between 100-150 °C, although MS data is inconclusive.

Neodymium

The major weight loss event occurs at 191-208 °C with about 81.6% sample lost. With a melting point range of 205-209 °C, most sample lost is believed to be due to sublimation,

not boiling following melting. A second event after this occurring up until the final temperature of 600 °C results in a total loss of 8.1 wt%, which coincides with an increase in masses 18 and 44 detected starting around 300 °C. This could be potential oxidation or degradation of the compound. There is around 1 wt% lost between 100-150 °C, although MS data is inconclusive.

Samarium

The major weight loss event occurs at 182-198 °C with about 89% sample lost. With a melting point range of 197-202 °C, most sample lost is believed to be due to sublimation, not boiling following melting. A second event after this occurring up until the final temperature of 600 °C results in a total loss of 8.9 wt%, which coincides with an increase in masses 18 and 44 detected starting around 300 °C. This could be potential oxidation or degradation of the compound. There is around 0.5 wt% lost between 100-150 °C, although MS data is inconclusive.

Europium

The major weight loss event occurs at 186-191 °C with about 80.8% sample lost. With a melting point range of 180-196 °C, most sample lost is believed to be due to sublimation, not boiling following melting. A second event after this occurring up until the final temperature of 600 °C results in a total loss of 6.2 wt%, which coincides with an increase in masses 18 and 44 detected starting around 300 °C. This could be potential oxidation or degradation of the compound. There is around 1.5 wt% lost between 100-150 °C, although MS data is inconclusive.

Gadolinium

The major weight loss event occurs at 181-183 °C with about 90.7% sample lost. With a melting point range of 178-188 °C, most sample lost is believed to be due to sublimation, not boiling following melting. A second event after this occurring up until the final temperature of 600 °C results in a total loss of 3.4 wt%, which coincides with an increase in masses 18 and 44 detected starting around 300 °C. This could be potential oxidation or

degradation of the compound. There is around 0.5 wt% lost between 100-150 °C, although MS data is inconclusive.

Terbium

The major weight loss event occurs at 168-186 °C with about 82.7% sample lost. With a melting point range of 177-179 °C, most sample lost is believed to be due to sublimation, not boiling following melting. A second event after this occurring up until the final temperature of 600 °C results in a total loss of 7.5 wt%, which coincides with an increase in masses 18 and 44 detected starting around 300 °C. This could be potential oxidation or degradation of the compound. There is around 3 wt% lost between 100-150 °C, although MS data is inconclusive.

Dysprosium

The major weight loss event occurs at 178-188 °C with about 86.3% sample lost. With a melting point range of 177-182 °C, most sample lost is believed to be due to sublimation, not boiling following melting. A second event after this occurring up until the final temperature of 600 °C results in a total loss of 9.1 wt%, which coincides with an increase in masses 18 and 44 detected starting around 300 °C. This could be potential oxidation or degradation of the compound. There is around 0.5 wt% lost between 100-150 °C, although MS data is inconclusive.

Holmium

The major weight loss event occurs at 172-187 °C with about 92.7% sample lost. With a melting point range of 181-185 °C, most sample lost is believed to be due to sublimation, not boiling following melting. A second event after this occurring up until the final temperature of 600 °C results in a total loss of 5.1 wt%, which coincides with an increase in masses 18 and 44 detected starting around 300 °C. This could be potential oxidation or degradation of the compound. There is around 2 wt% lost between 50-80 °C, although MS data is inconclusive.

Erbium

The major weight loss event occurs at 170-185 °C with about 83.3% sample lost. With a melting point range of 168-176 °C, most sample lost is believed to be due to sublimation, not boiling following melting. A second event after this occurring up until the final temperature of 600 °C results in a total loss of 11 wt%, which coincides with an increase in masses 18 and 44 detected starting around 300 °C. This could be potential oxidation or degradation of the compound. There is around 3 wt% lost between 50-80 °C, although MS data is inconclusive.

Thulium

The major weight loss event occurs at 168-178 °C with about 91.3% sample lost. With a melting point range of 169-172 °C, most sample lost is believed to be due to sublimation, not boiling following melting. A second event after this occurring up until the final temperature of 600 °C results in a total loss of 3.9 wt%, which coincides with an increase in masses 18 and 44 detected starting around 300 °C. This could be potential oxidation or degradation of the compound. There is around 1.5 wt% lost between 50-80 °C, although MS data is inconclusive.

Ytterbium

The major weight loss event occurs at 164-173 °C with about 93.2% sample lost. With a melting point range of 166-170 °C, most sample lost is believed to be due to sublimation, not boiling following melting. A second event after this occurring up until the final temperature of 600 °C results in a total loss of 4.1 wt%, which coincides with an increase in masses 18 and 44 detected starting around 300 °C. This could be potential oxidation or degradation of the compound. There is around 2 wt% lost between 60-120 °C, although MS data is inconclusive.

Lutetium

The major weight loss event occurs at 169-179 °C with about 93.7% sample lost. With a melting point range of 174-178 °C, most sample lost is believed to be due to sublimation,

not boiling following melting. A second event after this occurring up until the final temperature of 600 °C results in a total loss of 4.2 wt%, which coincides with an increase in masses 18 and 44 detected starting around 300 °C. This could be potential oxidation or degradation of the compound. There is around 0.5 wt% lost between 100-150 °C, although MS data is inconclusive.

4.1.3 Lanthanide Trifluoroacetylacetonates

The lanthanide tfac chelates, as noted earlier, are not ideal for the Langmuir method for sublimation enthalpy determination, and more importantly not ideal for gas phase separations explained in this work. The tfac chelates do not sublime appreciably, and the ammine tfac chelates introduced earlier do not sublime in amounts larger than 30 wt%. Total sublimation of the compound is ideal for the Langmuir method. Additionally, each lanthanide ammine chelate experiences a sublimation event different in weight to the others, so there is no quantitative method in correlating the weight lost to the elemental composition. The TGA-MS curves of the ammine forms of the chelate are discussed in more detail below, while the tfac chelates are omitted due to the lack of utility in this study. Langmuir method is not done on any of the lanthanide tfac compounds. The TGA-MS curves for the lanthanide trifluoroacetylacetonate ammines can be seen in the Appendix.

Lanthanum

The ammine chelate experiences a sublimation event of 20 wt% in the range 100-125 °C. Vaporization occurs for 21 wt% between 200-225 °C, and decomposition of 16 wt% occurs between 230-340 °C. Less than 1 wt% water is lost below 50 °C.

Cerium

The ammine chelate experiences a sublimation event of 21 wt% in the range 100-135 °C. Vaporization for the melted compound occurs for 15 wt% between 200-220 °C, and decomposition of 16 wt% occurs between 225-350 °C. Less than 1 wt% water is lost below 70 °C.

Praseodymium

The ammine chelate experiences a sublimation event of 15 wt% in the range 125-135 °C. Vaporization for the melted compound occurs for 24 wt% between 212-226 °C, and decomposition of 7 wt% occurs between 300-350 °C. Less than 6 wt% water is lost below 75 °C.

Europium

The ammine chelate experiences a sublimation event of 22 wt% in the range 125-145 °C. Vaporization for the melted compound occurs for 25 wt% between 200-240 °C, and decomposition of 9 wt% occurs between 275-325 °C. Less than 1 wt% water is lost below 85 °C.

Erbium

The ammine chelate experiences a sublimation event of 30 wt% in the range 110-160 °C. Vaporization for the melted compound occurs for 13 wt% between 190-200 °C, and decomposition of 24 wt% occurs between 200-370 °C. Less than 1 wt% water is lost below 95 °C.

Lutetium

The ammine chelate experiences a sublimation event of 10 wt% in the range 100-160 °C. Vaporization for the melted compound occurs for 16 wt% between 180-210 °C, and decomposition of 22 wt% occurs between 240-360 °C. Less than 1 wt% water is lost below 70 °C.

4.1.4 Lanthanide Heptafluorodimethyloctanedionates

The TGA-MS curves for the lanthanide heptafluorodimethyloctanedionates can be seen in the Appendix.

Lanthanum

The tris fod complex of lanthanum (III) experiences a major weight loss event of 93 wt% starting at 185 °C, with peak mass loss at 212 °C. This is believed to be vaporization of the melted compound due to a much lower melting point. Around 1 wt% or less of water is lost in the range of 70-95 °C. Decomposition of the compound starts to occur at 235 °C and is mostly completed by 350 °C but will continue as the temperature rises, evidenced by an increase in mass number 44 of the evolved gas, assumed to be carbon dioxide. Similarly, an increase in mass number 18 is seen which is believed to be mostly water.

Cerium

The tris fod complex of cerium (III) experiences a major weight loss event of 84 wt% starting at 144 °C, with peak mass loss at 164 °C. This is believed to be vaporization of the melted compound due to a much lower melting point. Around 1 wt% or less of water is lost in the range of 110-126 °C. Decomposition of the compound starts to occur at 260 °C and is mostly completed by 350 °C but will continue as the temperature rises, evidenced by an increase in mass number 44 of the evolved gas, assumed to be carbon dioxide. Similarly, an increase in mass number 18 is seen which is believed to be mostly water.

Praseodymium

The tris fod complex of praseodymium (III) experiences a major weight loss event of 90 wt% starting at 170 °C, with peak mass loss at 191 °C. This is believed to be vaporization of the melted compound due to a much lower melting point. Around 1 wt% or less of water is lost in the range of 90-130 °C. Decomposition of the compound starts to occur at 220 °C and is mostly completed by 350 °C but will continue as the temperature rises, evidenced by an increase in mass number 44 of the evolved gas, assumed to be carbon dioxide. Similarly, an increase in mass number 18 is seen which is believed to be mostly water.

Neodymium

The tris fod complex of neodymium (III) experiences a major weight loss event of 94 wt% starting at 140 °C, with peak mass loss at 155 °C. This is believed to be vaporization of the melted compound due to a much lower melting point. Around 1 wt% or less of water is lost in the range of 117-125 °C. Decomposition of the compound starts to occur at 285 °C and

is mostly completed by 350 °C but will continue as the temperature rises, evidenced by an increase in mass number 44 of the evolved gas, assumed to be carbon dioxide. Similarly, an increase in mass number 18 is seen which is believed to be mostly water.

Samarium

The tris fod complex of samarium (III) experiences a major weight loss event of 94 wt% starting at 142 °C, with peak mass loss at 160 °C. This is believed to be vaporization of the melted compound due to a much lower melting point. Around 1 wt% or less of water is lost in the range of 108-124 °C. Decomposition of the compound starts to occur at 188 °C and is mostly completed by 192 °C but will continue as the temperature rises, evidenced by an increase in mass number 44 of the evolved gas, assumed to be carbon dioxide. Similarly, an increase in mass number 18 is seen which is believed to be mostly water.

Europium

The tris fod complex of europium (III) experiences a major weight loss event of 93 wt% starting at 158 °C, with peak mass loss at 182 °C. This is believed to be vaporization of the melted compound due to a much lower melting point. Around 1 wt% or less of water is lost in the range of 65-75 °C. Decomposition of the compound starts to occur at 250 °C and is mostly completed by 400 °C but will continue as the temperature rises, evidenced by an increase in mass number 44 of the evolved gas, assumed to be carbon dioxide. Similarly, an increase in mass number 18 is seen which is believed to be mostly water.

Gadolinium

The tris fod complex of gadolinium (III) experiences a major weight loss event of 95 wt% starting at 150 °C, with peak mass loss at 168 °C. This is believed to be vaporization of the melted compound due to a much lower melting point. Around 1 wt% or less of water is lost in the range of 95-118 °C. Decomposition of the compound starts to occur at 220 °C and is mostly completed by 380 °C but will continue as the temperature rises, evidenced by an increase in mass number 44 of the evolved gas, assumed to be carbon dioxide. Similarly, an increase in mass number 18 is seen which is believed to be mostly water.

Terbium

The tris fod complex of gadolinium (III) experiences a major weight loss event of 91 wt% starting at 144 °C, with peak mass loss at 172 °C. This is believed to be vaporization of the melted compound due to a much lower melting point. Around 1 wt% or less of water is lost in the range of 94-115 °C. Decomposition of the compound starts to occur at 200 °C and is mostly completed by 350 °C but will continue as the temperature rises, evidenced by an increase in mass number 44 of the evolved gas, assumed to be carbon dioxide. Similarly, an increase in mass number 18 is seen which is believed to be mostly water.

Dysprosium

The tris fod complex of dysprosium (III) experiences a major weight loss event of 94 wt% starting at 148 °C, with peak mass loss at 163 °C. This is believed to be vaporization of the melted compound due to a much lower melting point. Around 1 wt% or less of water is lost in the range of 78-120 °C. Decomposition of the compound starts to occur at 190 °C and is mostly completed by 200 °C but will continue as the temperature rises, evidenced by an increase in mass number 44 of the evolved gas, assumed to be carbon dioxide. Similarly, an increase in mass number 18 is seen which is believed to be mostly water.

Holmium

The tris fod complex of holmium (III) experiences a major weight loss event of 91 wt% starting at 140 °C, with peak mass loss at 157 °C. This is believed to be vaporization of the melted compound due to a much lower melting point. Around 1 wt% or less of water is lost in the range of 85-118 °C. Decomposition of the compound starts to occur at 225 °C and is mostly completed by 235 °C but will continue as the temperature rises, evidenced by an increase in mass number 44 of the evolved gas, assumed to be carbon dioxide. Similarly, an increase in mass number 18 is seen which is believed to be mostly water.

Erbium

The tris fod complex of erbium (III) experiences a major weight loss event of 95 wt% starting at 138 °C, with peak mass loss at 163 °C. This is believed to be vaporization of the

melted compound due to a much lower melting point. Around 1 wt% or less of water is lost in the range of 83-109 °C. Decomposition of the compound starts to occur at 190 °C and is mostly completed by 200 °C but will continue as the temperature rises, evidenced by an increase in mass number 44 of the evolved gas, assumed to be carbon dioxide. Similarly, an increase in mass number 18 is seen which is believed to be mostly water.

Thulium

The tris fod complex of thulium (III) experiences a major weight loss event of 93 wt% starting at 133 °C, with peak mass loss at 143 °C. This is believed to be vaporization of the melted compound due to a much lower melting point. Around 1 wt% or less of water is lost in the range of 60-75 °C. Decomposition of the compound starts to occur at 175 °C and is mostly completed by 275 °C but will continue as the temperature rises, evidenced by an increase in mass number 44 of the evolved gas, assumed to be carbon dioxide. Similarly, an increase in mass number 18 is seen which is believed to be mostly water.

Ytterbium

The tris fod complex of ytterbium (III) experiences a major weight loss event of 93 wt% starting at 130 °C, with peak mass loss at 146 °C. This is believed to be vaporization of the melted compound due to a much lower melting point. Around 1 wt% or less of water is lost in the range of 82-102 °C. Decomposition of the compound starts to occur at 200 °C and is mostly completed by 350 °C but will continue as the temperature rises, evidenced by an increase in mass number 44 of the evolved gas, assumed to be carbon dioxide. Similarly, an increase in mass number 18 is seen which is believed to be mostly water.

Lutetium

The tris fod complex of lutetium (III) experiences a major weight loss event of 92 wt% starting at 127 °C, with peak mass loss at 143 °C. This is believed to be vaporization of the melted compound due to a much lower melting point. Around 1 wt% or less of water is lost in the range of 77-102 °C. Decomposition of the compound starts to occur at 200 °C and is mostly completed by 350 °C but will continue as the temperature rises, evidenced by an

increase in mass number 44 of the evolved gas, assumed to be carbon dioxide. Similarly, an increase in mass number 18 is seen which is believed to be mostly water.

4.2 Langmuir Method

The results of the Langmuir method are presented in Table 9. As mentioned earlier, the hfac and fod complexes are run over a 30 °C range, while the dpm complexes are run over a 24 °C range. This is due to a shorter sublimation event, therefore a smaller range gives a better estimation and fit of the weight loss event. Similarly, for the neodymium and holmium hfac complexes, the major sublimation event appeared to be over a shorter temperature range than 30 °C, and to ensure enough data points covered this event range, the measured range was shortened to 24 °C, by using isotherms every 4 °C instead of every 5 °C. Still using 7 isotherms for 5 min each, the data improved in linearity. Some of the samples necessitated a change in the isothermal scheme because of unique sublimation or vaporization curves. It can be seen that the dysprosium chelate has two sets of sublimation data, corresponding to the two major weight loss events during sublimation. The dysprosium homologue sublimes in a two-step process, with a 15 wt% loss event followed by a brief period of no weight loss, and then immediately followed by a 50 wt% loss event. The sample was analyzed by running the isotherm scheme for each step over 15 °C ranges, as noted in Table 9. The isotherms were taken every 3 °C, and still for 5 min each, but with only 6 isotherms per step. Also, note that the enthalpy value for lanthanum hfac corresponds to the enthalpy of vaporization, not sublimation, due to the low melting point. Also, the jump between isotherms for all samples resulted in <1 min of set point temperature fluctuations in the furnace, therefore the straight line fitted to each isotherm typically includes the latter portion of the curve that is within >99% precision of the set point temperature. As will be discussed later, five different linear fits of the mass loss curve for each isotherm are taken and averaged, which allows for uncertainty analysis with a standard deviation of the mass loss rate value.

The values of sublimation (or vaporization) enthalpy for all compounds for each of the three ligands are shown in Figure 17. The cyclical nature of the thermodynamics across the series is shown, and there is no clear trend that holds true for all three chelate types. It should be noted that the values across the series are connected by smooth lines to better see

Table 9. Sublimation Enthalpy values for the hfac, dpm and fod complexes of the lanthanides

Compound	Color	*mp* (°C)	Range (°C)	ΔH_{sub} (kJ mol^{-1})	±σ (kJ mol^{-1})	Δwt%	P_v (150 °C) (torr)
Hfac complexes							
La[hfac]$_4$	white	82-89	120-150	137.52	3.79	40.0	2.040
Pr[hfac]$_4$	green	172-180	115-145	159.97	5.65	44.7	4.548
Nd[hfac]$_4$	reddish blue	188-197	126-150	193.81	5.84	35.9	1.542
Sm[hfac]$_4$	yellow white	180-193	110-140	99.36	3.05	20.2	1.945
Eu[hfac]$_4$	yellow white	200-208	115-145	86.04	3.29	24.8	1.136
Gd[hfac]$_4$	white	217-220	125-155	103.88	3.6	35.7	0.843
Tb[hfac]$_4$	white	214-218	125-155	103.91	3.64	39.2	0.923
Dy[hfac]$_4$	yellow white	196-205	115-130	150.19	10.99	15.0	3.737
			140-155	56.54	7.75	52.9	0.772
Ho[hfac]$_4$	red	170-180	112-136	105.81	6.07	30.7	1.827
Er[hfac]$_4$	reddish white	218-226	120-150	121.66	4.61	23.8	1.120
Tm[hfac]$_4$	yellow white	214-217	125-155	95.12	4.27	29.4	0.888
Yb[hfac]$_4$	yellow white	212-215	120-150	114.41	4.66	42.1	1.703
Lu[hfac]$_4$	white	194-198	115-145	123.42	4.62	33.3	2.121
Dpm complexes							
La[dpm]$_4$	white	224-230	204-228	137.03	5.05	49.7	0.004
Ce[dpm]$_4$	reddish brown	275-283	196-220	87.62	6.07	26.2	0.027
Pr[dpm]$_3$	light green	214-220	184-208	153.25	11.74	45.1	0.016
Nd[dpm]$_3$	reddish blue	205-209	178-202	158.9	5.35	33.6	0.012
Sm[dpm]$_3$	yellowish white	197-202	164-188	145.89	4.04	26.1	0.023
Eu[dpm]$_3$	yellow	186-191	164-188	145.05	4.10	25.0	0.042
Gd[dpm]$_3$	white	181-183	162-186	184.16	4.02	54.7	0.033
Tb[dpm]$_3$	white	177-179	154-178	130.98	4.83	29.8	0.238
Dy[dpm]$_3$	yellowish white	177-182	162-186	145.44	5.13	29.8	0.095
Ho[dpm]$_3$	light red	181-185	158-182	130.59	3.89	25.9	0.127
Er[dpm]$_3$	pink	168-176	154-178	135.01	4.82	41.7	0.213
Tm[dpm]$_3$	yellowish white	169-172	152-176	145.91	3.85	37.5	0.173
Yb[dpm]$_3$	white	166-170	148-172	147.72	3.76	27.0	0.197
Lu[dpm]$_3$	white	174-178	154-178	158.75	3.78	47.3	0.167
Fod complexes							
La[fod]$_3$	yellowish white	95-105	180-210	116.22	4.51	13.8	0.007
Ce[fod]$_3$	reddish brown	88-94	134-164	85.94	2.87	12.7	0.169
Pr[fod]$_3$	green	80-90	160-190	66.03	5.58	18.0	0.126
Nd[fod]$_3$	light purple	110-114	125-155	95.51	2.71	12.1	0.203
Sm[fod]$_3$	yellowish white	122-129	130-160	92.47	2.76	14.3	0.206
Eu[fod]$_3$	yellowish white	82-98	152-182	86.48	3.95	31.9	0.125
Gd[fod]$_3$	white	85-103	138-168	89.45	2.88	20.4	0.169
Tb[fod]$_3$	white	80-103	142-172	86.29	2.95	22.3	0.196
Dy[fod]$_3$	yellowish white	112-120	133-163	104.17	3.65	14.6	0.221
Ho[fod]$_3$	yellow	98-128	127-157	119.87	2.78	16.8	0.261
Er[fod]$_3$	pink	57-62	133-163	69.05	2.86	23.6	0.311
Tm[fod]$_3$	white	107-112	113-143	127.88	2.58	15.5	0.860
Yb[fod]$_3$	yellowish white	85-108	116-146	80.42	3.52	23.8	0.624
Lu[fod]$_3$	white	54-72	113-143	66.14	4.60	17.3	0.517

the cyclical nature of the lanthanide series, but are in no way related to each other. It is also worth noting how the fod complexes have vaporization enthalpy values smaller in magnitude than the sublimation enthalpy values for most of the dpm and hfac complexes. This indicates it takes less energy to vaporize the fod chelates given the same system. If we assume the linear correlation between sublimation enthalpy and adsorption enthalpy, this means the fod chelates would have smaller retention times on a chromatography column, given the same column parameters. Although, the faster experiment times may be negligible, especially when compared to the fact that what is most important is the differences in enthalpic values for different lanthanides of the same chelate type. In a hypothetical post-detonation forensics situation, an unknown mixture of lanthanide oxides or salts will need to be put through the same chemical process. The sample will be chemically converted to a mixture of volatile chelates, potentially hfac, dpm or fod, and the mixture will be separated in the gas phase on a gas chromatograph. The quality of separations on that column will be dependent on the enthalpic differences between the lanthanides present.

The adsorption enthalpy values for all 41 complexes are tabulated in Table 10 below and were calculated from equation 9, corresponding to lanthanide chlorides or oxychlorides on a quartz surface. Although this data may not be accurate because these compounds are β-diketonates and not chloride salts, this is still a useful example of the linear relation between sublimation and adsorption enthalpy values. This is useful information as it pertains to chromatographic separations of the compound. A kinetic model such as a Monte Carlo simulation of single-atom chemistry can predict retention time from adsorption enthalpy and other column specific parameters. Although there is a need to find adsorption enthalpy values via another method because this correlation is not meant for hfac chelates, to the authors knowledge, this is the first report of enthalpic values of adsorption for the hfac dpm and fod complexes of the lanthanides. Knowing the relative differences in enthalpy across the series allows for the proper manipulation of chromatographic parameters to experimentally separate each lanthanide complex on a column. It can be noted that these enthalpic values do not show a smooth or consistent linear trend across the series, as some of the other properties show.

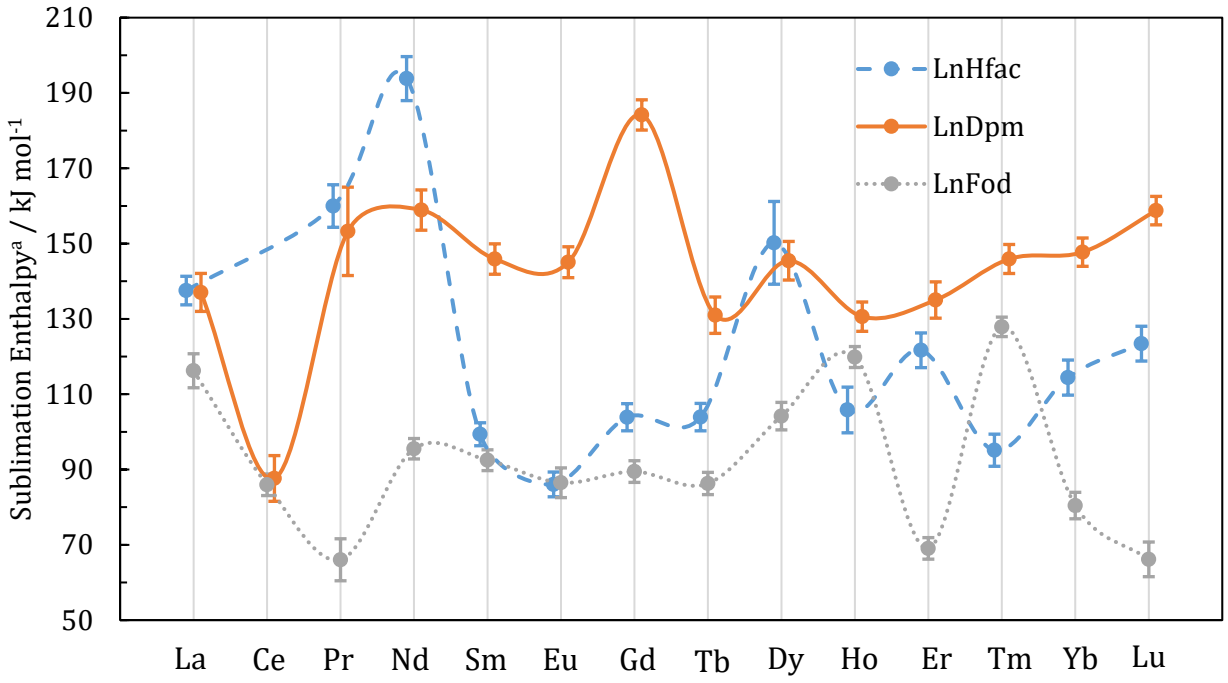

Figure 17: Sublimation (or vaporization) enthalpy values for all lanthanide chelates analyzed. [a]The enthalpy values for the Ln[fod]$_3$ complexes and for La[hfac]$_4$ are the enthalpies of vaporization. Note that the enthalpy values are connected by smooth lines to better see the cyclical nature but are not related.

Table 10. Adsorption enthalpy values for the hfac, dpm and fod complexes of the lanthanides

Compound	$-\Delta H_{ads}$ (kJ mol^{-1})	±σ (kJ mol^{-1})	Compound	$-\Delta H_{ads}$ (kJ mol^{-1})	±σ (kJ mol^{-1})	Compound	$-\Delta H_{ads}$ (kJ mol^{-1})	±σ (kJ mol^{-1})
La[hfac]$_4$	104.01	6.64	La[dpm]$_4$	103.72	6.92	La[fod]$_3$	91.23	6.54
			Ce[dpm]$_4$	74.07	6.72	Ce[fod]$_3$	73.07	5.88
Pr[hfac]$_4$	117.48	7.38	Pr[dpm]$_3$	113.45	9.56	Pr[fod]$_3$	61.12	6.40
Nd[hfac]$_4$	137.79	7.92	Nd[dpm]$_3$	116.84	7.29	Nd[fod]$_3$	78.81	5.95
Sm[hfac]$_4$	81.12	6.05	Sm[dpm]$_3$	109.03	6.80	Sm[fod]$_3$	76.98	5.93
Eu[hfac]$_4$	73.12	5.96	Eu[dpm]$_3$	108.53	6.80	Eu[fod]$_3$	73.39	6.11
Gd[hfac]$_4$	83.83	6.20	Gd[dpm]$_3$	132.00	7.35	Gd[fod]$_3$	75.17	5.92
Tb[hfac]$_4$	83.85	6.21	Tb[dpm]$_3$	100.09	6.79	Tb[fod]$_3$	73.27	5.90
Dy[hfac]$_4$	111.61	9.20	Dy[dpm]$_3$	108.76	7.05	Dy[fod]$_3$	84.00	6.21
Ho[hfac]$_4$	84.99	6.88	Ho[dpm]$_3$	99.85	6.57	Ho[fod]$_3$	93.42	6.23
Er[hfac]$_4$	94.50	6.63	Er[dpm]$_3$	102.51	6.84	Er[fod]$_3$	62.93	5.74
Tm[hfac]$_4$	78.57	6.27	Tm[dpm]$_3$	109.05	6.76	Tm[fod]$_3$	98.23	6.30
Yb[hfac]$_4$	90.15	6.56	Yb[dpm]$_3$	110.13	6.77	Yb[fod]$_3$	69.75	5.96
Lu[hfac]$_4$	95.55	6.65	Lu[dpm]$_3$	116.75	6.92	Lu[fod]$_3$	61.18	6.12

Because the 4f electrons of the lanthanide series are very close to the nucleus, the increasing nuclear charge across the period corresponds to decreasing ionic radius. This would lead us to assume that the lanthanide chelates decrease sterically across the period and thus are more volatile for the heavier lanthanides. It is important to note that despite this, the spectrochemical series of ligands only indicates that the ligand field splitting parameter increases down a group, i.e., volatility decreases. Although, there is no correlation across a period. According to this TGA data, we do see a general decrease in vaporization temperatures, i.e. increasing volatility, as we move from lanthanum to lutetium, with slight exceptions due to improved valency of some neighboring lanthanides.

When analyzing the energetics of the lanthanide series, it can be said that both the physical properties and chemical properties are influencing the sorption thermodynamics. This is also partially why the enthalpic values of the series appear cyclical in nature. It can be hypothesized that the volatilization of the compounds is more due to the chemical properties rather than the physical properties such as size. Physisorption of the compound on a chromatography column would be more prevalent if the series followed a trend with ionic radius, and although this may exist for parts of the series, it is not the trend we are seeing in enthalpy values. Chemisorption must play a larger role when differentiating elements directly next to each other. Neighboring lanthanides are similar in size, but can differ greatly in chemistry due to the filling of the 4f orbitals and/or addition of a 5d electron. This is important because the effect of physisorption decreases and the effect of chemisorption increases as chromatographic temperatures increase, up to a certain peak temperature. Therefore, the differences seen in this data may be exploited in various chromatographic experiments or simulations.

4.3 Varying Experimental Parameters in Langmuir Method

The effect of sample weight, crystal size and surface area on the sublimation enthalpy estimation was studied. It was hypothesized that crystal size would have less of an impact on the result as the overall weight of the sample, while surface area was believed to be most important. Maintaining a constant surface area for the same sample is important because the mass loss rate can change based on surface area. Because the Langmuir method is based on

the isothermal mass loss rate at various temperatures, and because the higher temperature isotherms are run on samples of decreased sample weight, it was important that this decrease in sample weight did not also correlate to a decrease in sample surface area. Sample surface areas were measured before and after running, and the average is taken for use in calculations. A more constant surface area is typically seen for larger weight samples, while most samples of at least 10 mg did not lose more than 5% surface area.

Additional parameters tested were the hydration of the compound for the hfac complexes, such as how long the compound is left in open air. Because many lanthanide compounds are hygroscopic, hydration or coordination of water ions may be noticed during lower temperatures of TGA. It is important to differentiate between impurities in compound synthesis and TGA sample preparation, as well as study its effect on the end result. It was noticed that samples run immediately from vial to instrument had significantly less water coordinated, as noted by dehydration around 100 °C. All hfac samples were eventually run with open air exposure for around 2 hours. This resulted in between 2-10% weight lost before the first isotherm, typically around 5% and mostly due to molecular water, which was confirmed by the TGA-MS. Some samples were left much longer than 2 hours and it was noted that hydration possibly reaches a saturation point after several hours, as much more water was not necessarily detected.

It was also necessary to compare the effect of the heating rates and time allowed for each isothermal region within the Langmuir method. Some studies have used longer isothermal heating times, farther jumps in temperature, fewer isothermal temperatures and other adjustments. It was noted that less than 4 minutes per isotherm did not result in as precise data due to the slow temperature adjustment of the instrument after each jump. This instrument took around 1 min just to stabilize at the new temperature, and it was found that at least 3 minutes of data collection was sufficient. The range of the Langmuir method used was found to rely on the size and range of the TGA and DTG curve. Ranges anywhere from 15 to 30 °C produced positive results, but the biggest factor was the rate at which the DTG curve sloped upwards towards its peak. If the weight loss event started and peaked over a 30 °C range, then that was used. For some samples, two smaller yet separate sublimation events took place, each over 15 °C. The goal is to space out the isotherms enough so that they

don't produce similar values, while making sure they aren't so far apart that one starts before the sublimation and one finishes after it.

The effect of the parameter for molar mass was tested on the equation. It was found that the molar mass did not have any effect on the value of sublimation enthalpy. This is due to the fact that the sublimation enthalpy is only dependent on the slope of the trendline, which is only dependent on the changing variables of mass loss rate and temperature. Additionally, taking the value of molar mass to its lower and upper extremes had a considerable effect on the calculated vapor pressure. Lowering the molar mass by 50% or increasing it by 100% each resulted in a decrease or increase by 25%, respectively. For more accurate estimations of vapor pressure, it will be necessary to understand the exact molecular structure of the chelate, as multiple coordination geometries seem to be possible for these amorphous compounds.

4.4 Quantifying Uncertainty in Langmuir Method

Although the result of the Langmuir method is the value of the sublimation enthalpy, the accuracy and precision of this value is also necessary information. Because there is often little published data on these compounds, the accuracy of the results may not be confirmed, except for the trends seen across the series compared to that seen for enthalpic data of other lanthanide compounds. Fortunately, the precision of the data produced here can be quantified by error propagation. This can be done by quantifying the uncertainty in the isothermal mass loss rate at each temperature, which is the variable that is used to calculate values fitted by a linear trendline. A Monte Carlo model has been produced to find a normal distribution of trendline slopes and y-intercepts given these uncertainties. Thus, a normal distribution of sublimation enthalpy values is found and the distribution of data allows for the solution of a standard deviation. The standard deviation values are tabulated with the corresponding data in the previous section, while the approach is outlined below.

4.4.1 Standard Deviation of Sublimation Enthalpy

Calculating uncertainty in the value of sublimation enthalpy begins with the uncertainty in estimating the value of the mass loss rate for each isotherm in the TGA curve. Because the rate is dependent on how the curve is selected and fit to a line, five random

values of this mass loss rate for each isotherm are found using the software's line fitting feature. The average and standard deviation of the five are taken. The value of "y" in the linear equation used in the Langmuir method is calculated along with corresponding standard deviation by using the average surface area of the sample, molar mass and corresponding temperatures.

$$y = \ln\left(\mu_{m_{sub}}\sqrt{\frac{T}{M_W}}\right) \qquad (14)$$

$$\delta_y = \sqrt{\left(\frac{\delta_{m_{sub}}}{\mu_{m_{sub}}}\right)^2 + \left(\frac{\delta_{SA}}{\mu_{SA}}\right)^2} \qquad (15)$$

The uncertainty associated with the surface area determination is assumed to be 5% of the mean surface area value. The Monte Carlo model consists of a "while loop" taken to 20,000 histories. In each history, an array of "y" values, corresponding to each temperature, is created according to a normal random distribution function, which utilizes the standard deviation values. A trendline fitting these "y" values with the corresponding temperatures ("x" values) is found. The slope is used to calculate the value of sublimation enthalpy for that history, and this is repeated for all histories. The mean enthalpy and the standard deviation are found using MATLAB's built in functions "mean" and "std".

4.5 Thermal Analysis of Lanthanide Chlorides

Most of the lanthanide trichlorides were characterized with a TGA to understand the potential volatility and phase changes upon heating. The trichlorides were synthesized from the rare earth oxides by adding enough hydrochloric acid and stirring. Only ten lanthanide trichlorides were tested because of instrument breakdown during the experiment. The remaining compounds can be visited in future experiments, although the results found here indicate that the chlorides do not sublime up to 1000 °C, proving them unsuitable for low temperature vaporization. The same Discovery TGA-MS and TGA Q50 that were used in the thermal analysis experiments for the lanthanide chelates were used here. Discovery TGA-MS

(TA Instruments, USA) was used with HT Pt pans and between 3-10 mg samples with a heating rate of 5 °C/min up to at least 600 °C. Evolved gas analysis achieved with quadrupole mass spectrometer, and the furnace was run under 20 psi N_2. TGA Q50 (TA Instruments, USA) was used for some samples with heating rate of 10 °C/min up to 1000 °C, between 10-20 mg of sample and HT Pt pans, and the furnace was run under 20 psi N_2.

Notable mass numbers detected are 1, 16, 17, 18, 32, 36, 38, 40, and 44. All samples except for Dy exhibited hydration with 6 H_2O molecules; similarly all contained 1 H_2O aqua ion coordinated with the metal. Masses 36 and 38 correspond to HCl formed as a byproduct of oxychloride formation during hydrolysis; note that the equilibrium constant is large in the forward direction for the following reaction.

$$LnCl_3 + OH^- \leftrightarrow LnOCl + HCl \qquad (16)$$

Oxychloride formation occurs as water is removed from the sample and at increasing temperatures; in the case of Sm and Eu, this occurs first when the aqua ion is removed, and again at a higher temperature. Figure 18 and Figure 19 show mass peaks of the vapor phase for mass 18 and mass 36 for the chlorides of Sm and Dy, respectively.

A strong signal for mass 36 is seen for Sm and Eu, a medium signal is seen for La, Pr, Nd, Er and Tm, and a weak signal is seen for Gd, Tb and Dy. La, Pr, Eu and Dy form oxychlorides consistently as temperatures increase; Nd, Sm, Gd, Tb, Er and Tm experience peak oxychloride formation within noted temperature ranges. Also worth noting is how masses 32, 40 and 44 typically increases with temperature. No samples tested entered the gas phase at a pressure of 20 psi. Table 11 details the results of the thermal analysis.

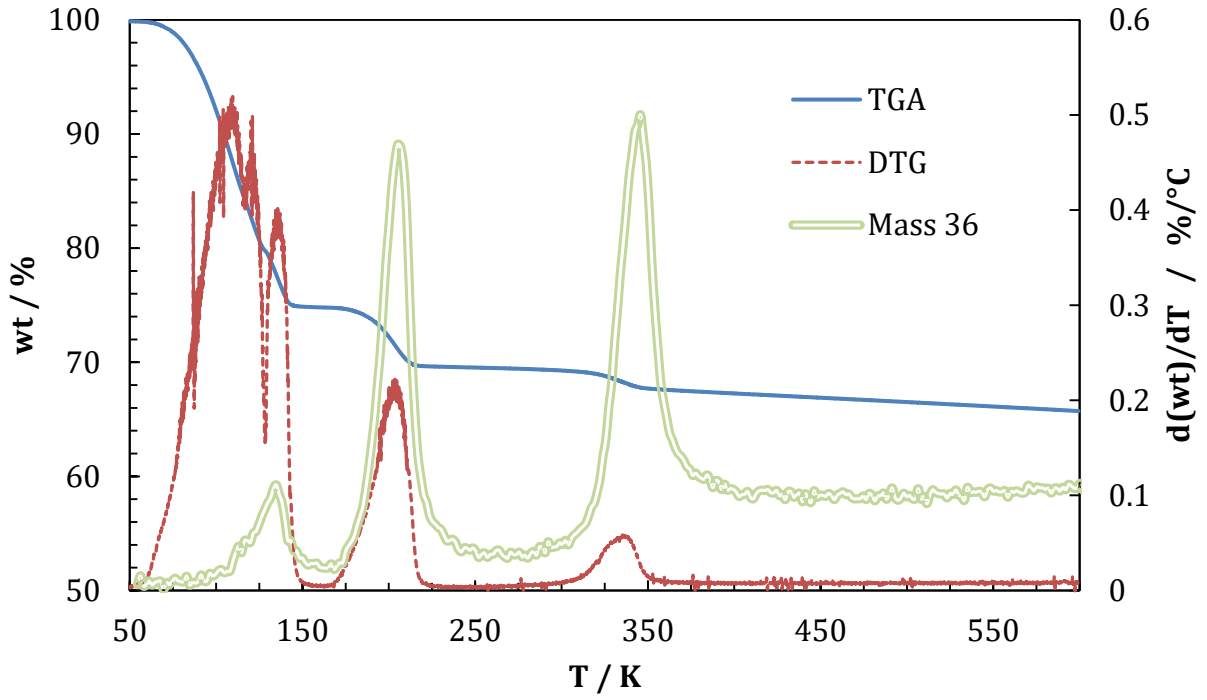

Figure 18: $SmCl_3$: TGA-DTG and MS data for mass 36. Note the peak of the MS data is normalized to 0.5 units on the DTG axis for convenience.

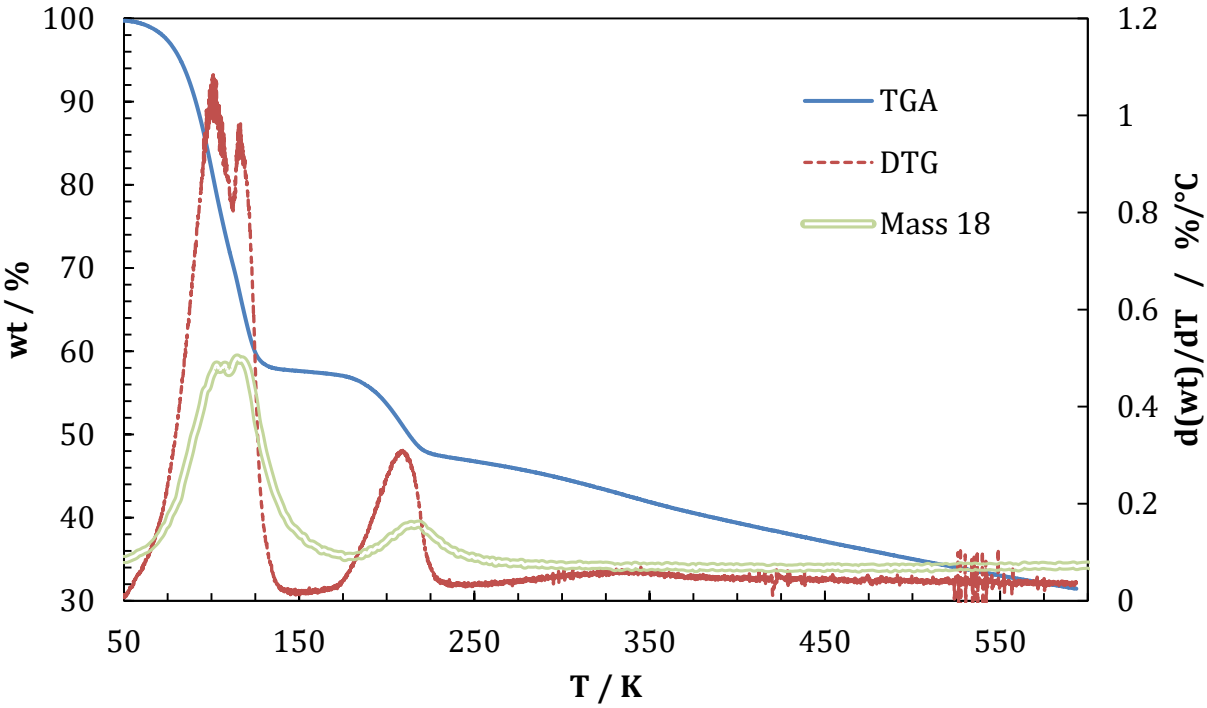

Figure 19: $DyCl_3$: TGA-DTG and MS data for mass 18. Note the peak of the MS data is normalized to 0.5 units on the DTG axis for convenience.

Table 11. Properties and results from thermal analysis of ten hydrated lanthanide trichlorides

	Lanthanum	Praseodymium	Neodymium	Samarium	Europium	Gadolinium	Terbium	Dysprosium	Erbium	Thulium
Atomic Number	57	59	60	62	63	64	65	66	68	69
Most Common Isotope	139	141	142, 144, 146	147, 152, 154	151, 153	156, 158, 160	159	162, 163, 164	166, 167, 168	169
# of Stable Isotopes	1	1	5	5	1	6	1	7	6	1
Electron Configuration [Xe]	$5d^1\ 6s^2$	$4f^3\ 6s^2$	$4f^4\ 6s^2$	$4f^6\ 6s^2$	$4f^7\ 6s^2$	$4f^7\ 5d^1\ 6s^2$	$4f^9\ 6s^2$	$4f^{10}\ 6s^2$	$4f^{12}\ 6s^2$	$4f^{13}\ 6s^2$
Oxidation States	3+	3+, 4+	3+	2+, 3+	2+, 3+	3+	3+, 4+	3+	3+	3+
Crystal structure: $LnCl_3$	hex-UCl_3	hex-UCl_3	hex-UCl_3	hex-UCl_3	hex-UCl_3	hex-UCl_3	ortho-$PuBr_3$	mono-$AlCl_3$	mono-$AlCl_3$	mono-$AlCl_3$
Crystal structure: LnOCl	tet-PbFCl	tet-PbFCl	tet-PbFCl	tet-PbFCl	tet-PbFCl	tet-PbFCl	tet-PbFCl	tet-PbFCl	both	rhom-SmSI
M_w/g/mol	245.264	247.267	250.601	256.72	258.323	263.61	265.284	268.859	273.618	275.293
Color and appearance	wh hex cry; hyg	grn hex needles; hyg	viol hex cry	yel cry	grn-yel needles	wh monocl cry; hyg	wh orth cry; hyg	wh or yel cry	viol monocl cry; hyg	yel hyg cry
Literature mp/°C	858	786	759	682	623	602	582	718	776	845
Discovery TGA-MS temp limit/°C	600	600	600	600	600	600	600	600	1000	750
Q50 TGA temp limit/°C	1000	1000	-	1000	1000	900	-	-	-	-
Dehydration/°C	38-100	54-100	54-114	85-135	73-130	89-145	83-138	80-122	89-209	87-133
Aqua ion removal/°C	127-150	148-170	158-177	189-212	196-217	208-229	210-233	190-220	318-361	212-235
Oxychloride formation/°C	374-600*	331-600*	305-333	189-212 319-346	196-217 513-600*	332-356	322-353	280-600*	318-361	324-355
wt % remaining at 600 °C	59.7	64.2	66.5	65.7	60.2	64.0	63.2	31.2	67.1	60.4
wt % remaining at 1000 °C	57.2	54.1	-	55.2	56.9	-	-	-	61.8	-

Chapter 5: Conclusions and Recommendations

Lanthanide β-Diketonates

Presented here is the determination of the sublimation enthalpies of lanthanide chelates for three different ligands via the Langmuir method using isothermal TGA. The ligands used include hfac, dpm, fod, and tfac, although the tfac complexes did not sublime fully and were later omitted from further research. This analysis allows for the comparison of the relative adsorptive qualities of each of the lanthanide homologues in the series, as well as that for different chelate complexes. By comparing the chelates of these four ligands, we can better understand the thermodynamics of lanthanide β-diketonates. We can learn how partial or total fluorination and sterics of the ligand play a role in the compound's volatility. The cyclical nature of the enthalpy values across the lanthanide series tells us that the chemical properties of the lanthanides play a larger role in the compound's volatility, as opposed to physical properties, i.e. decreasing ionic radius. Finally, chromatographic separations can be achieved by exploiting enthalpic differences between different lanthanides chelated with the same ligand.

Additionally, there was investigation into the degradation or decomposition of the compound via standard heating TGA-MS up to higher temperatures. This was evidenced by the increase in mass numbers 18 and 44 at higher temperatures, indicating the possible product formation of water and carbon dioxide, respectively. The TGA-MS data also provided information on the onset and end set temperatures of major weight loss stages, as well as the peak temperature at which total sublimation occurs. This data was utilized in setting the temperature ranges for each compound's unique sublimation range in the Langmuir method. Melting point analysis of the compounds confirmed the occurrence of sublimation during the major weight loss event, as opposed to the melting of the compound followed by vaporization. Although, the fod complexes did melt prior to the major weight loss event, the Langmuir method was still employed to find the vaporization enthalpy values. Finally, although all three ligand options seem adequate, the fod ligand posed a slightly more difficult synthesis route.

Lanthanide Chlorides

The detection of mass numbers 36 and 38 in the evolved gas indicates the transition from the trichloride state to the oxychloride state. This poses additional problems in attempting to separate different elements in the gas phase, as oxychlorides represent an additional set of vaporization characteristics. Oxychlorides begin to form at relatively low temperatures for hydrated lanthanide trichlorides; this can be avoided in the absence of oxygen or water. This can be achieved by altering the furnace gases, specifically by increasing the partial pressure of chlorine and reducing the partial pressure of oxygen or water. Fortunately, three of the lanthanide trichlorides tested exhibit little to no oxychloride formation upon heating, which can be utilized when separating. Lower pressures are potentially needed to achieve sublimation at temperatures below the melting point, although this is not confirmed yet; future work involves obtaining an instrument that can achieve near vacuum furnace pressures. Additional future work involves combining TGA with tube furnace and chromatography column connected to ICP-MS to allow for elemental chromatographic separations with isotopic detection for nuclear forensics. Finally, it has been shown before that complexing the lanthanide chloride with aluminum chloride can help volatilize the sample and allow for sublimation at a much lower temperature; this is a potential avenue for exploration for this project.

Estimating Adsorption Enthalpy

The importance of adsorption enthalpy to separations has been shown, and thus there is continued motivation in estimating this value by one or more methods. There will be continued efforts in using DFT to characterize the compounds. Additionally, it is recommended that efforts be continued in injecting the compounds on a working chromatography column and finding the retention time. The retention time can be used in several different published models to solve for the adsorption enthalpy, although the accuracy of these methods isn't quite known for these types of compounds. When adsorption enthalpy values are known, they can be correlated to the sublimation enthalpy values and will be useful data to publish.

Bibliography

[1] K.J. Moody, I.D. Hutcheon, P.M. Grant, Nuclear Forensic Analysis, 2nd ed., CRC Press, 2014.

[2] V. Fedchenko, The Role of Nuclear Forensics in Nuclear Security, Strateg. Anal. 38 (2014) 230–247. doi:10.1080/09700161.2014.884442.

[3] D. Hanson, J. Garrison, H. Hall, Assessing thermochromatography as a separation method for nuclear forensics: current capability vis-a-vis forensic requirements, J. Radioanal. Nucl. Chem. 289 (2011) 213–223. doi:10.1007/s10967-011-1063-5.

[4] K. Eisentraut, R. Sievers, Volatile Rare Earth Chelates, J. Am. Chem. …. 87 (1965) 5254–5256. doi:10.1021/ja00950a051.

[5] R.E. Sievers, B.W. Ponder, M.L. Morris, R.W. Moshier, Gas Phase Chromatography of Metal Chelates of Acetylacetone, Trifluoroacetylacetone, and Hexafluoroacetylacetone, Inorg. Chem. 2 (1963) 693–698. doi:10.1021/ic50008a006.

[6] C.S. Springer Jr., D.W. Meek, R.E. Sievers, Rare Earth Chelates of 1,1,1,2,2,3,3-Heptafluoro-7,7-dimethyl-,6-octanedione, Inorg. Chem. 6 (1966) 1105–1110.

[7] J.D. Auxier, J.A. Jordan, S.A. Stratz, S. Shahbazi, D.E. Hanson, D. Cressy, et al., Thermodynamic analysis of volatile organometallic fission products, J. Radioanal. Nucl. Chem. 307 (2016) 1621–1627. doi:10.1007/s10967-015-4653-9.

[8] C.E. Düllmann, B. Eichler, R. Eichler, H.W. Gäggeler, A. Türler, On the stability and volatility of group 8 tetroxides, MO4 (M = ruthenium, osmium, and hassium (Z = 108)), J. Phys. Chem. B. 106 (2002) 6679–6684. doi:10.1021/jp0257146.

[9] M. Schädel, D.A. Shaughnessy, The Chemistry of Superheavy Elements, Springer, 2013. doi:10.1007/b100152.

[10] B. Eichler, A. Türler, H.W. Gäggeler, Thermochemical Characterization of Seaborgium Compounds in Gas Adsorption Chromatography, J. Phys. Chem. A. 103 (1999) 9296–9306.

[11] A. Serov, R. Eichler, R. Dressler, D. Piguet, A. Türler, A. Vögele, et al., Gas chromatography of indium in macroscopic and carrier-free amounts using quartz and gold as stationary phases, Radiochim. Acta. 99 (2011) 95–101. doi:10.1524/ract.2011.1797.

[12] A.W. Coats, J.P. Redfern, Kinetic Parameters from Thermogravimetric Data, Nature.

201 (1964) 68–69.

[13] H.H. Horowitz, G. Metzger, A new analysis of thermogravimetric traces, Anal. Chem. 35 (1963) 1464–1468. doi:10.1021/ac60203a013.

[14] E.S. Freeman, B. Carroll, The application of thermoanalytical techniques to reaction kinetics: the thermogravimetric evaluation of the kinetics of the decomposition of calcium oxalate monohydrate, J. Phys. Chem. 62 (1958) 394–397. doi:10.1021/j150562a003.

[15] J.H. Flynn, L.A. Wall, General treatment of the thermogravimetry of polymers, J. Res. Natl. Bur. Stand. Sect. A Phys. Chem. 70A (1966) 487. doi:10.6028/jres.070A.043.

[16] S.A. Sadeek, Synthesis, thermogravimetric analysis, infrared, electronic and mass spectra of Mn(II), Co(II) and Fe(III) norfloxacin complexes, J. Mol. Struct. 753 (2005) 1–12. doi:10.1016/j.molstruc.2005.06.011.

[17] S.J. Ashcroft, The measurement of enthalpies of sublimation by thermogravimetry, Thermochim. Acta. 2 (1971) 512–514. doi:10.1016/0040-6031(71)80021-7.

[18] B.D. Fahlman, A.R. Barron, Substituent Effects on the Volatility of Metal β-diketonates, Adv. Mater. Opt. Electron. 10 (2000) 223–232. doi:10.1002/1099-0712(200005/10)10:3/5<223::AID-AMO411>3.0.CO;2-M.

[19] E.G. Gillan, S.G. Bott, A.R. Barron, Volatility Studies on Gallium Chalcogenide Cubanes: Thermal Analysis and Determination of Sublimation Enthalpies, Chem. Mater. 9 (1997) 796–806.

[20] I. Langmuir, The vapor pressure of metallic tungsten, Phys. Rev. 2 (1913) 329–342. doi:10.1103/PhysRev.2.329.

[21] D. Hanson, Synthesis and Thermodynamic Analysis of Volatile Beta-Diketone Complexes of Select Lanthanides via Gas-Phase Separations, The University of Tennessee, Knoxville, 2014.

[22] J. Rudolph, K. Bachmann, A Gaschromatography Apparatus for the Investigation and Separation of Radioactively Labelled Inorganic Compounds at High Temperatures, Mikrochim. Acta. 71 (1979) 477–493. doi:10.1007/BF01197420.

[23] V. Pershina, A. Borschevsky, M. Ilias, A. Turler, Theoretical predictions of properties and volatility of chlorides and oxychlorides of group-4 elements. II. Adsorption of tetrachlorides and oxydichlorides of Zr, Hf, and Rf on neutral and modified surfaces, J

Chem Phys. 141 (2014) 64315. doi:10.1063/1.4891531.

[24] I. Zvára, The Inorganic Radiochemistry of Heavy Elements, Springer Netherlands, Dordrecht, 2008. doi:10.1007/978-1-4020-6602-3.

[25] I. Zvara, Simulation of thermochromatographic processes by the Monte Carlo method, Radiochim. Acta. 1 (1985) 95–102. doi:10.1524/ract.1985.38.2.95.

[26] J.R. Garrison, D.E. Hanson, H.L. Hall, Monte Carlo analysis of thermochromatography as a fast separation method for nuclear forensics, J. Radioanal. Nucl. Chem. 291 (2011) 885–894. doi:10.1007/s10967-011-1367-5.

[27] K. Binnemans, Rare-earth beta-diketonates, Handb. Phys. Chem. Rare Earths. 35 (2005) 107–272. doi:10.1016/S0168-1273(05)35003-3.

[28] S. Mohammadi-Jam, K.E. Waters, Inverse gas chromatography applications: A review, Adv. Colloid Interface Sci. 212 (2014) 21–44. doi:10.1016/j.cis.2014.07.002.

[29] V. Pershina, J. Anton, T. Jacob, Fully relativistic density-functional-theory calculations of the electronic structures of M O4 (M=Ru, Os, and element 108, Hs) and prediction of physisorption, Phys. Rev. A - At. Mol. Opt. Phys. 78 (2008) 1–5. doi:10.1103/PhysRevA.78.032518.

[30] V. Pershina, T. Bastug, Electronic structure and properties of group 7 oxychlorides, MO3Cl, where M=Tc, Re, and element 107, Bh, J. Chem. Phys. 113 (2000) 1441–1446. doi:10.1063/1.481961.

[31] M. Leskela, L. Niinisto, E. Nykanen, P. Soininen, M. Tiitta, Thermoanalytical and Mass Spectrometric Studies on Volatile Beta-Diketone Chelates, Thermochim. Acta. 175 (1991) 91–98.

[32] A.C. Gigante, F.J. Caires, D.J.C. Gomes, L.S. Lima, O. Treu-Filho, M. Pivatto, et al., Spectroscopic study and thermal behavior of trivalent lanthanides and yttrium(III) chelates of EDTA using TG-DSC, FTIR, and TG-DSC coupled to FTIR, J. Therm. Anal. Calorim. 115 (2014) 127–135. doi:10.1007/s10973-013-3284-z.

[33] M. Leskelä, R. Sillanpää, L. Niinistö, M. Tiitta, M. Sjöström, S. Wold, et al., Structural and Thermal Studies of Tetrakis(2,2,6,6-tetramethyl-3,5-heptanedionato)cerium(IV)., Acta Chem. Scand. 45 (1991) 1006–1011. doi:10.3891/acta.chem.scand.45-1006.

[34] M.F. Richardson, R.E. Sievers, Volatile rare earth chelates of 1,1,1,5,5,5-hexafluoro-

2,4-pentanedione and 1,1,1,2,2,3,3,7,7,7-decafluoro-4,6-heptanedione, Inorg. Chem. 10 (1971) 498–504. doi:10.1021/ic50097a012.

[35] P.A. Barnes, M.B. Parkes, E.L. Charsley, High-Performance Evolved Gas Analysis System for Catalyst Characterization, 66 (1994) 2226–2231.

[36] T.S. Arul Jeevan, K.S. Nagaraja, Sublimation Kinetic Studies of the Zr(tmhd)4 Complex, Hindawi J. Chem. 2013 (2013) 1–5. doi:10.1155/2013/350937.

[37] H. Nishizaki, K. Yoshida, J.H. Wang, Comparative study of various methods for thermogravimetric analysis of polystyrene degradation, J. Appl. Polym. Sci. 25 (1980) 2869–2877. doi:10.1002/app.1980.070251218.

[38] A. Ji, S. Zhang, X. Lu, Y. Liu, A new method for evaluating the sewage sludge pyrolysis kinetics., Waste Manag. 30 (2010) 1225–9. doi:10.1016/j.wasman.2009.10.003.

[39] D. Li, L. Chen, J. Zhao, X. Zhang, Q. Wang, H. Wang, et al., Evaluation of the pyrolytic and kinetic characteristics of Enteromorpha prolifera as a source of renewable bio-fuel from the Yellow Sea of China, Chem. Eng. Res. Des. 88 (2010) 647–652. doi:10.1016/j.cherd.2009.10.011.

[40] D.M. Price, Vapor pressure determination by thermogravimetry, Thermochim. Acta. 367-368 (2001) 253–262. doi:10.1016/S0040-6031(00)00676-6.

[41] D.M. Price, M. Hawkins, Calorimetry of two disperse dyes using thermogravimetry, Thermochim. Acta. 315 (1998) 19–24. doi:10.1016/S0040-6031(98)00272-X.

[42] D.M. Price, S. Bashir, P.R. Derrick, Sublimation properties of x,y-dihydroxybenzoic acid isomers as model matrix assisted laser desorption ionisation (MALDI) matrices, Thermochim. Acta. 327 (1999) 167–171. doi:10.1016/S0040-6031(98)00606-6.

[43] S.P. Verevkin, R. V. Ralys, D.H. Zaitsau, V.N. Emel'Yanenko, C. Schick, Express thermo-gravimetric method for the vaporization enthalpies appraisal for very low volatile molecular and ionic compounds, Thermochim. Acta. 538 (2012) 55–62. doi:10.1016/j.tca.2012.03.018.

[44] Y. Pauleau, O. Dulac, Vaporization Processes of Aluminum Beta-Diketone Chelates, Chem. Mater. 3 (1991) 280–286. doi:10.1021/cm00014a015.

[45] S. Shahbazi, S.A. Stratz, J.D. Auxier, D.E. Hanson, M.L. Marsh, H.L. Hall, Characterization and thermogravimetric analysis of lanthanide hexafluoroacetylacetone chelates, J. Radioanal. Nucl. Chem. (2016).

doi:10.1007/s10967-016-5005-0.

[46] M. Stradiotto, R.J. Lundgren, eds., Ligand Design in Metal Chemistry, John Wiley & Sons, Ltd, Chichester, UK, 2016. doi:10.1002/9781118839621.

[47] D.A. Johnson, Principles of lanthanide chemistry, J. Chem. Educ. 57 (1980) 475. doi:10.1021/ed057p475.

[48] S. Cotton, Lanthanide and Actinide Chemistry, John Wiley & Sons, Ltd, Chichester, UK, 2006. doi:10.1002/0470010088.

[49] Z. Ahmed, K. Iftikhar, Solution studies of lanthanide (III) complexes based on 1,1,1,5,5,5-hexafluoro-2,4-pentanedione and 1,10-phenanthroline Part-I: Synthesis, 1H NMR, 4f–4f absorption and photoluminescence, Inorganica Chim. Acta. 363 (2010) 2606–2615. doi:10.1016/j.ica.2010.04.040.

[50] Z. Ahmed, K. Iftikhar, Synthesis, luminescence and NMR studies of lanthanide (III) complexes with hexafluoroacetylacetone and phenanthroline. Part II, Inorganica Chim. Acta. 392 (2012) 165–176. doi:10.1016/j.ica.2012.06.032.

[51] E.W. Berg, J.J.C. Acosta, Fractional Sublimation of the B-Diketone Chelates of the Lanthanide and Related Elements, Anal. Chim. Acta. 40 (1968) 101–113.

[52] F. Halverson, J.S. Brinen, J.R. Leto, Luminescence of Europium Hexafluoroacetylacetonate, J. Chem. Phys. 40 (1964) 2790. doi:10.1063/1.1724907.

[53] F. Halverson, J.S. Brinen, J.R. Leto, Photoluminescence of Lanthanide Complexes. II. Enhancement by an Insulating Sheath, J. Chem. Phys. 41 (1964) 157. doi:10.1063/1.1725616.

[54] N.P. Kaz'mina, G.N. Kupriyanova, S.I. Troyanov, Crystal Structure and Vacuum Sublimation of the Product of Reaction of Yttrium Hexafluoroacetylacetonate and Copper Acetylacetonate [Y(Hfa)3(H2O)2Cu(Acac)2], Russ. J. Coord. Chem. 26 (2000) 390–395.

[55] K. Eisentraut, R. Sievers, Volatile Rare Earth Chelates, J. Am. Chem. Soc. (1965) 20–22. doi:10.1021/ja00950a051.

[56] R.E. Thoma, Rare-Earth Halides, 1965.

[57] L.R. Morss, Thermochemical Properties of Yttrium, Lanthanum, and the Lanthanide Elements and Ions, Chem. Rev. 76 (1975) 827–841. doi:10.1016/B978-0-08-054819-7.00020-0.

[58] C.E. Myers, D.T. Graves, Vaporization thermodynamics of lanthanide trihalides, J. Chem. Eng. Data. 22 (1977) 440–445. doi:10.1021/je60075a023.

[59] K. Bachmann, SEPARATION OF TRACE ELEMENTS IN SOLID SAMPLES BY FORMATION OF VOLATILE INORGANIC COMPOUNDS, Talanta Rev. 29 (1982) 1–25.

[60] G. Meyer, The synthesis and structures of complex rare-earth halides, Prog. Solid State Chem. 14 (1982) 141–219. doi:10.1016/0079-6786(82)90005-X.

[61] B. Brunetti, A.R. Villani, V. Piacente, P. Scardala, Vaporization studies of dysprosium trichloride, tribromide, and triiodide, J. Chem. Eng. Data. 44 (1999) 509–515.

[62] B. Brunetti, A.R. Villani, V. Piacente, P. Scardala, Vaporization studies of lanthanum trichloride, tribromide, and triiodide, J. Chem. Eng. Data. 45 (2000) 231–236. doi:10.1021/je9902037.

[63] L.R. Morss, N.M. Edelstein, J. Fuger, The Chemistry of the Actinide and Transactinide Elements, Springer Netherlands, Dordrecht, 2011. doi:10.1007/978-94-007-0211-0.

[64] D. Gaede, CHLORINATION AND SELECTIVE VAPORIZATION OF RARE EARTH ELEMENTS, 2016.

[65] W.W. Wendlandt, The thermal decomposition of yttrium, scandium, and some rare-earth chloride hydrates, J. Inorg. Nucl. Chem. 5 (1957) 118–122. doi:10.1016/0022-1902(57)80052-9.

[66] W.W. Wendlandt, The Thermal Decomposition of the Heavier Rare Earth Metal Chloride Hydrates, J. Inorg. Nucl. Chem. 9 (1959) 136–139.

[67] D.M. Gruen, H. a. Oye, VAPOR COMPLEX OF NEODYMIUM CHLORIDE WITH ALUMINUM CHLORIDE, J. Inorg. Nucl. Chem. 3 (1967) 453–455.

[68] D.M. Gruen, R.L. McBeth, Uranium Tetrachloride - Aluminum Trichloride Vapor Complex, J. Inorg. Nucl. Chem. 4 (1968) 299–303.

[69] H. a. Oye, D.M. Gruen, Neodymium chloride-aluminum chloride vapor complexes, J. Am. Chem. Soc. 91 (1969) 2229–2236. doi:10.1021/ja01037a008.

[70] G. Adachi, K. Shinozaki, Y. Hirashima, Rare-earth separation using chemical vapor transport with LnCl3-AlCl3 gas-phase complexes, 169 (1990) 4–7.

[71] L.S. Wang, R.J. Gao, Y. Su, Z.C. Wang, Formation Thermodynamics of the Rare Earth Vapour Complexes - Dyal3cl12 and Dyal2cl9, J. Chem. Thermodyn. 28 (1996) 1093–1102. doi:10.1006/jcht.1996.0094.

[72] K.T. Jacob, A. Dixit, A. Rajput, Stability field diagrams for Ln-O-Cl systems, Bull. Mater. Sci. 39 (2016) 603–611. doi:10.1007/s12034-016-1219-6.

[73] D.K. Sahoo, R. Mishra, H. Singh, N. Krishnamurthy, Determination of thermodynamic stability of lanthanum chloride hydrates (LaCl3??xH2O) by dynamic transpiration method, J. Alloys Compd. 588 (2014) 578–584. doi:10.1016/j.jallcom.2013.11.115.

[74] M.L. Marsh, Synthesis and Characterization of Ln [hfac] x and Ln [fod] x Complexes for Thermochromatographic Separations, The University of Tennessee, Knoxville, 2014.

[75] S.B. Turnipseed, R.M. Barkley, R.E. Sievers, Synthesis and characterization of alkaline-earth-metal beta-diketonate complexes used as precursors for chemical vapor deposition of thin film superconductors, Inorg. Chem. 30 (1991) 1164–1170. doi:10.1021/ic00006a003.

[76] L.G. Hubert-Pfalzgraf, Metal alkoxides and β-diketonates as precursors for oxide and non-oxide thin films, Appl. Organomet. Chem. 6 (1992) 627–643. doi:10.1002/aoc.590060805.

[77] I.I. Gromova, K.M. Islamova, N.A. Lebedev, N.G. Zaitseva, Chemical states of radioactive lanthanide atoms in Pr and Nd fluorinated β-diketonates, J. Inorg. Nucl. Chem. 38 (1976) 961–964. doi:10.1016/0022-1902(76)80006-1.

[78] J.B. Westmore, M.L.J. Reimer, C. Reichert, Ionization energies of metal chelates. Acetylacetonates, trifluoroacetylacetonates, and hexafluoroacetylacetonates of trivalent metals of the first transition series, Can. J. Chem. 59 (1981) 1797–1804. doi:10.1139/v81-268.

[79] T. Moeller, H.E. Kremers, The Basicity Characteristics of Scandium, Yttrium, and the Rare Earth Elements, The William Albert Noyes Laboratory, University of Illinois, Urbana, Illinois, 1945.

[80] J. Mcaleese, J.C. Plakatouras, B.C.H. Steele, The use of Ce(fod)4 as a precursor for the growth of ceria films by metal--organic chemical vapour deposition, Thin Solid Films. 280 (1996) 152–159. doi:10.1016/0040-6090(95)08193-3.

[81] A.T. Johnson, T.G. Parker, S.M. Dickens, J.K. Pfeiffer, A.G. Oliver, D. Wall, et al., Synthesis and Crystal Structures of Volatile Neptunium(IV) β-Diketonates, Inorg. Chem. 56 (2017) 13553–13561. doi:10.1021/acs.inorgchem.7b02290.

Appendix

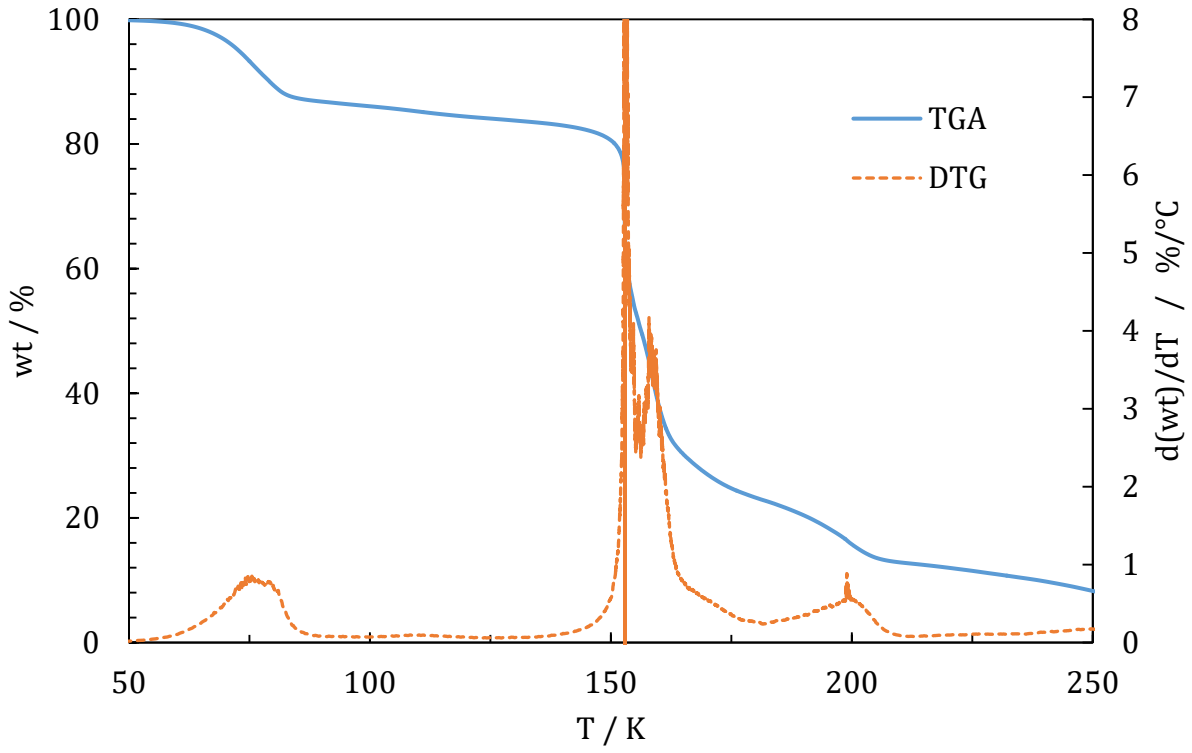

Figure 20: TGA-DTG spectrum for La[hfac]$_4$.

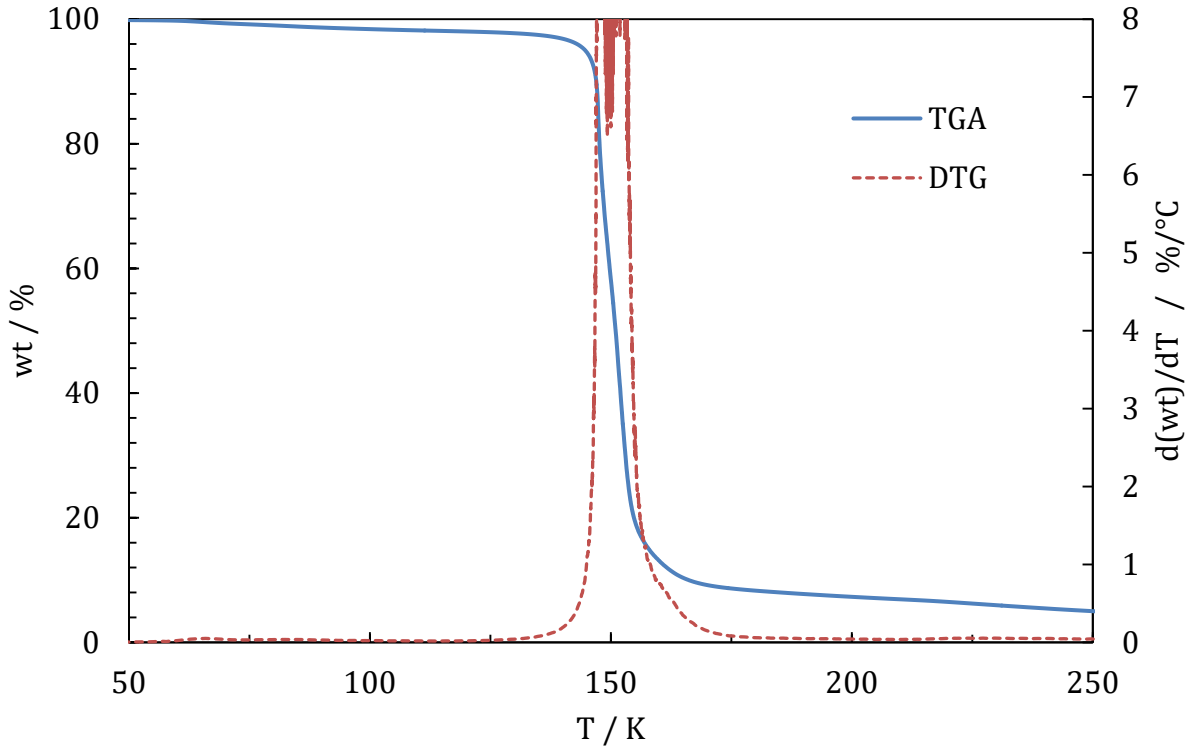

Figure 21: TGA-DTG spectrum for Pr[hfac]$_4$.

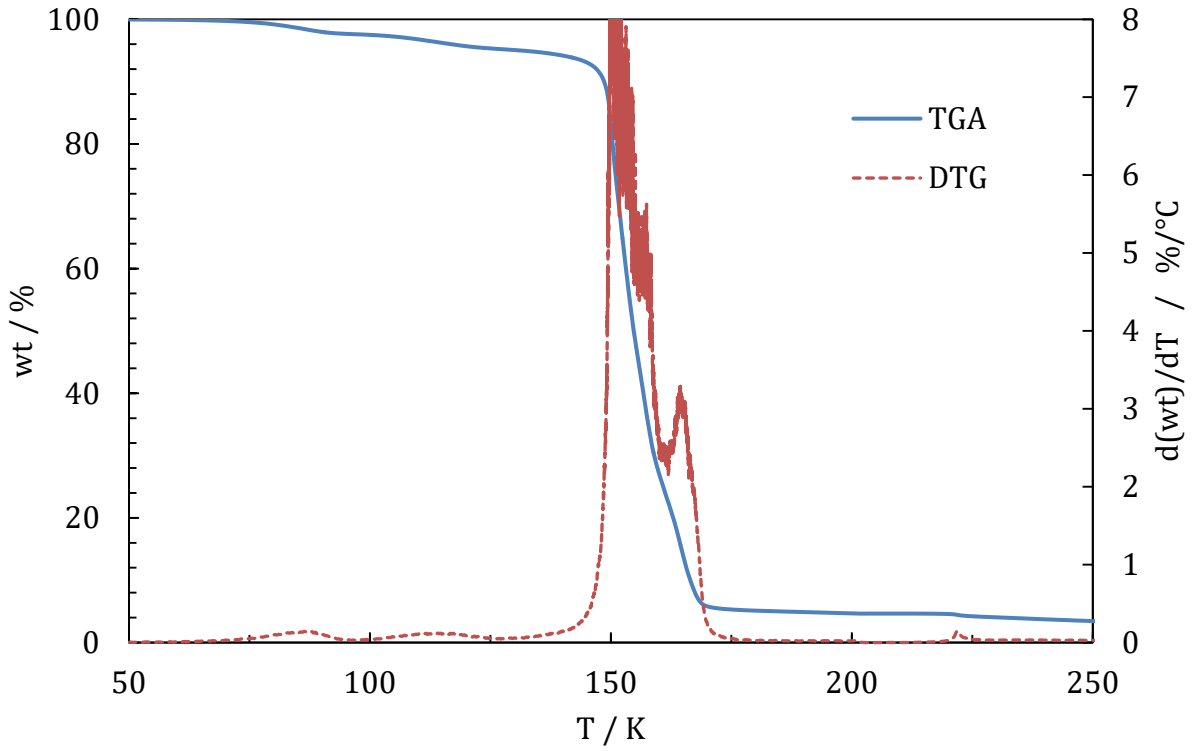

Figure 22: TGA-DTG spectrum for $Nd[hfac]_4$.

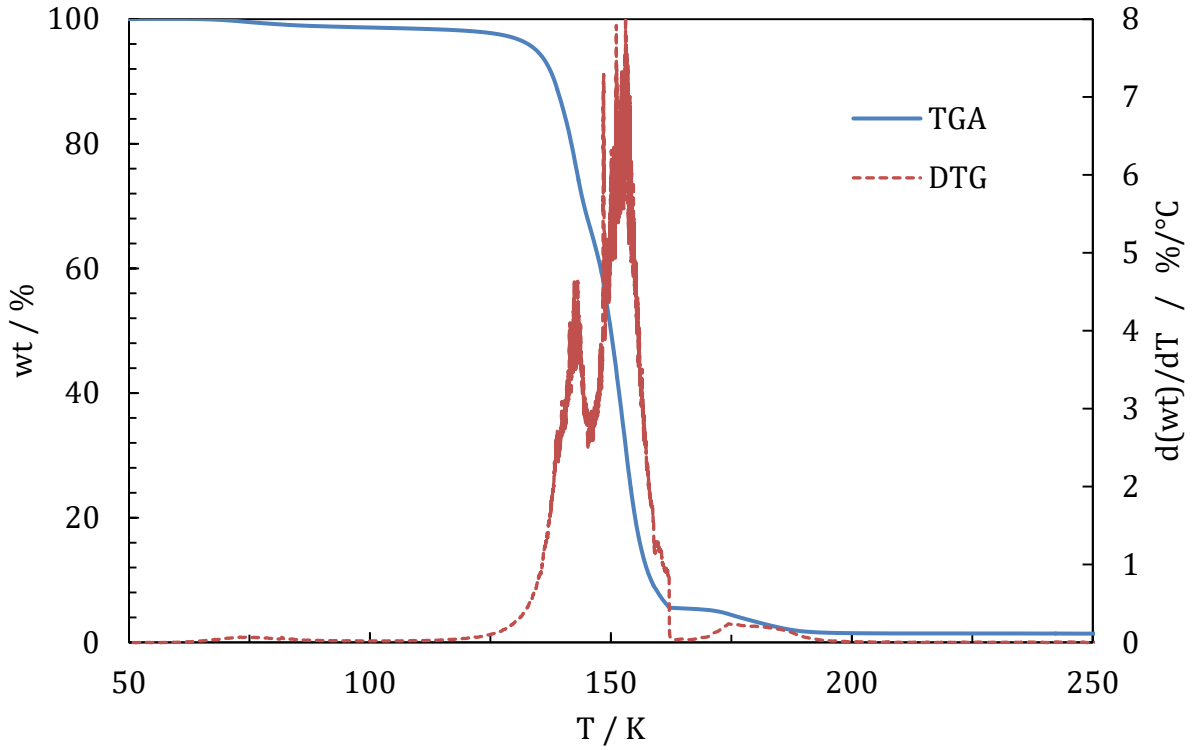

Figure 23: TGA-DTG spectrum for $Sm[hfac]_4$.

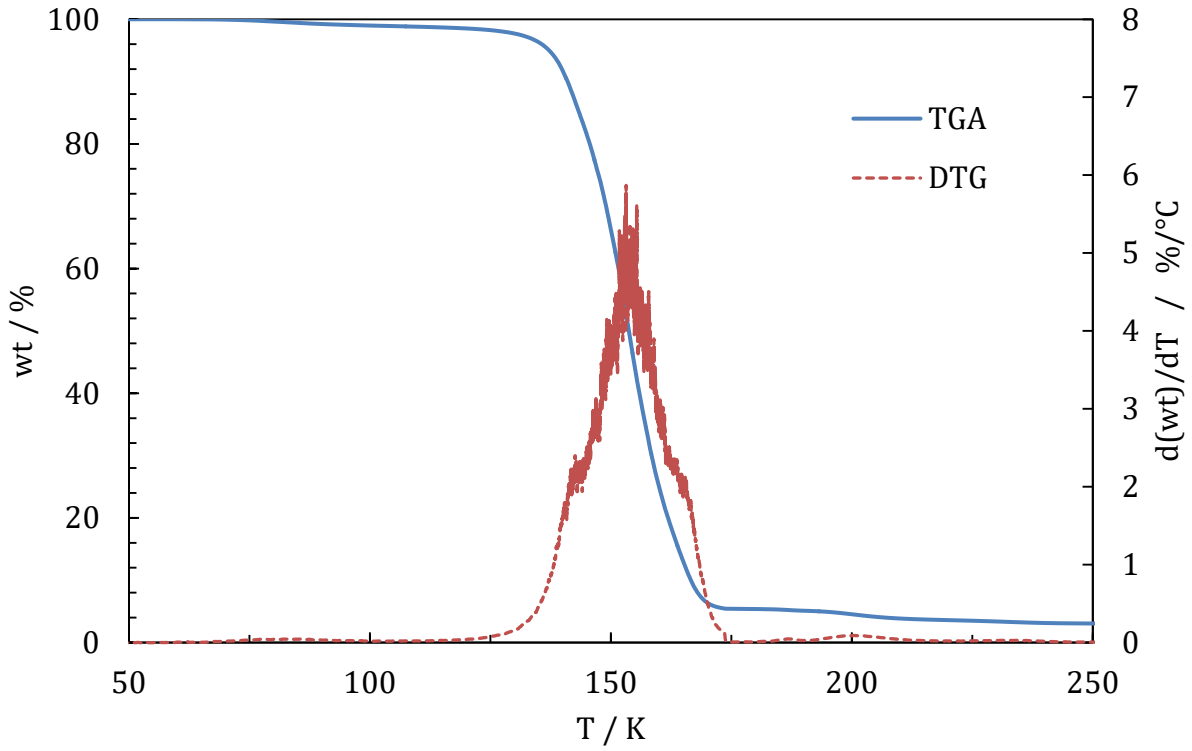

Figure 24: TGA-DTG spectrum for Eu[hfac]$_4$.

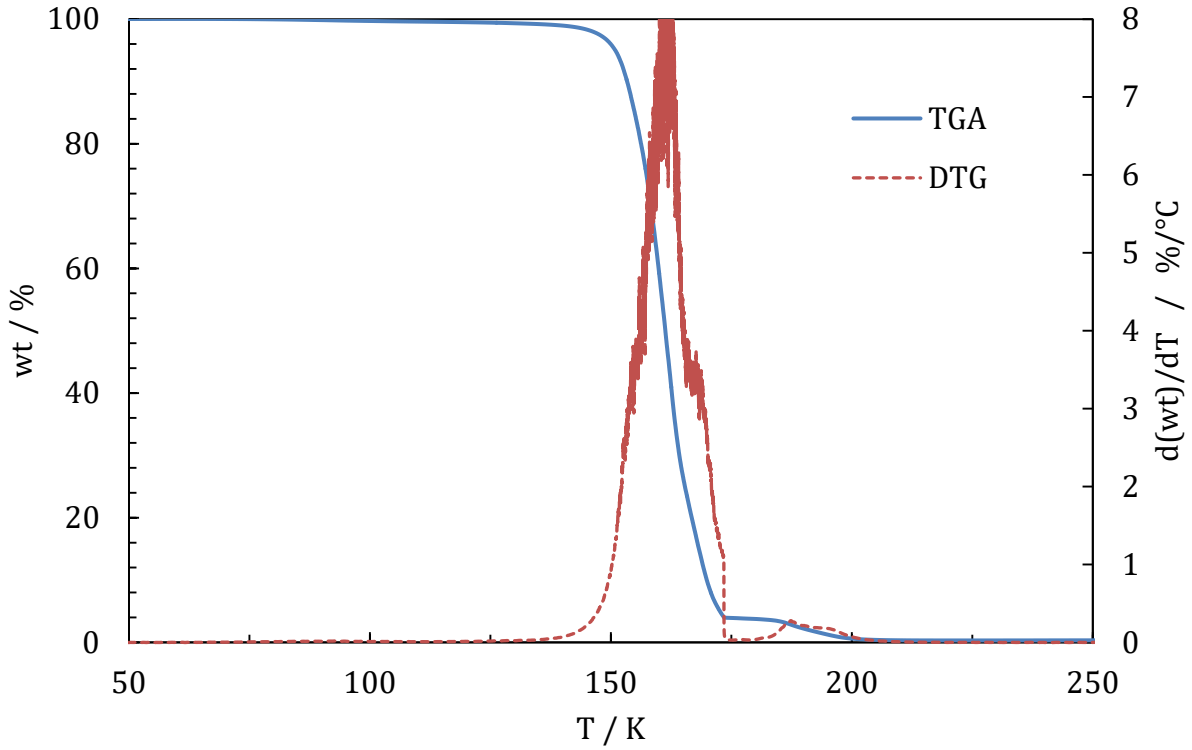

Figure 25: TGA-DTG spectrum for Gd[hfac]$_4$.

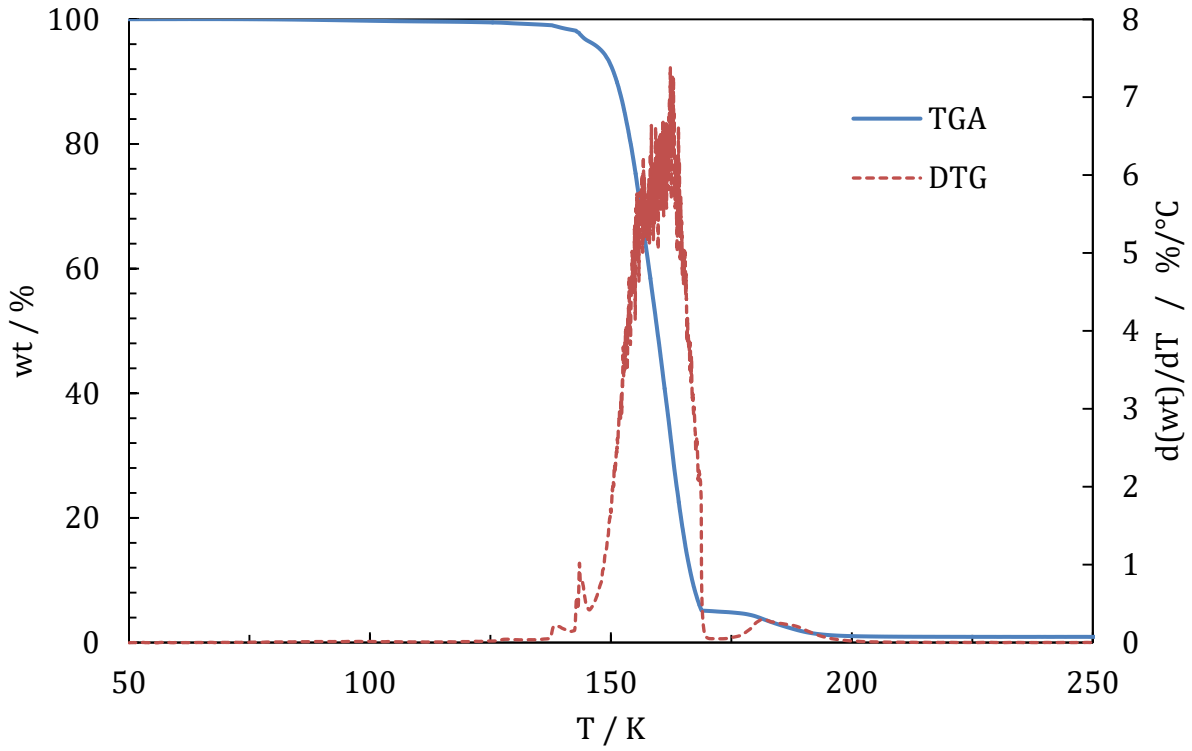

Figure 26: TGA-DTG spectrum for Tb[hfac]$_4$.

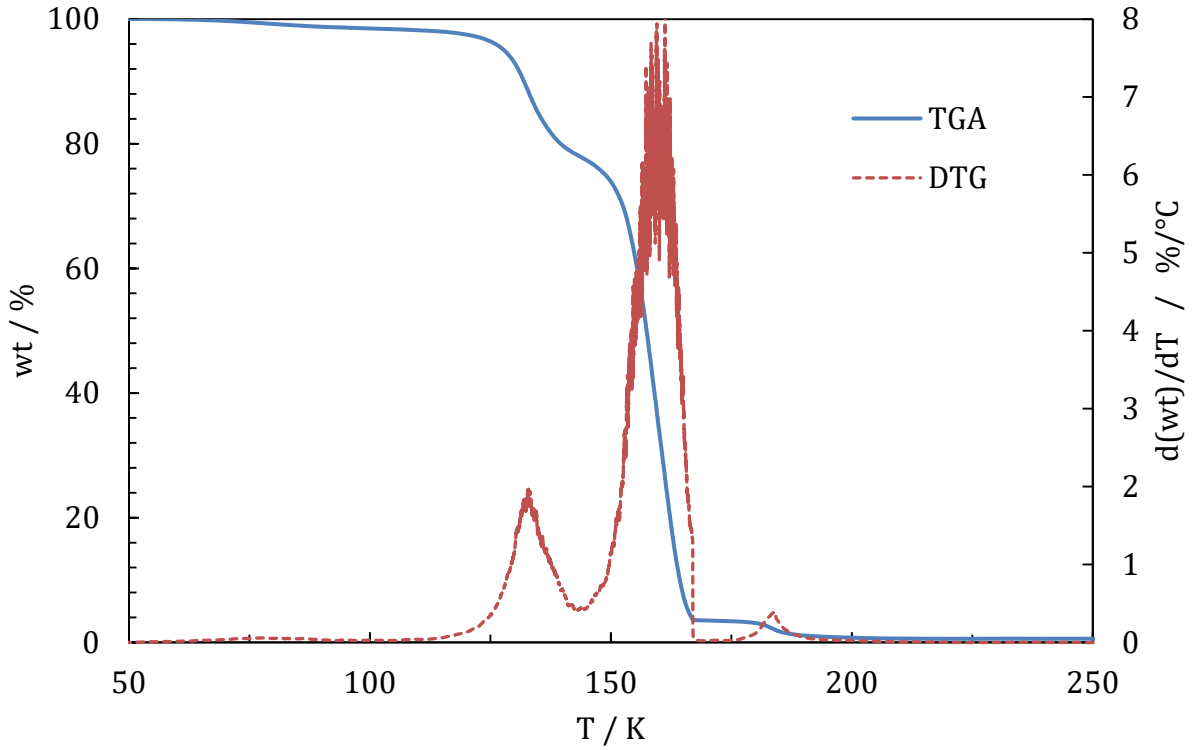

Figure 27: TGA-DTG spectrum for Dy[hfac]$_4$.

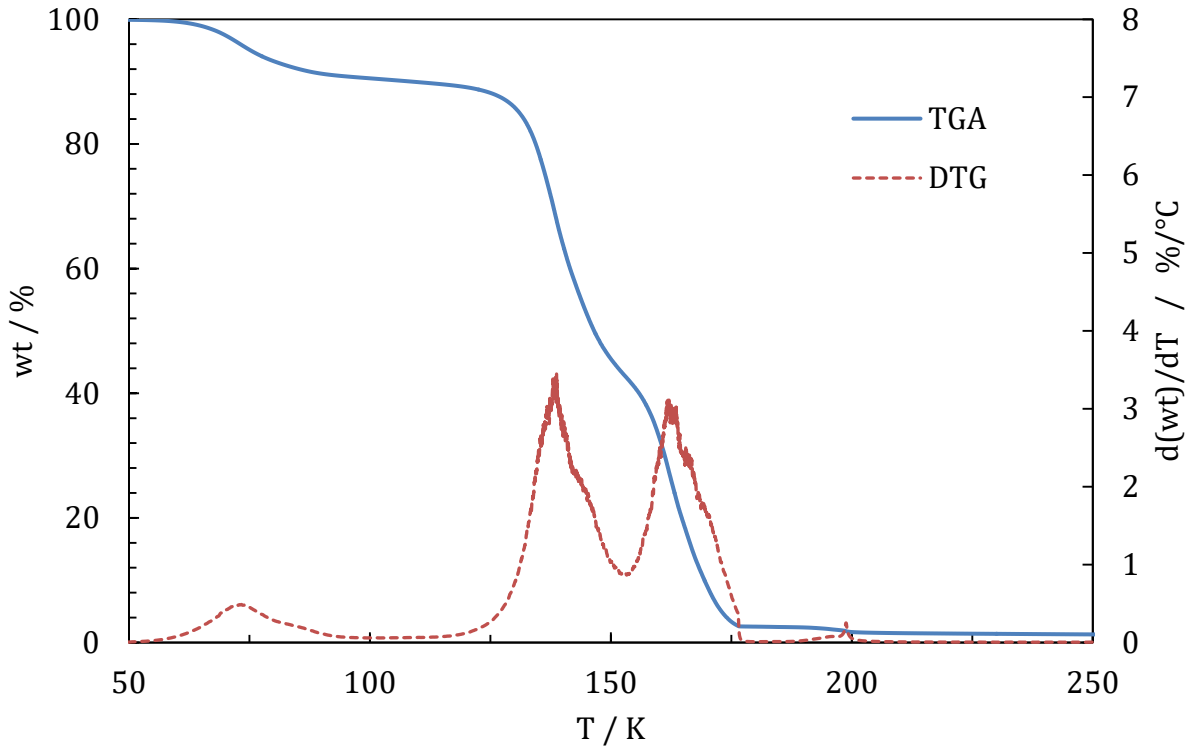

Figure 28: TGA-DTG spectrum for Ho[hfac]$_4$.

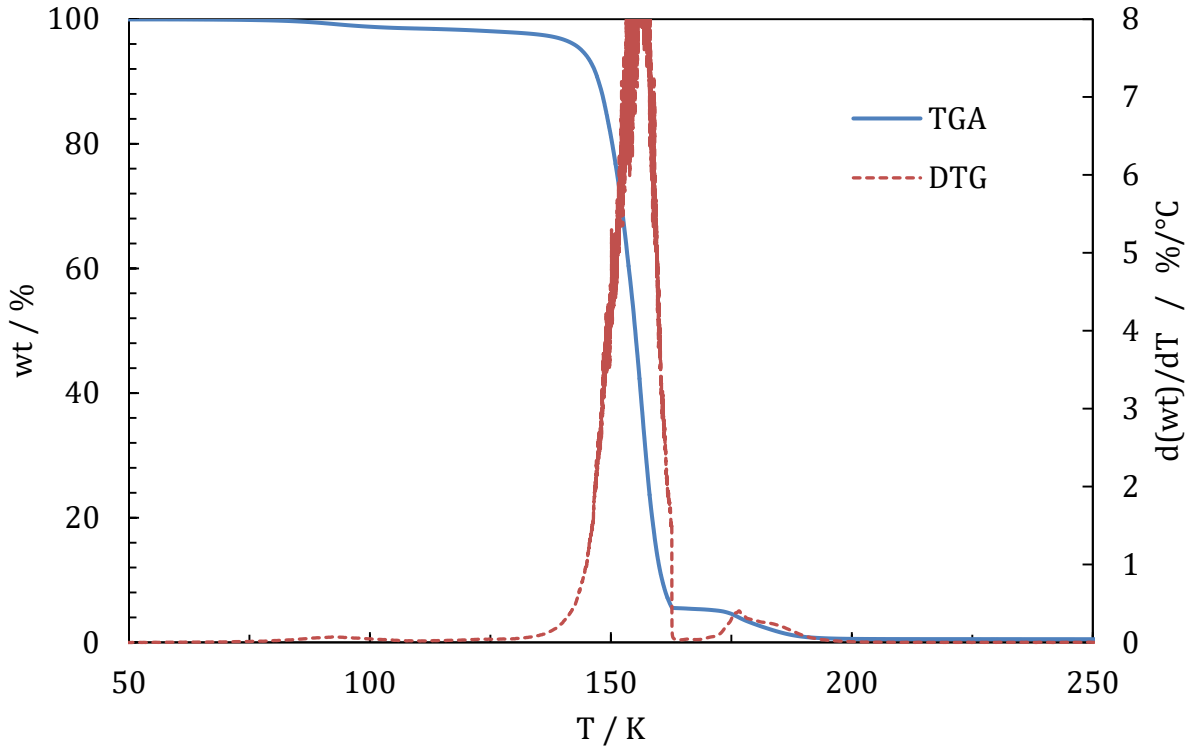

Figure 29: TGA-DTG spectrum for Er[hfac]$_4$.

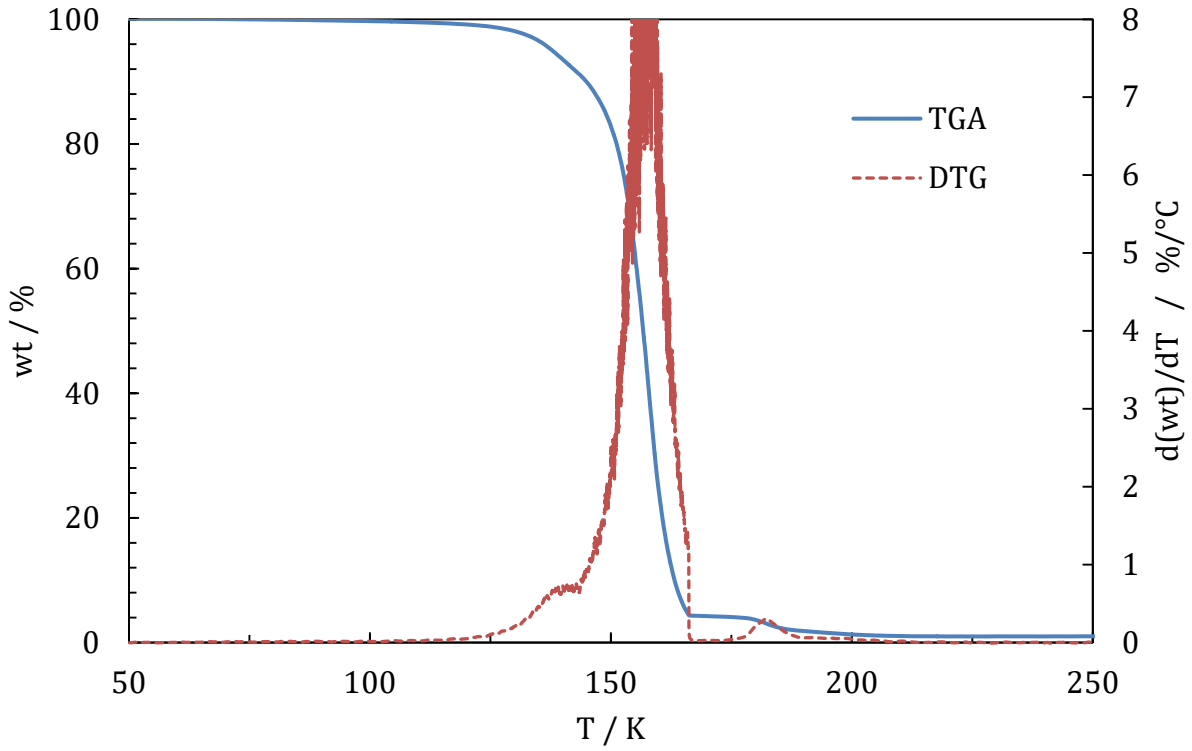

Figure 30: TGA-DTG spectrum for Tm[hfac]$_4$.

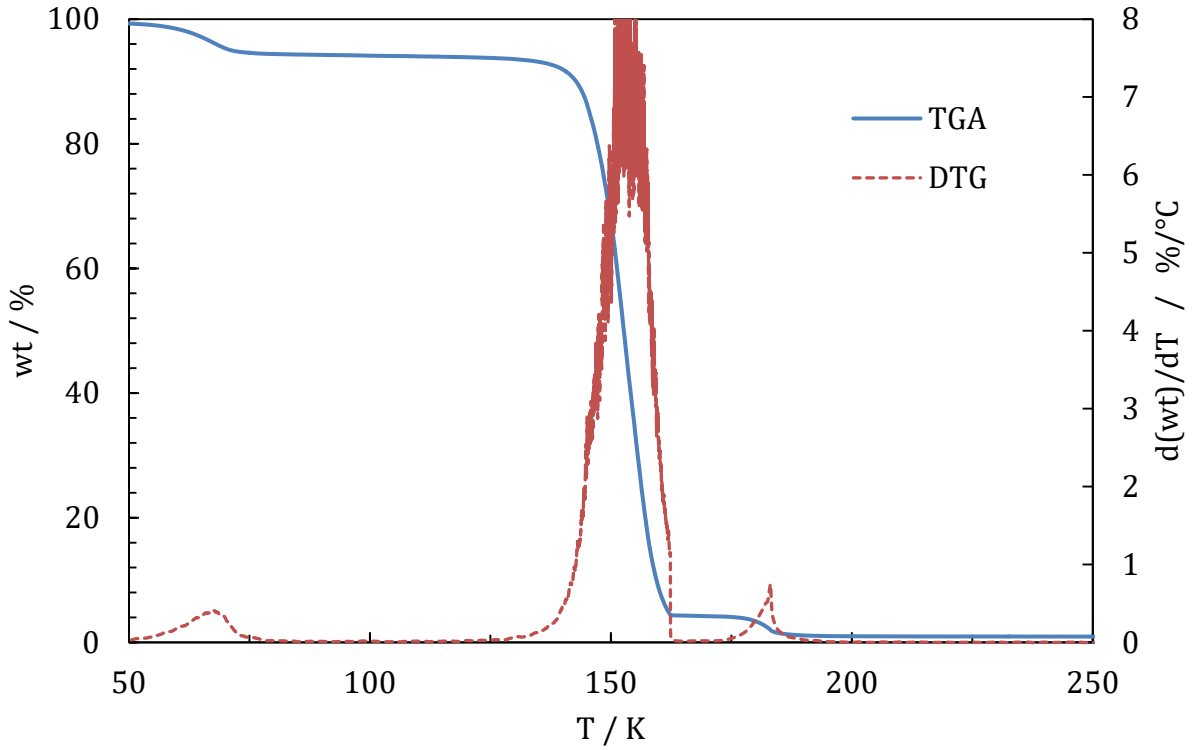

Figure 31: TGA-DTG spectrum for Yb[hfac]$_4$.

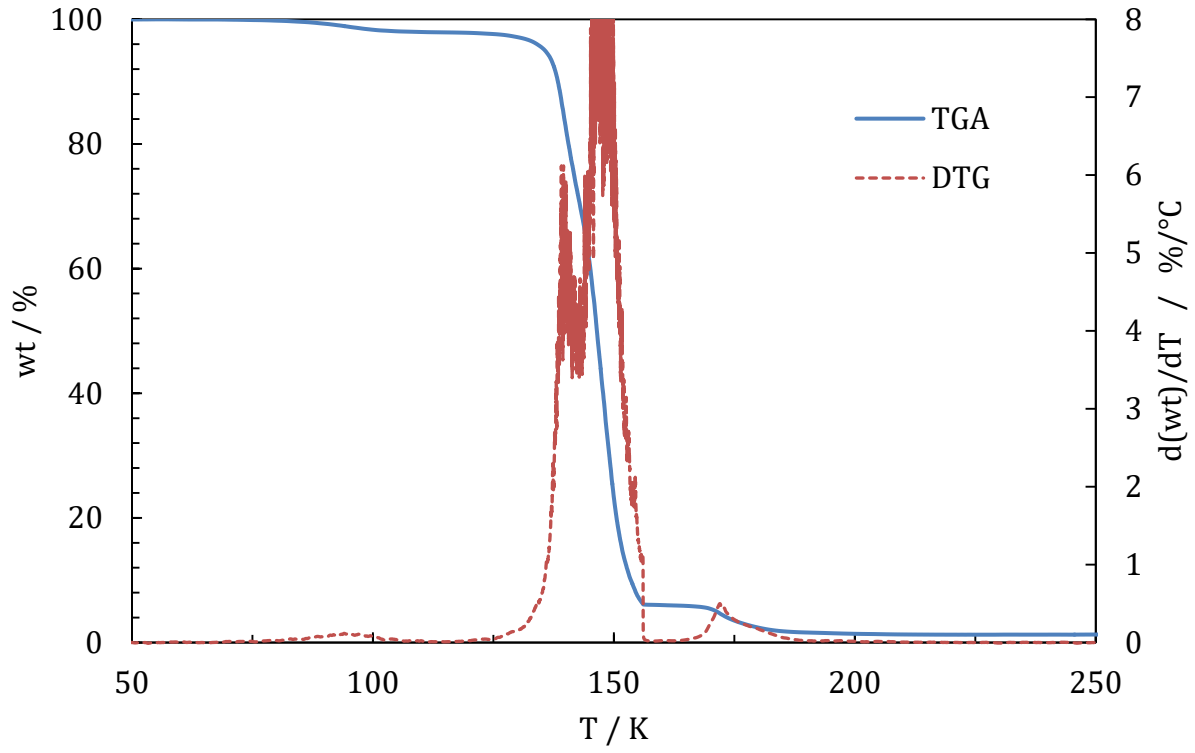

Figure 32: TGA-DTG spectrum for Lu[hfac]$_4$.

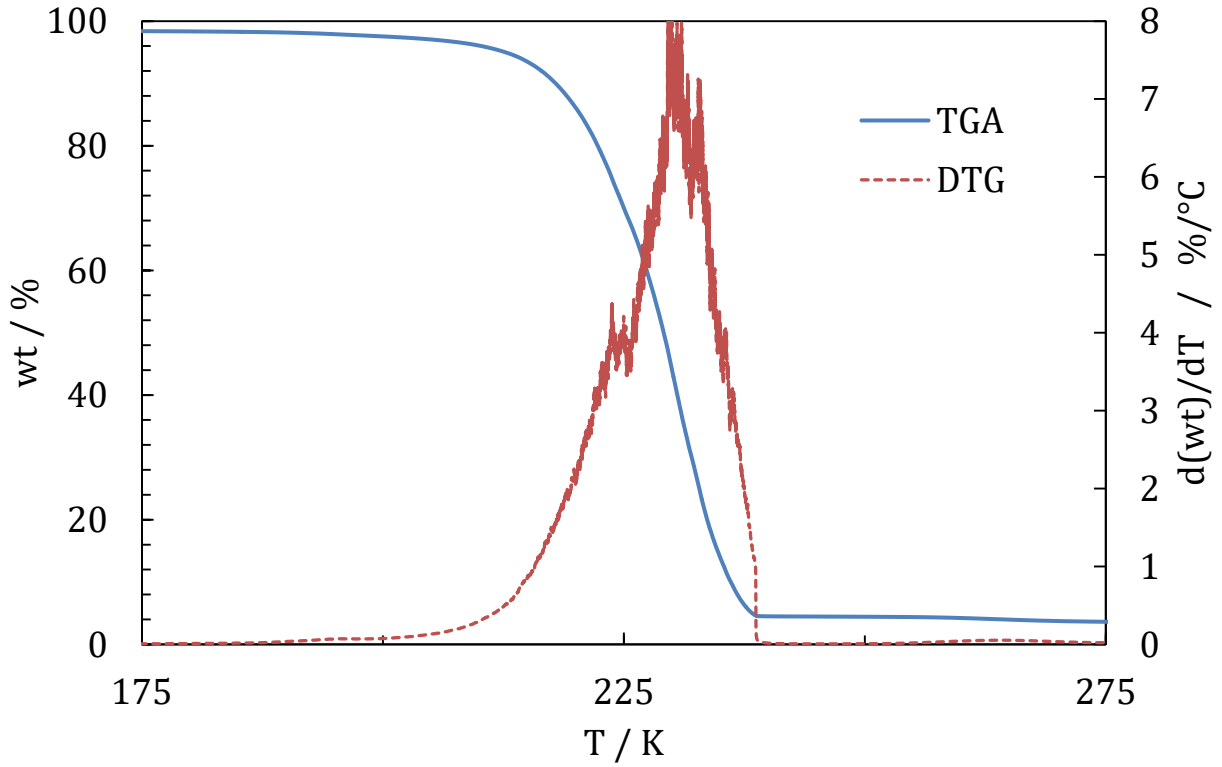

Figure 33: TGA-DTG spectrum for La[dpm]$_4$.

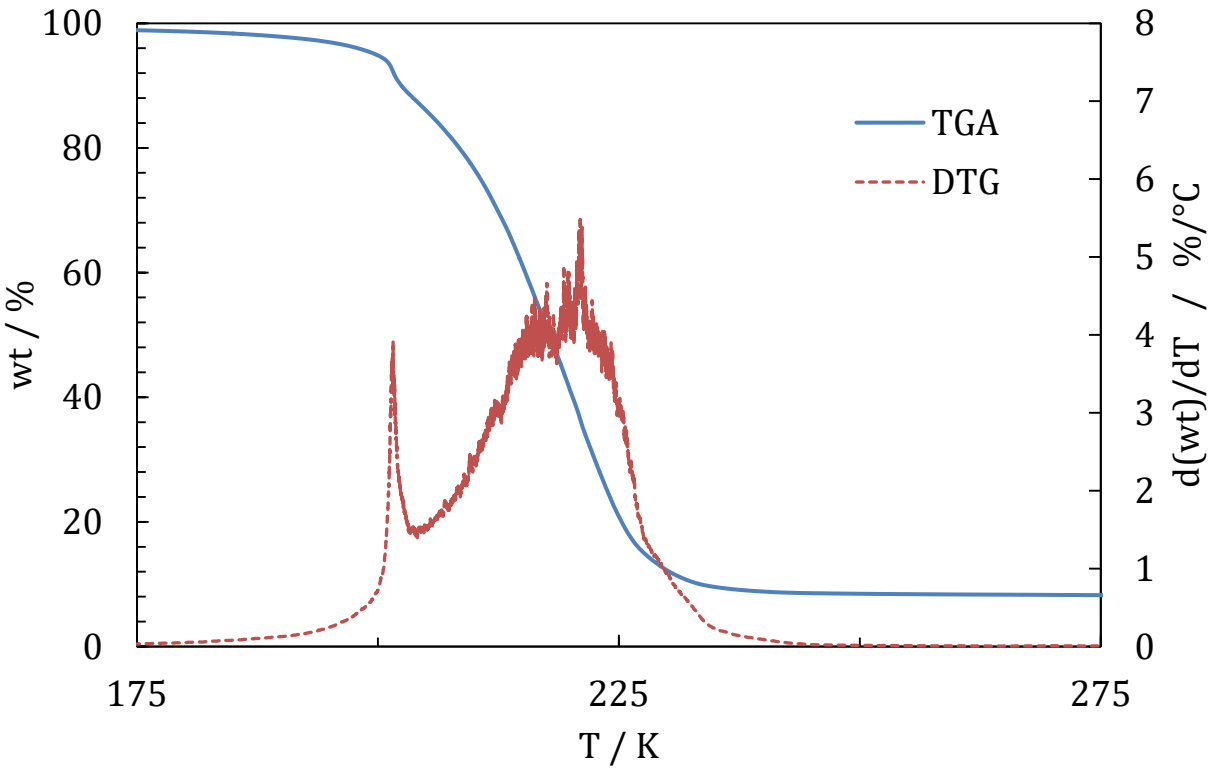

Figure 34: TGA-DTG spectrum for $Ce[dpm]_4$.

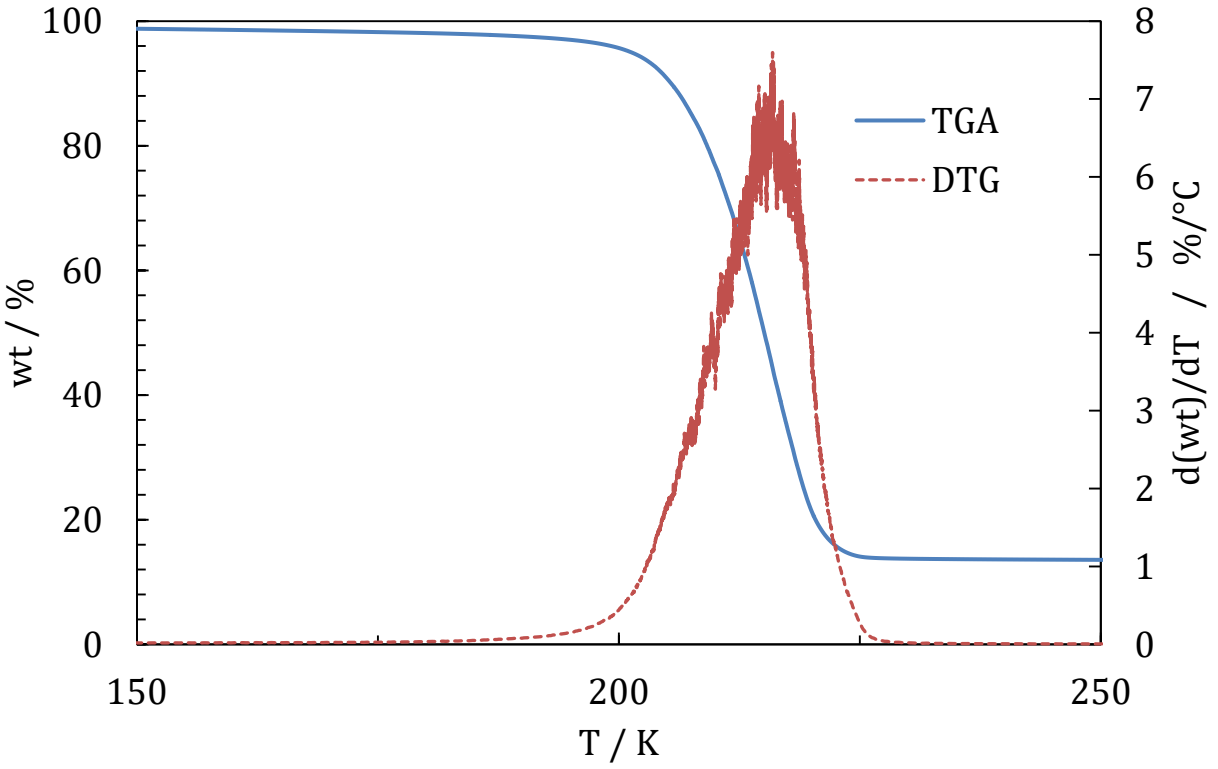

Figure 35: TGA-DTG spectrum for $Pr[dpm]_3$.

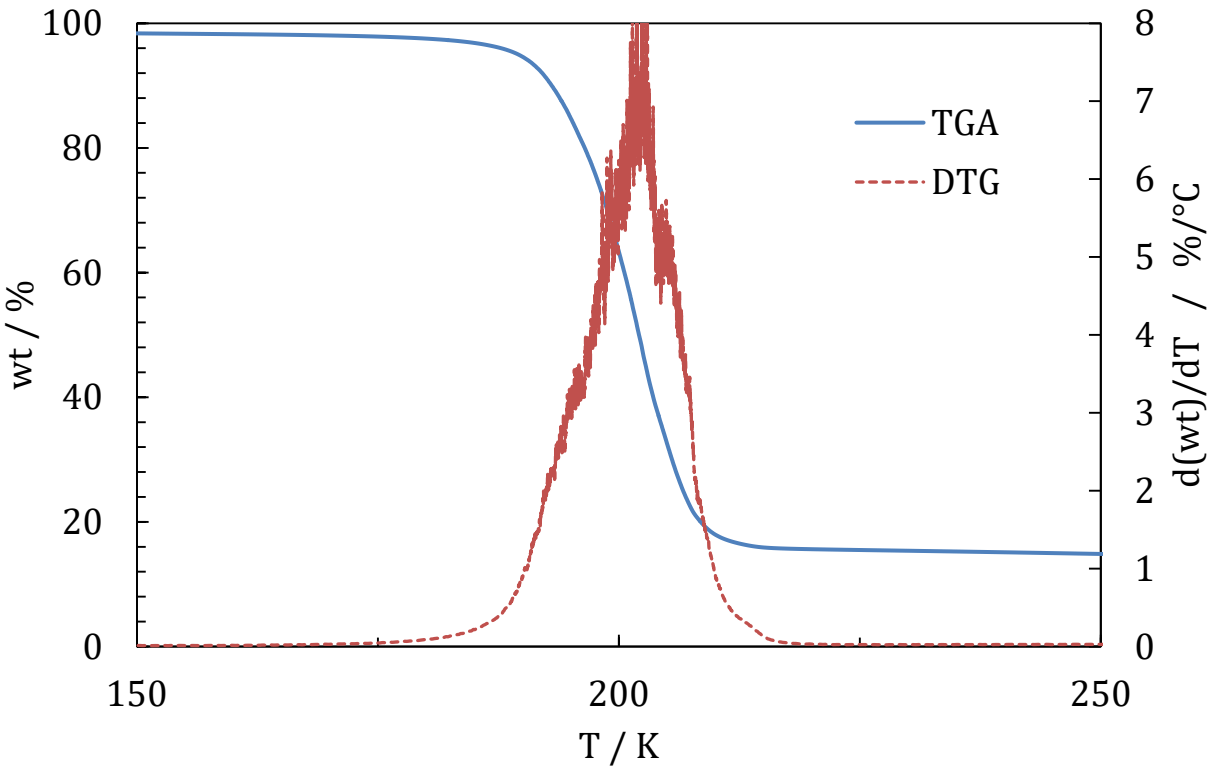

Figure 36: TGA-DTG spectrum for $Nd[dpm]_3$.

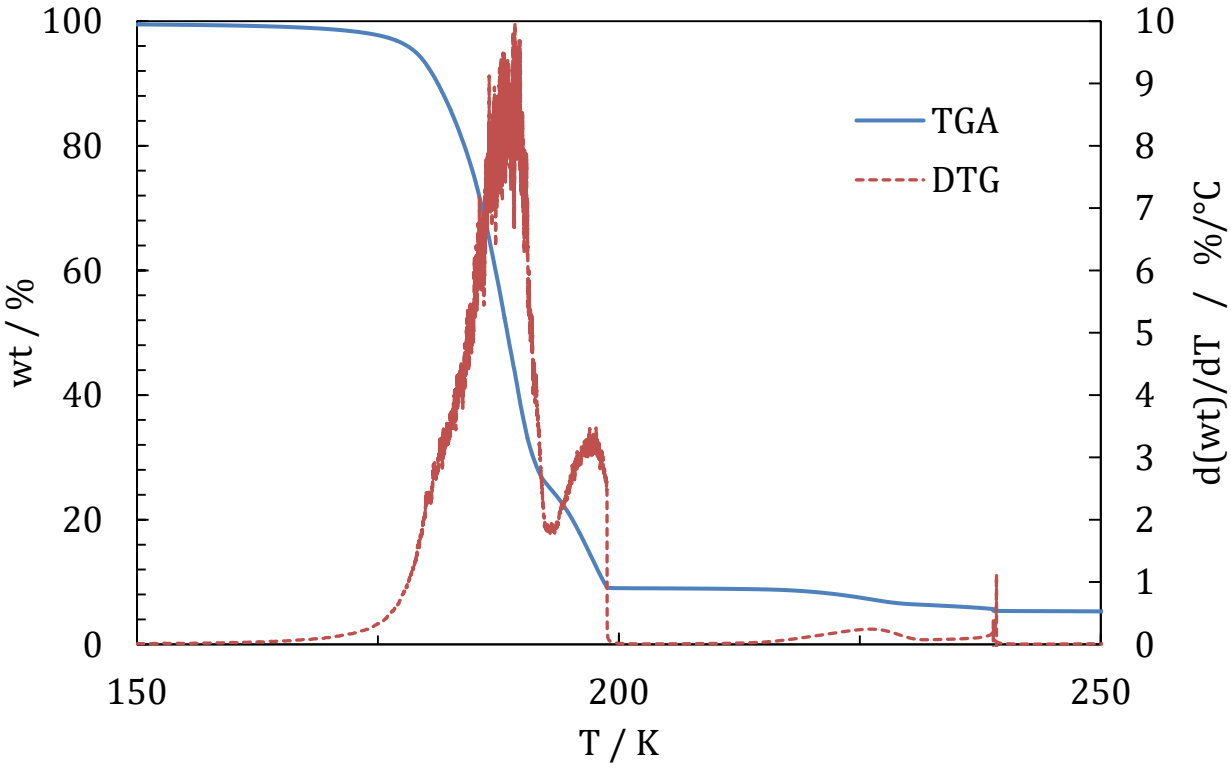

Figure 37: TGA-DTG spectrum for $Sm[dpm]_3$.

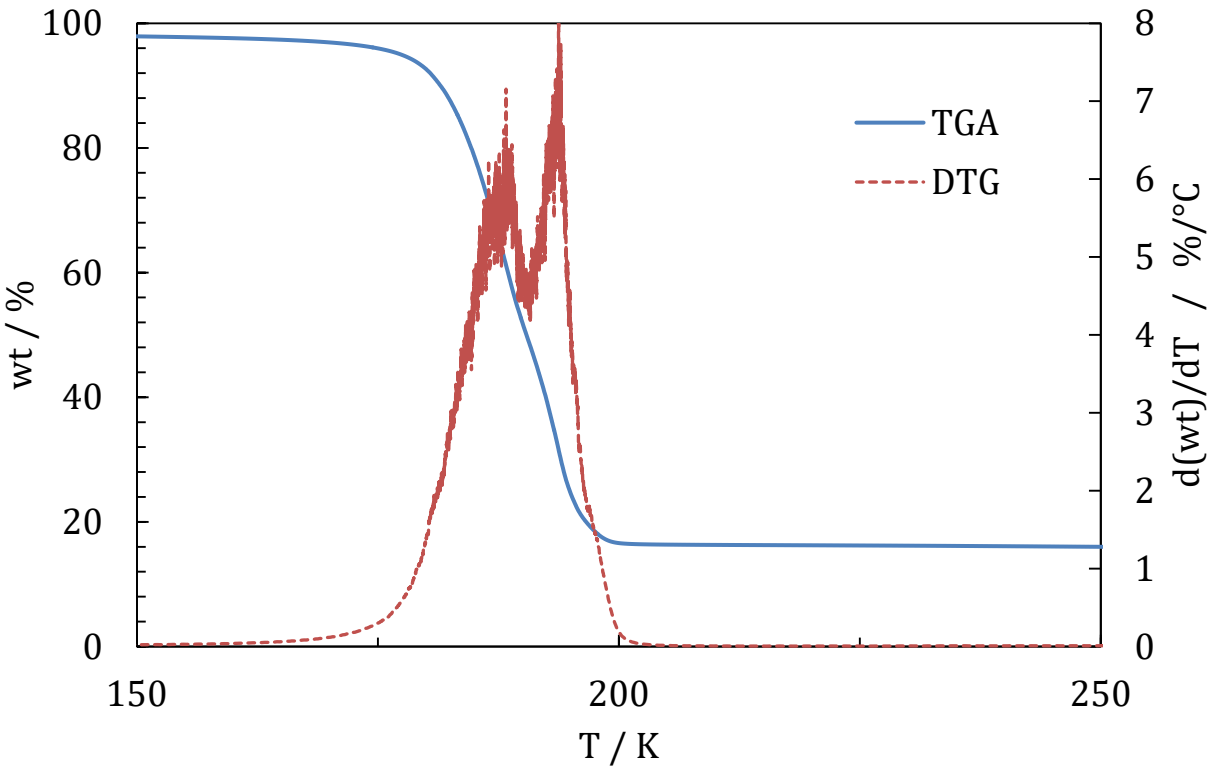

Figure 38: TGA-DTG spectrum for $Eu[dpm]_3$.

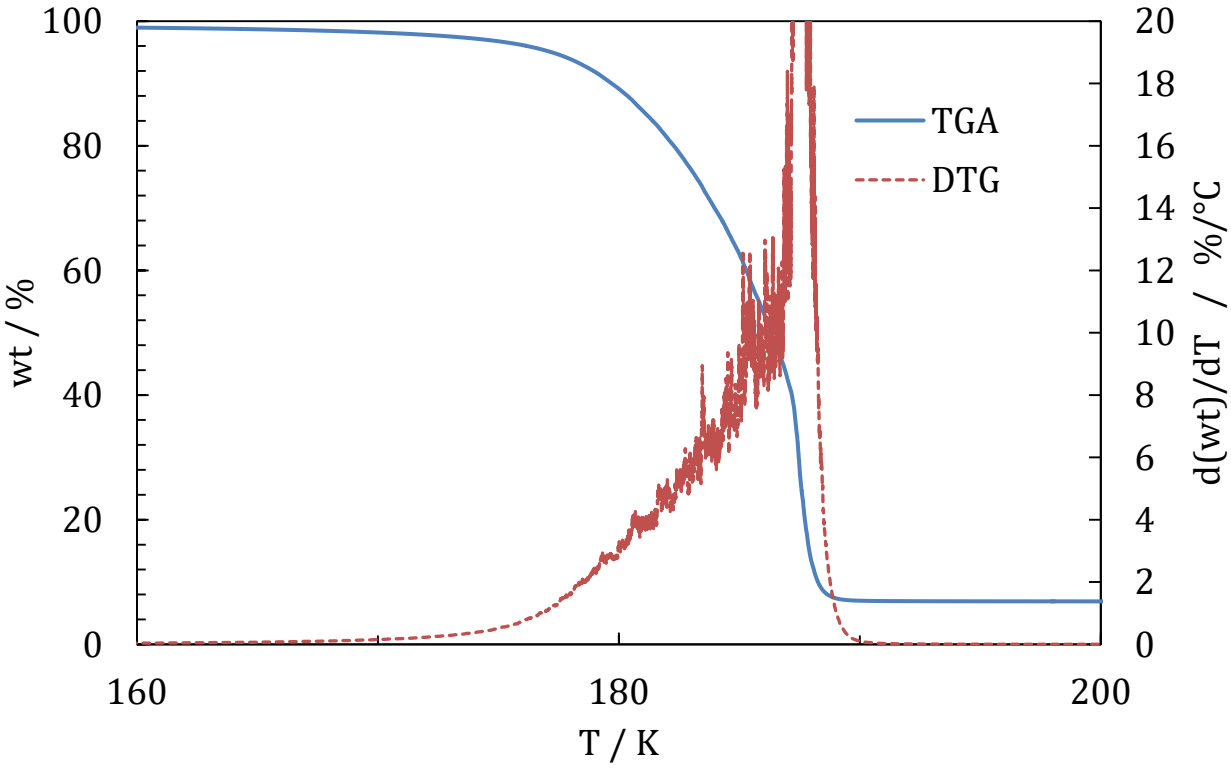

Figure 39: TGA-DTG spectrum for $Gd[dpm]_3$.

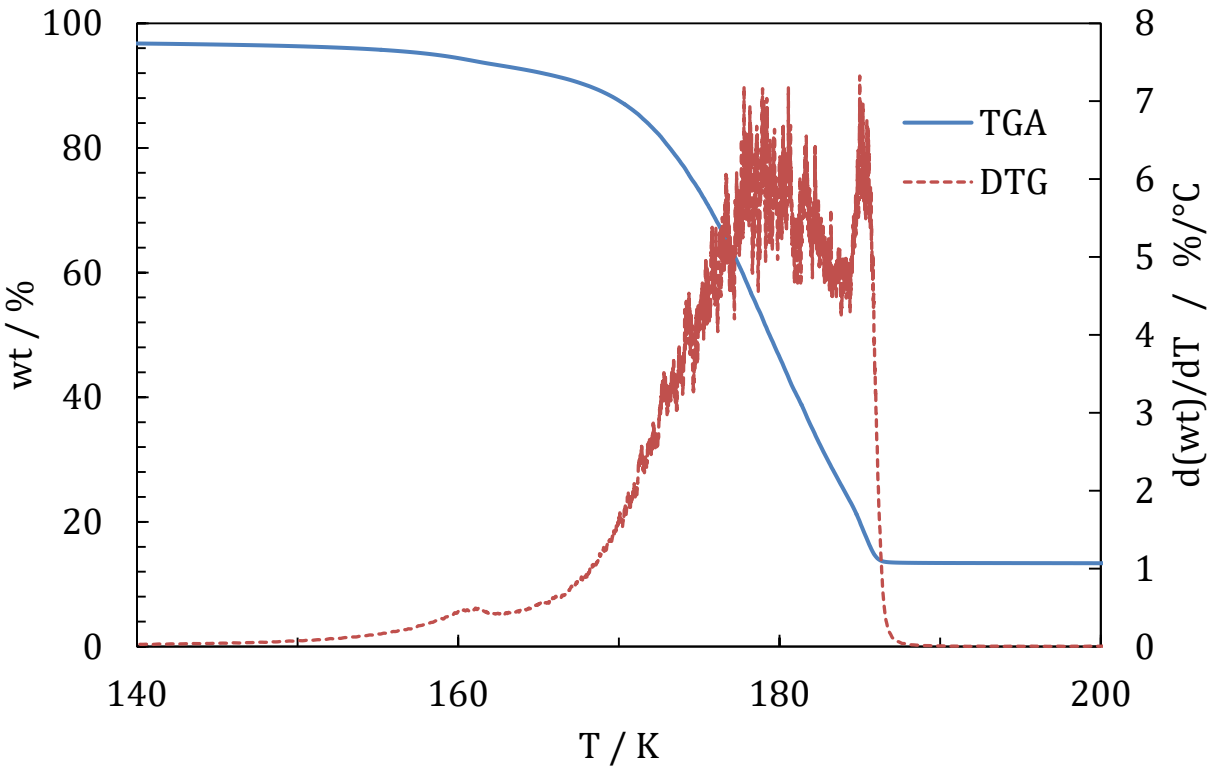

Figure 40: TGA-DTG spectrum for $Tb[dpm]_3$.

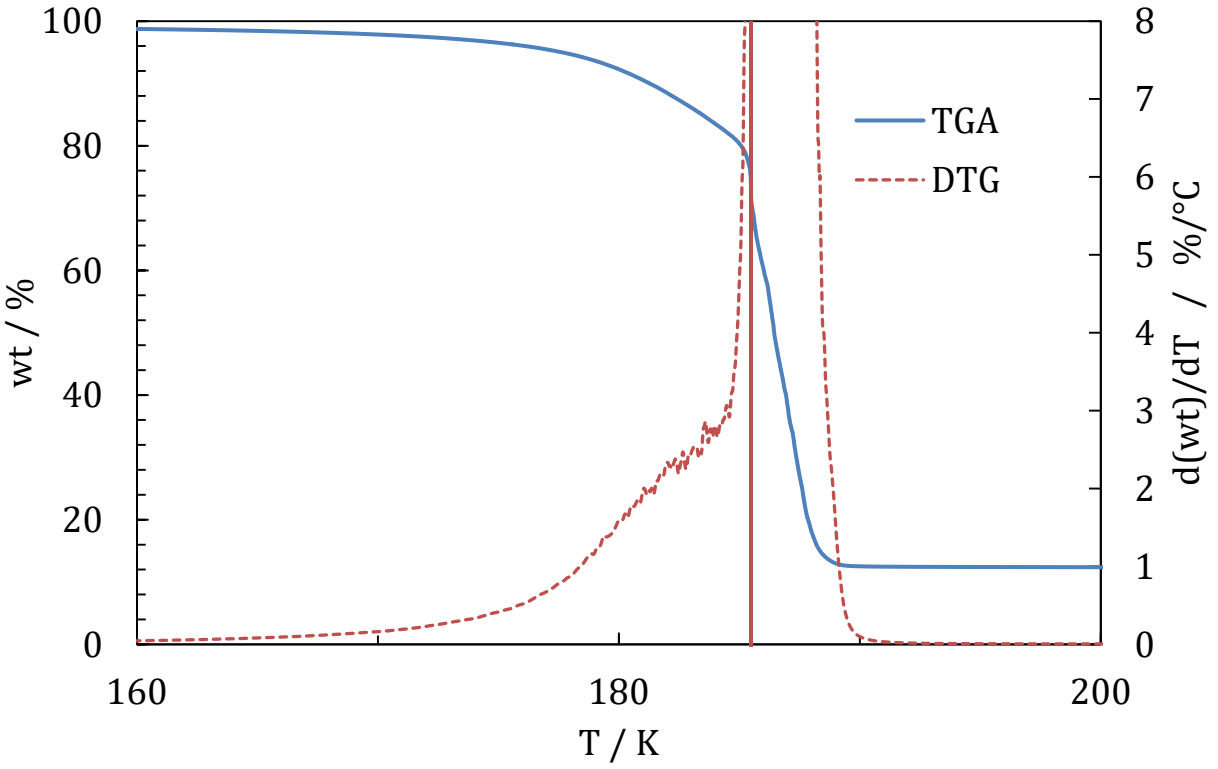

Figure 41: TGA-DTG spectrum for $Dy[dpm]_3$.

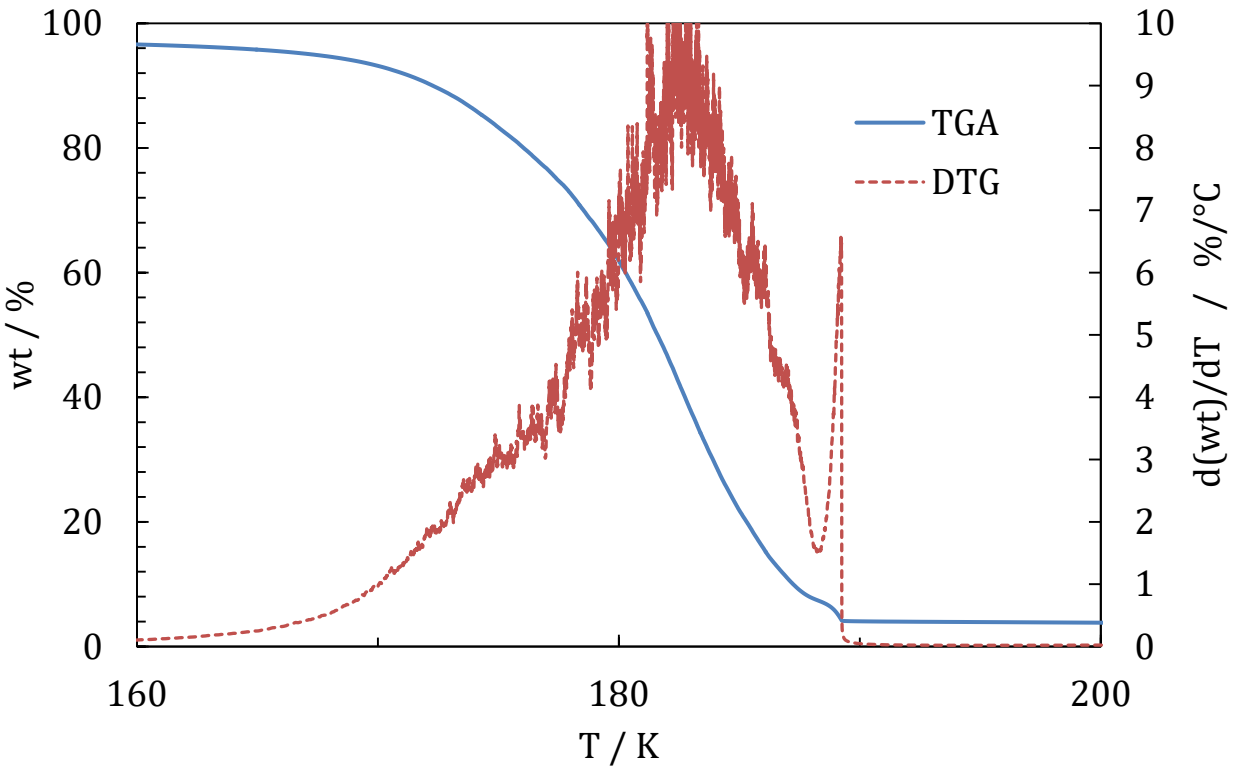

Figure 42: TGA-DTG spectrum for Ho[dpm]$_3$.

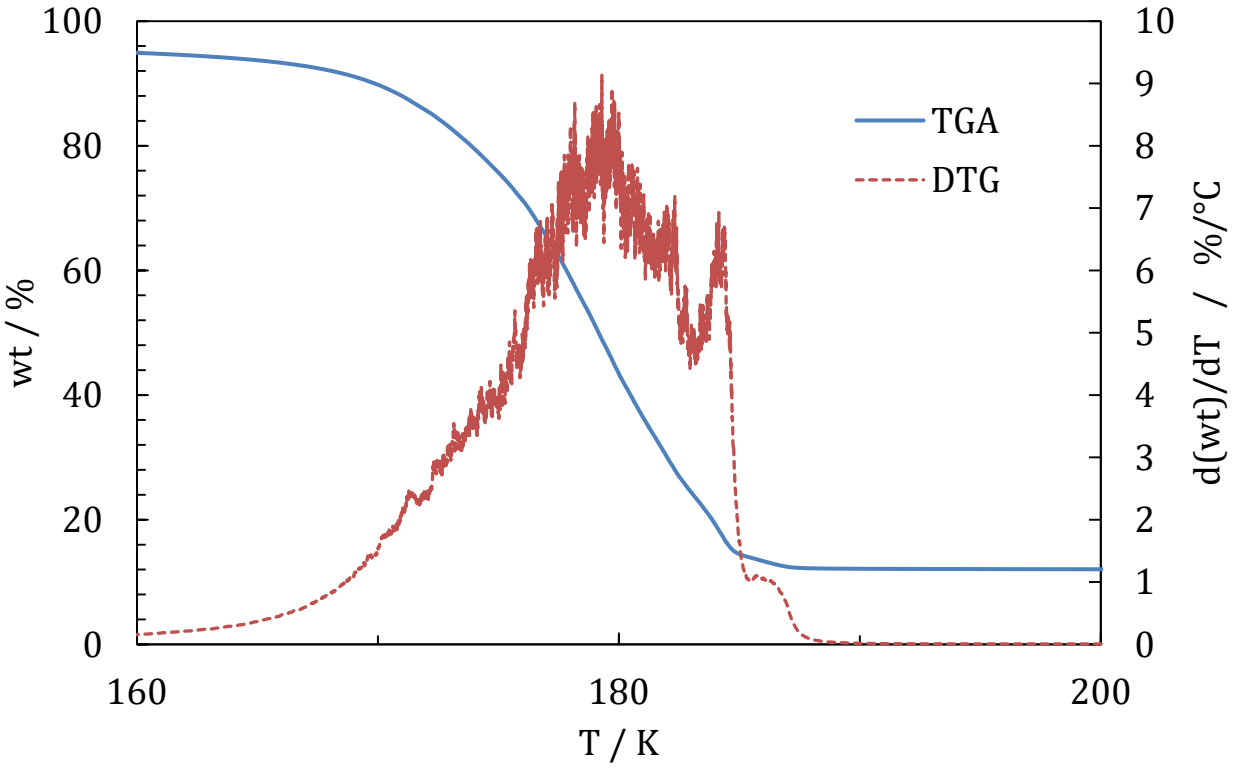

Figure 43: TGA-DTG spectrum for Er[dpm]$_3$.

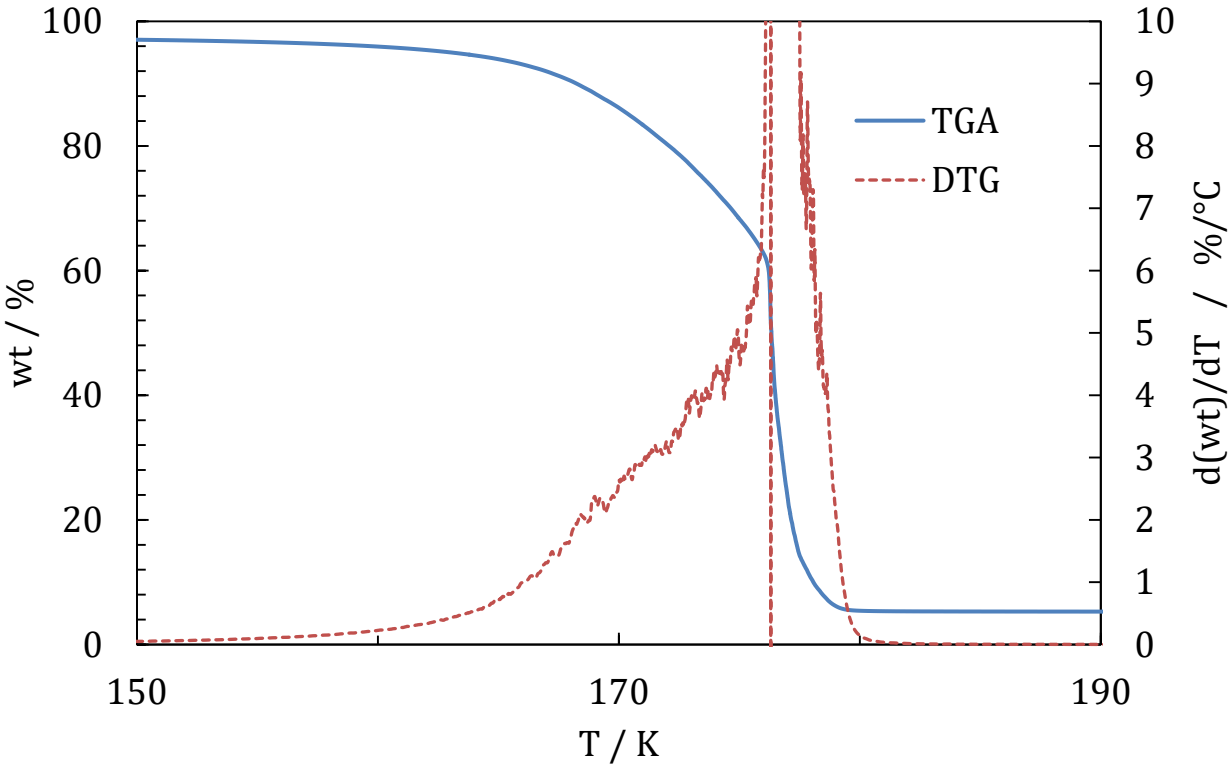

Figure 44: TGA-DTG spectrum for $Tm[dpm]_3$.

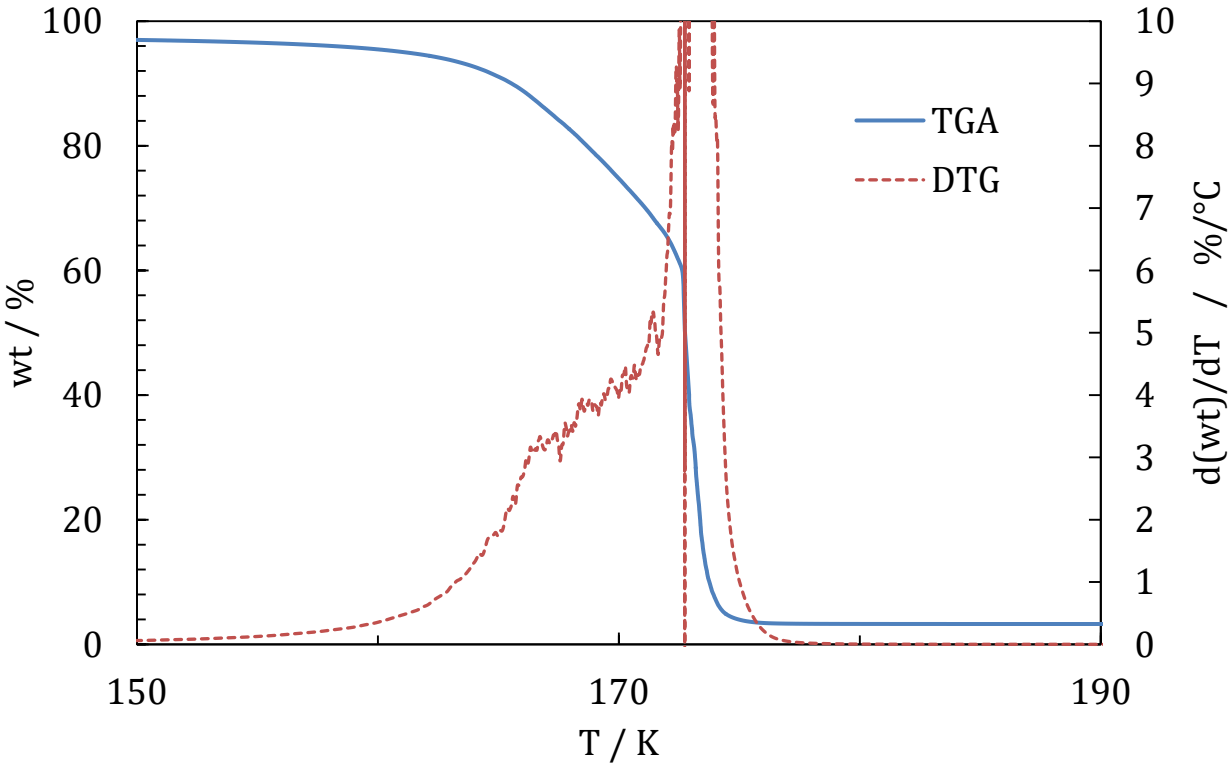

Figure 45: TGA-DTG spectrum for $Yb[dpm]_3$.

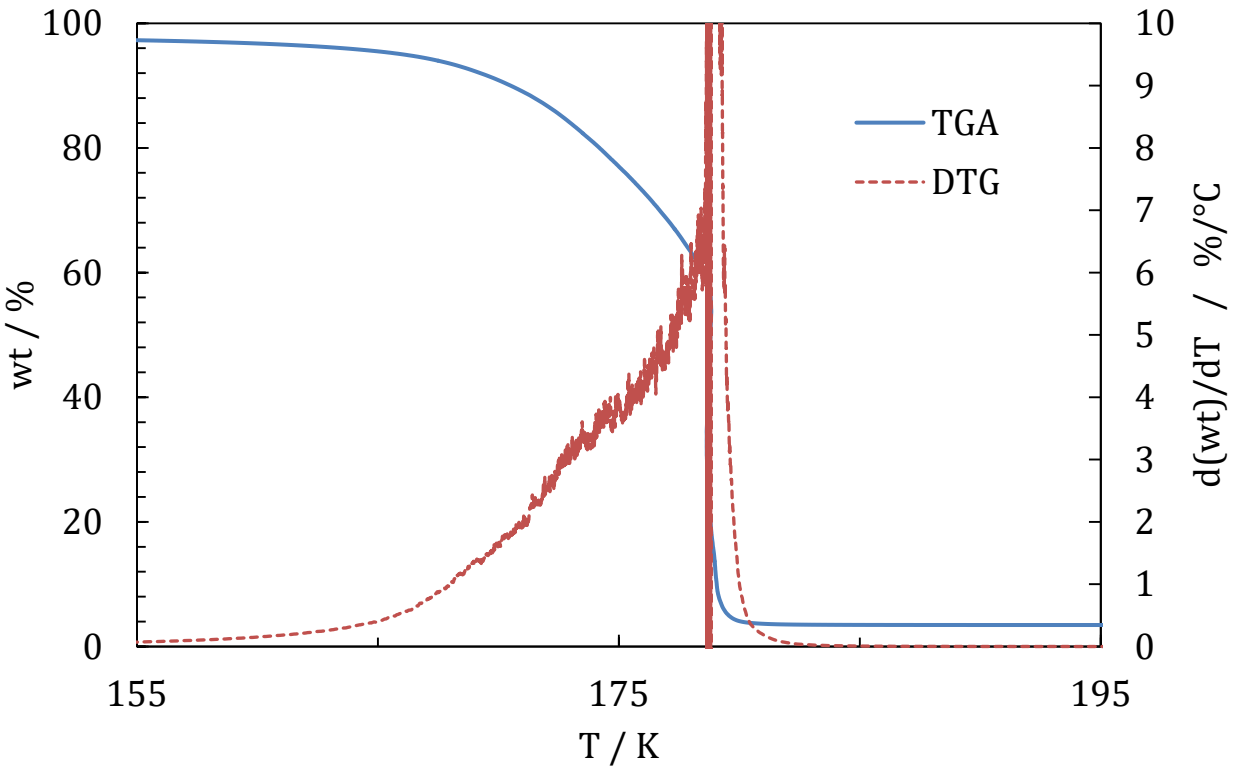

Figure 46: TGA-DTG spectrum for Lu[dpm]$_3$.

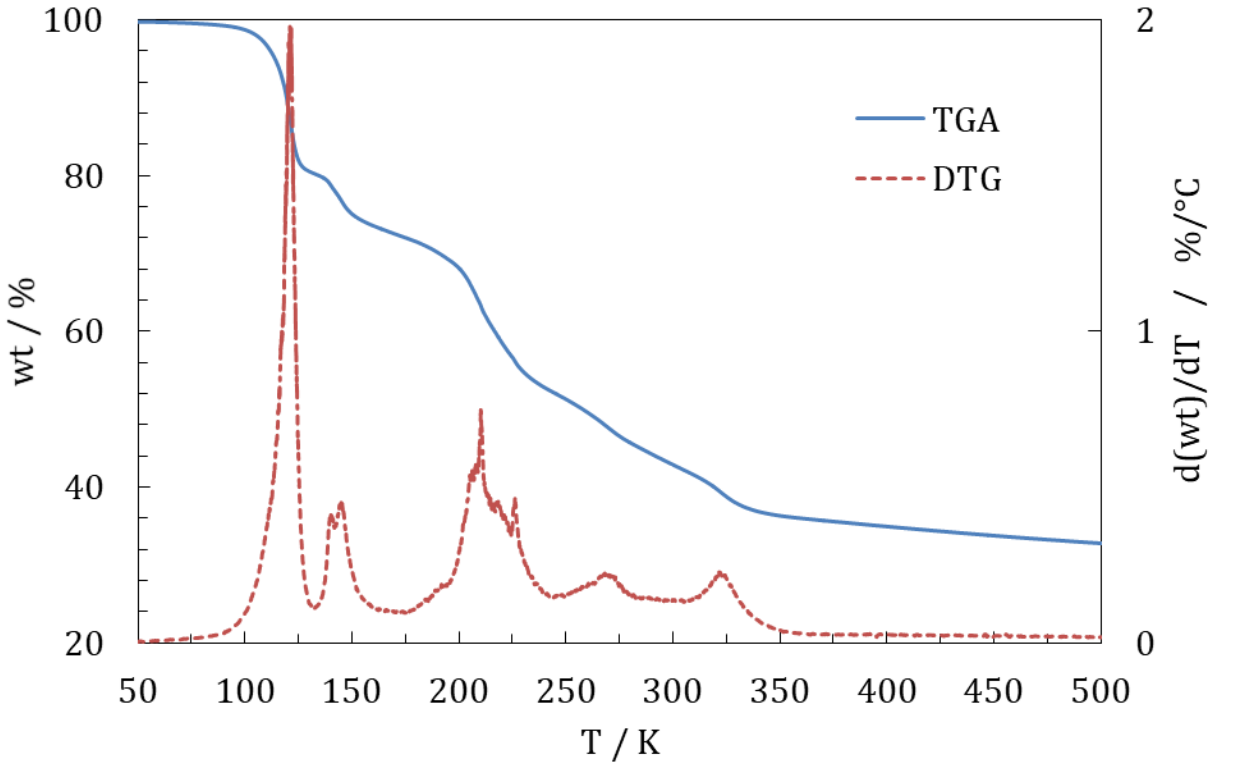

Figure 47: TGA-DTG spectrum for La[tfac]$_3$ ammine.

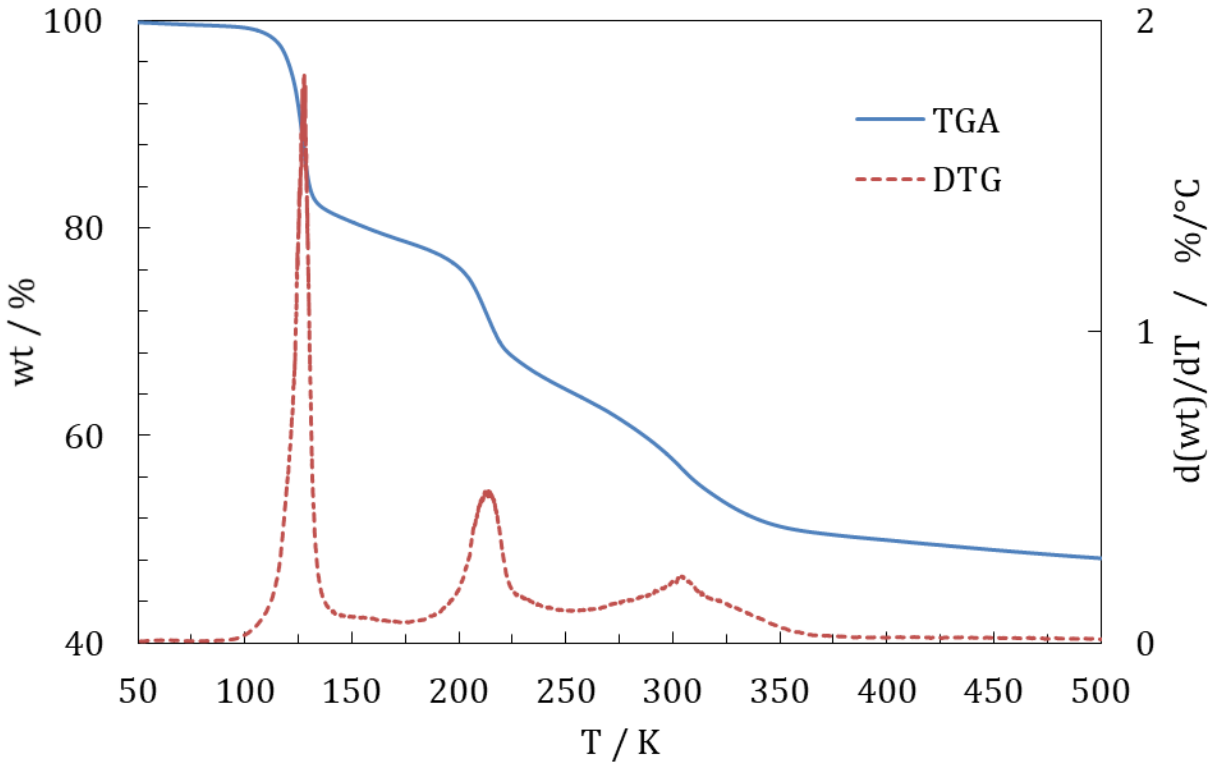

Figure 48: TGA-DTG spectrum for Ce[tfac]$_3$ ammine.

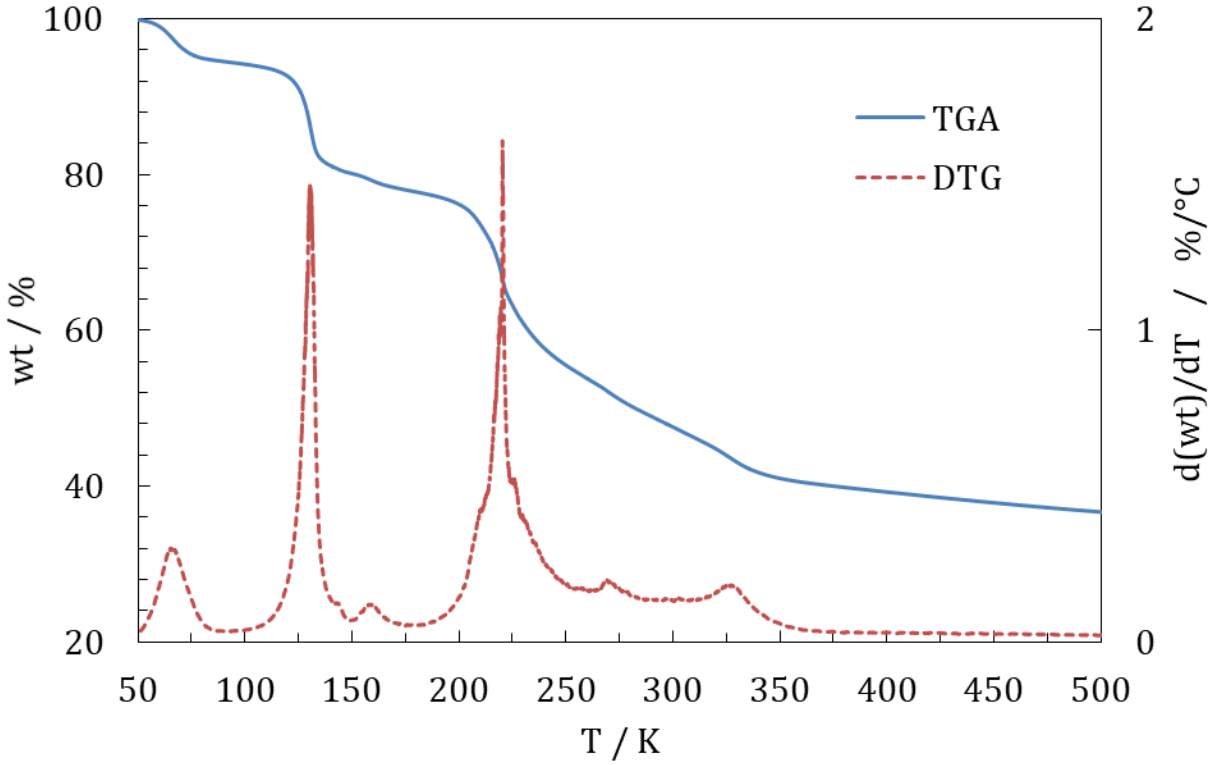

Figure 49: TGA-DTG spectrum for Pr[tfac]$_3$ ammine.

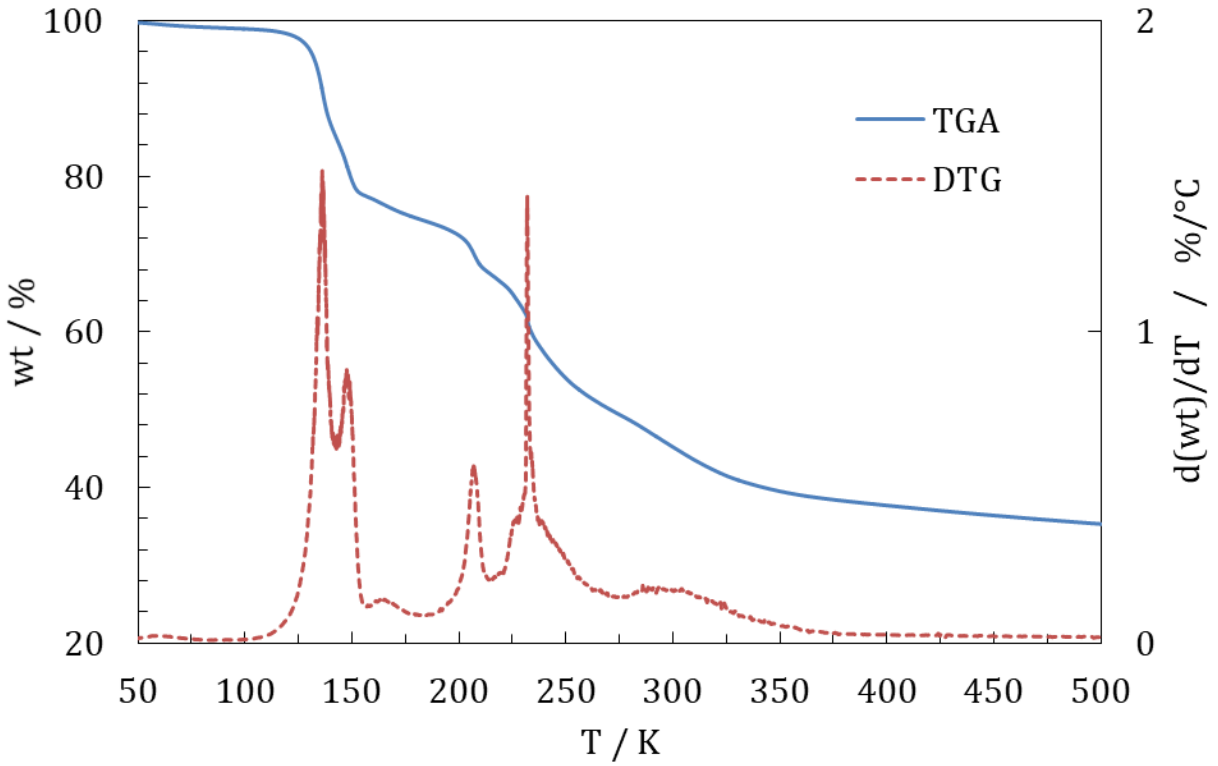

Figure 50: TGA-DTG spectrum for Eu[tfac]$_3$ ammine.

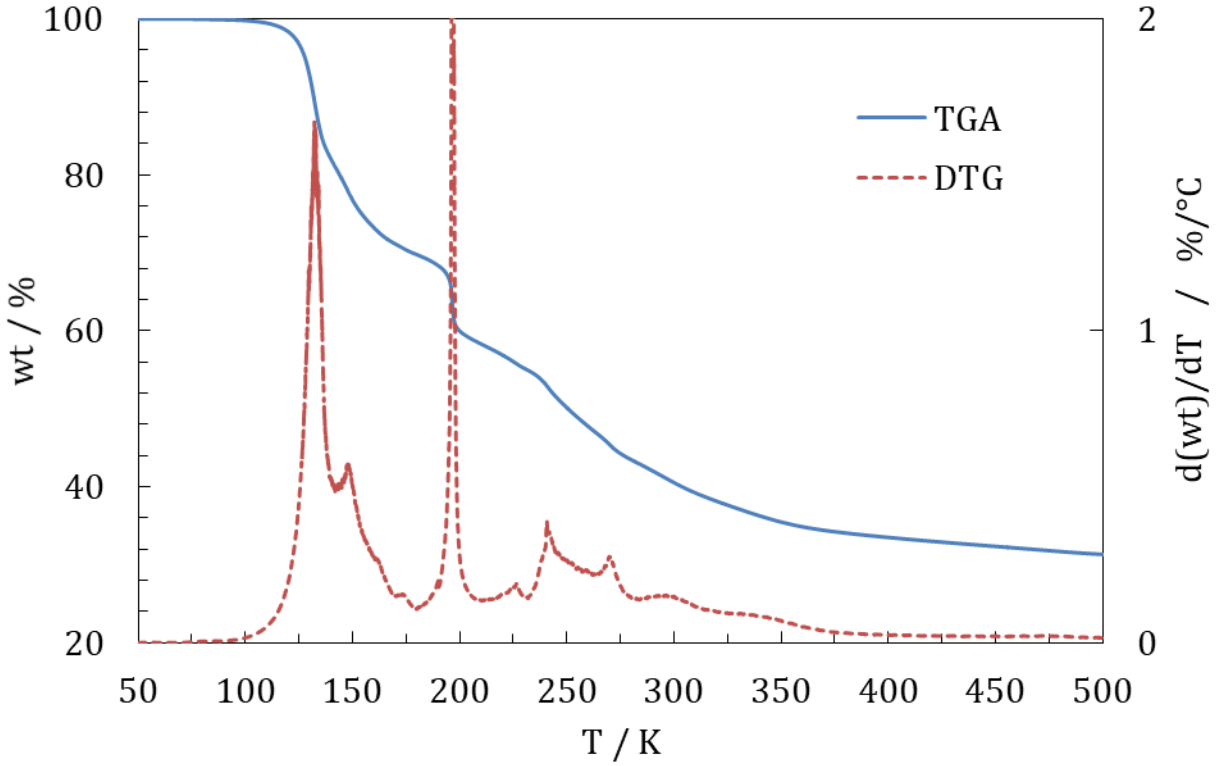

Figure 51: TGA-DTG spectrum for Er[tfac]$_3$ ammine.

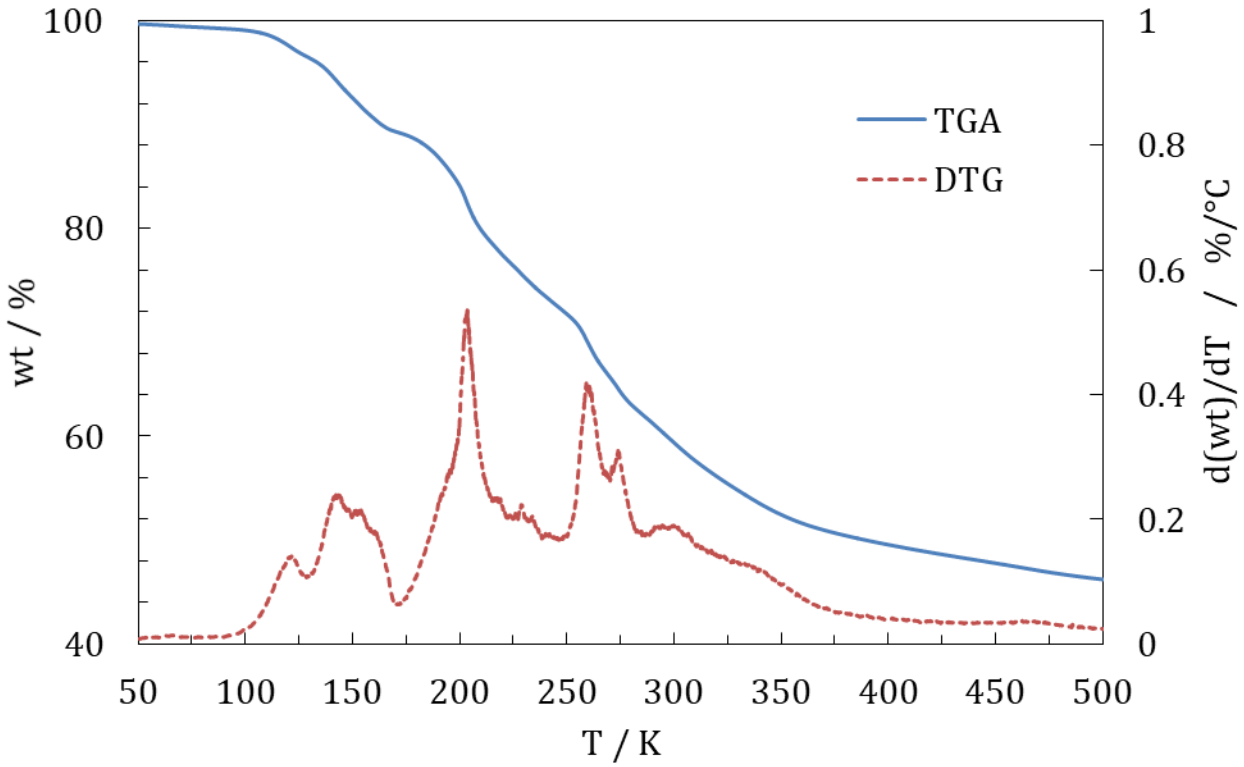

Figure 52: TGA-DTG spectrum for Lu[tfac]$_3$ ammine.

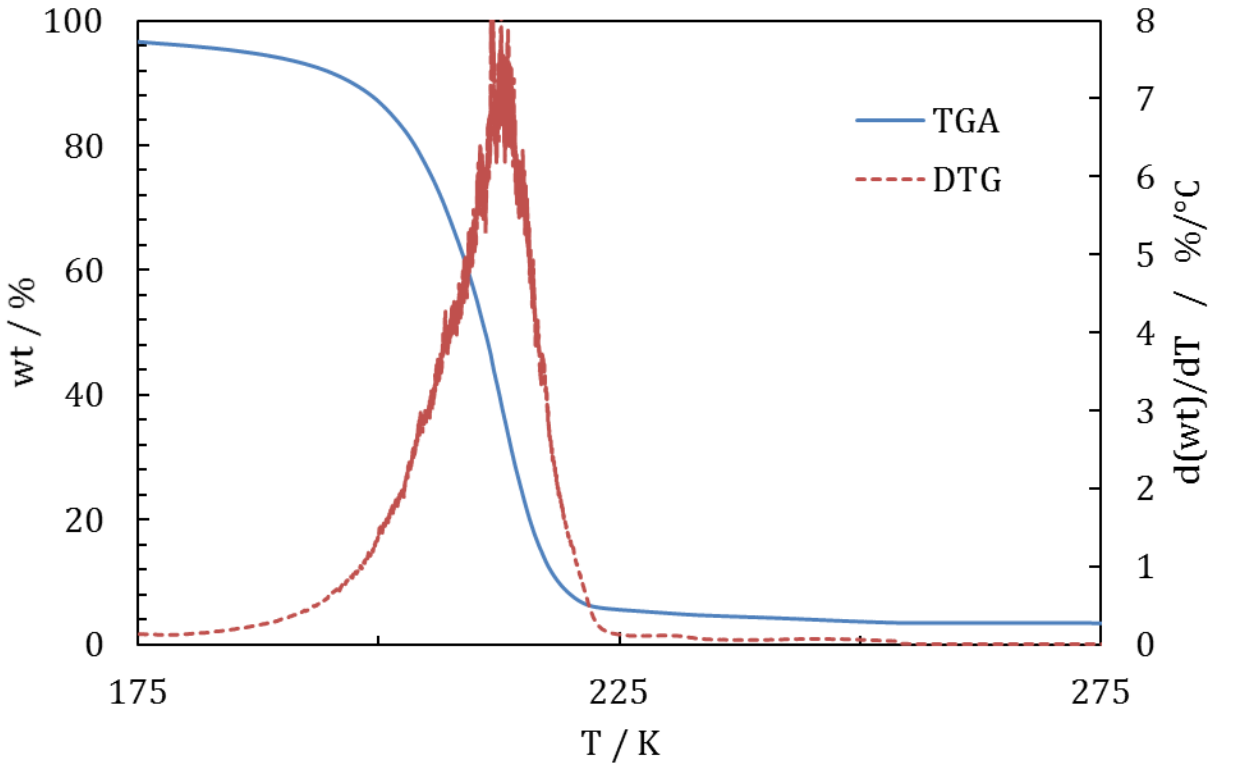

Figure 53: TGA-DTG spectrum for La[fod]$_3$.

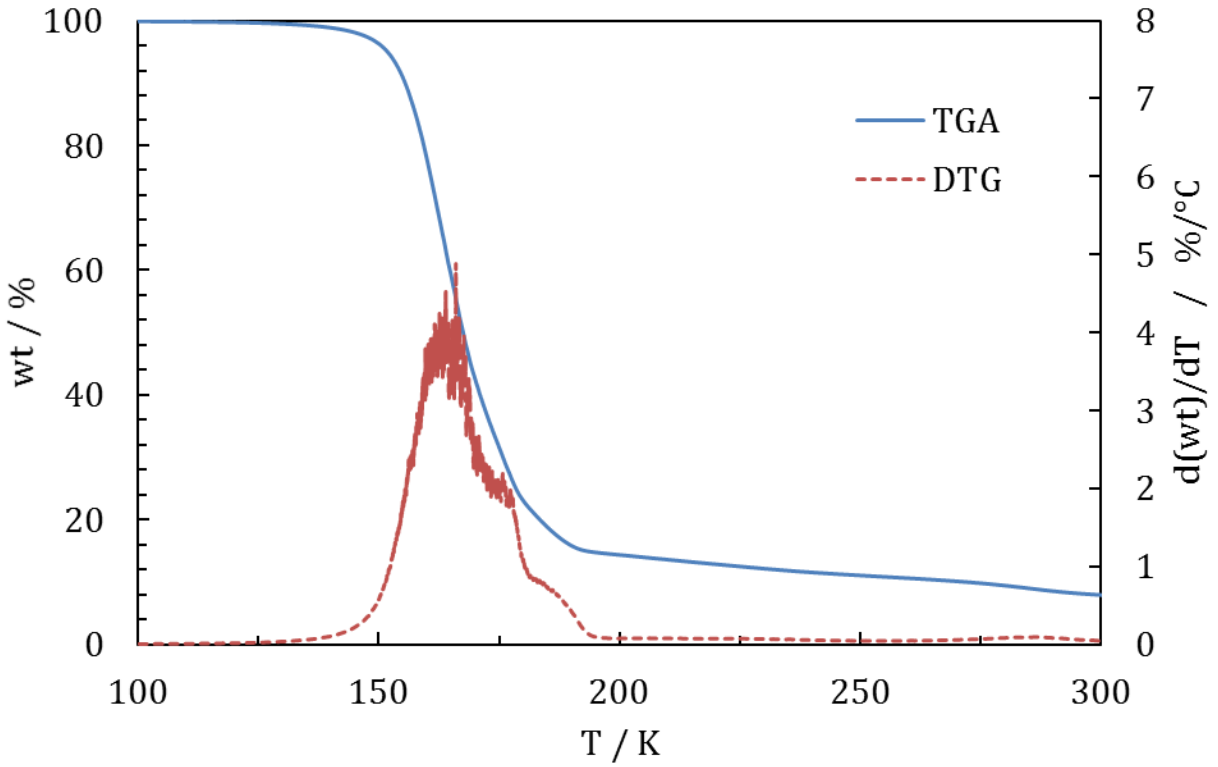

Figure 54: TGA-DTG spectrum for Ce[fod]$_3$.

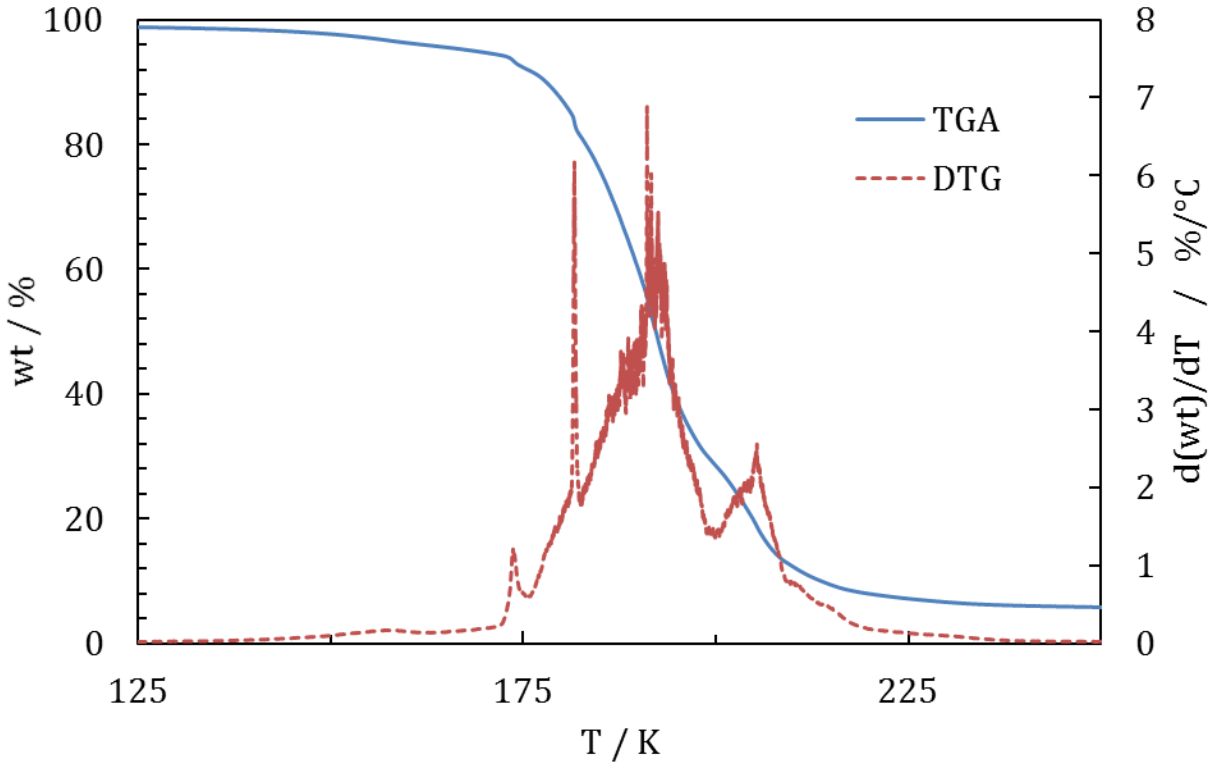

Figure 55: TGA-DTG spectrum for Pr[fod]$_3$.

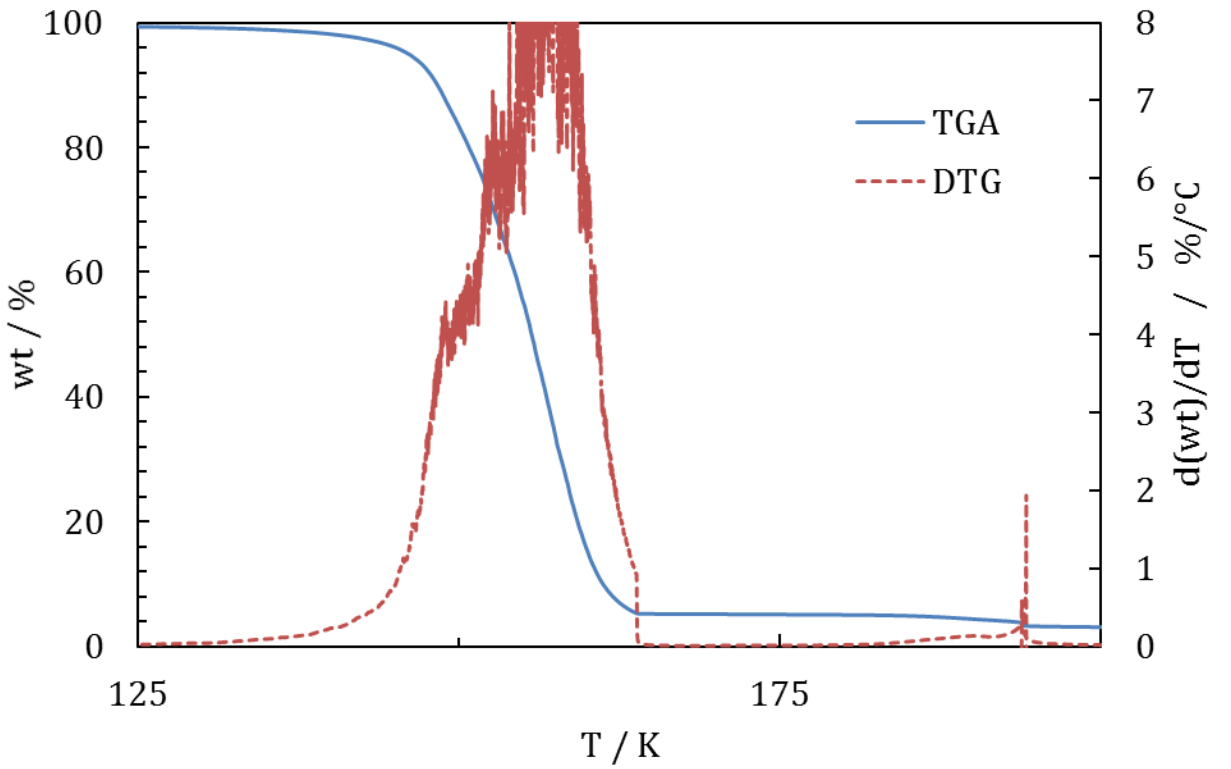

Figure 56: TGA-DTG spectrum for Nd[fod]$_3$.

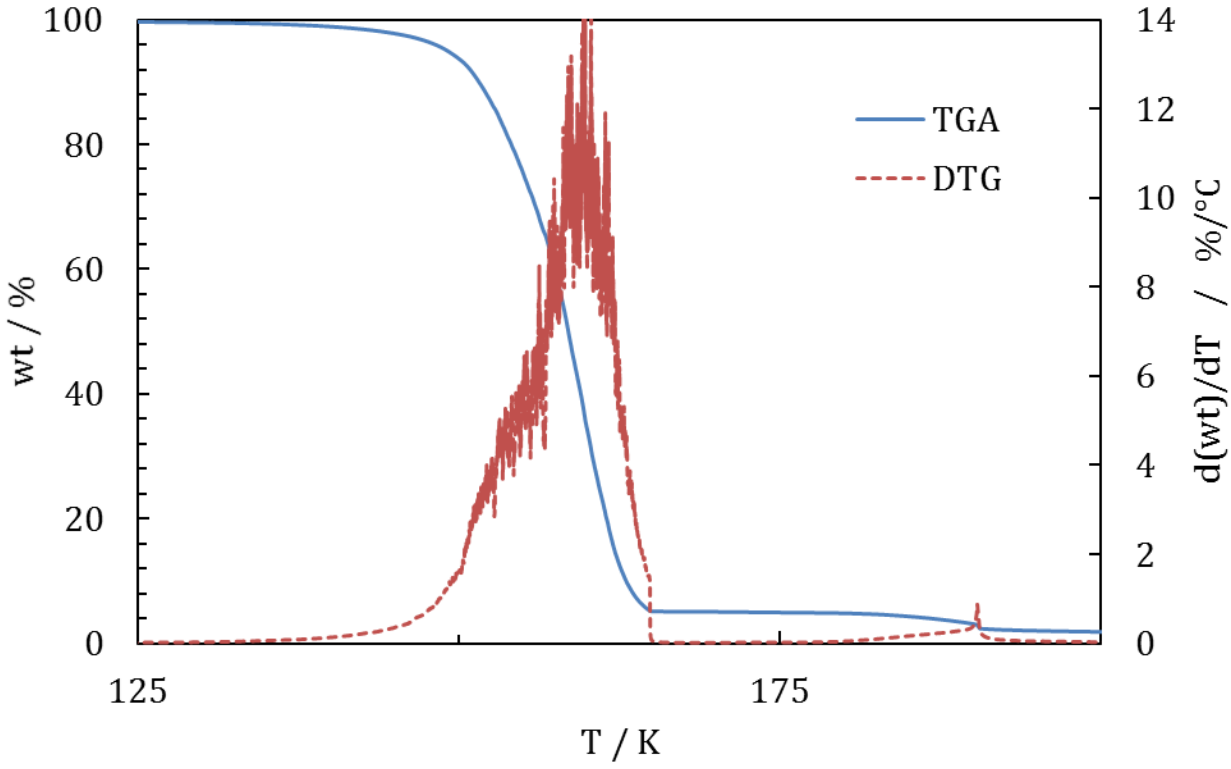

Figure 57: TGA-DTG spectrum for Sm[fod]$_3$.

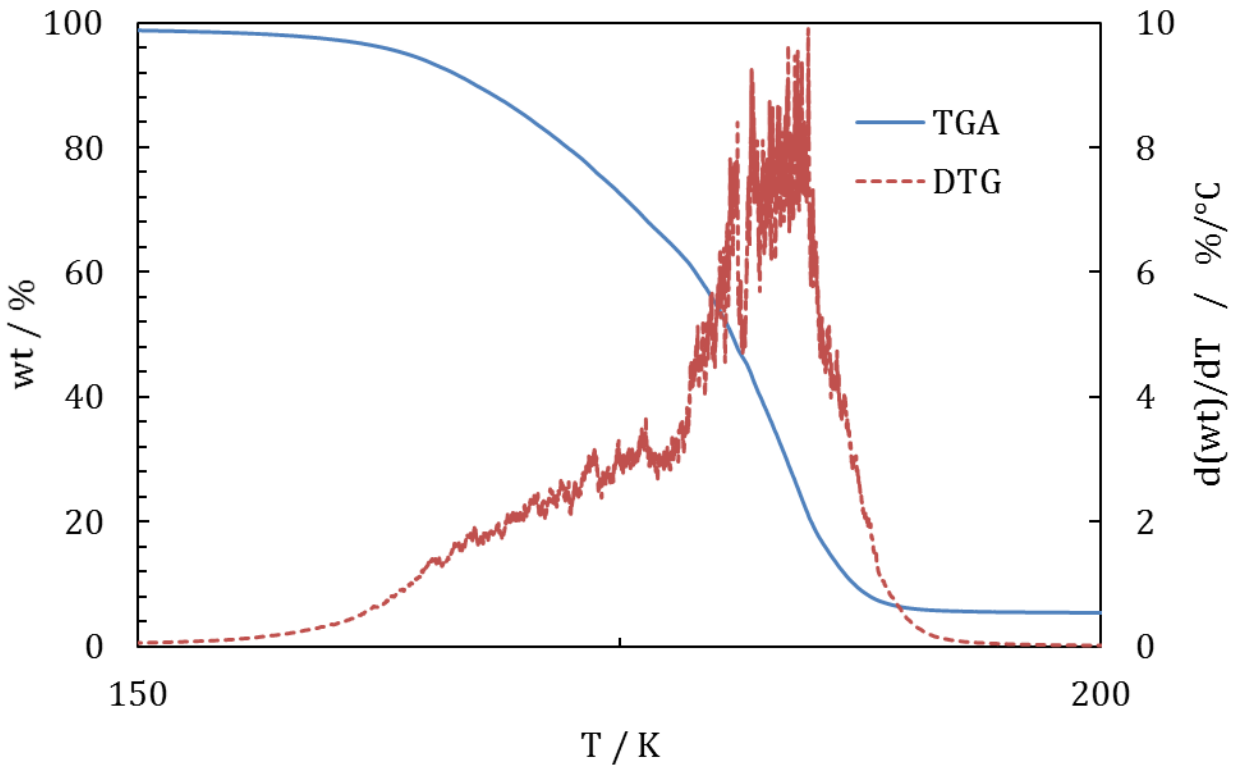

Figure 58: TGA-DTG spectrum for Eu[fod]$_3$.

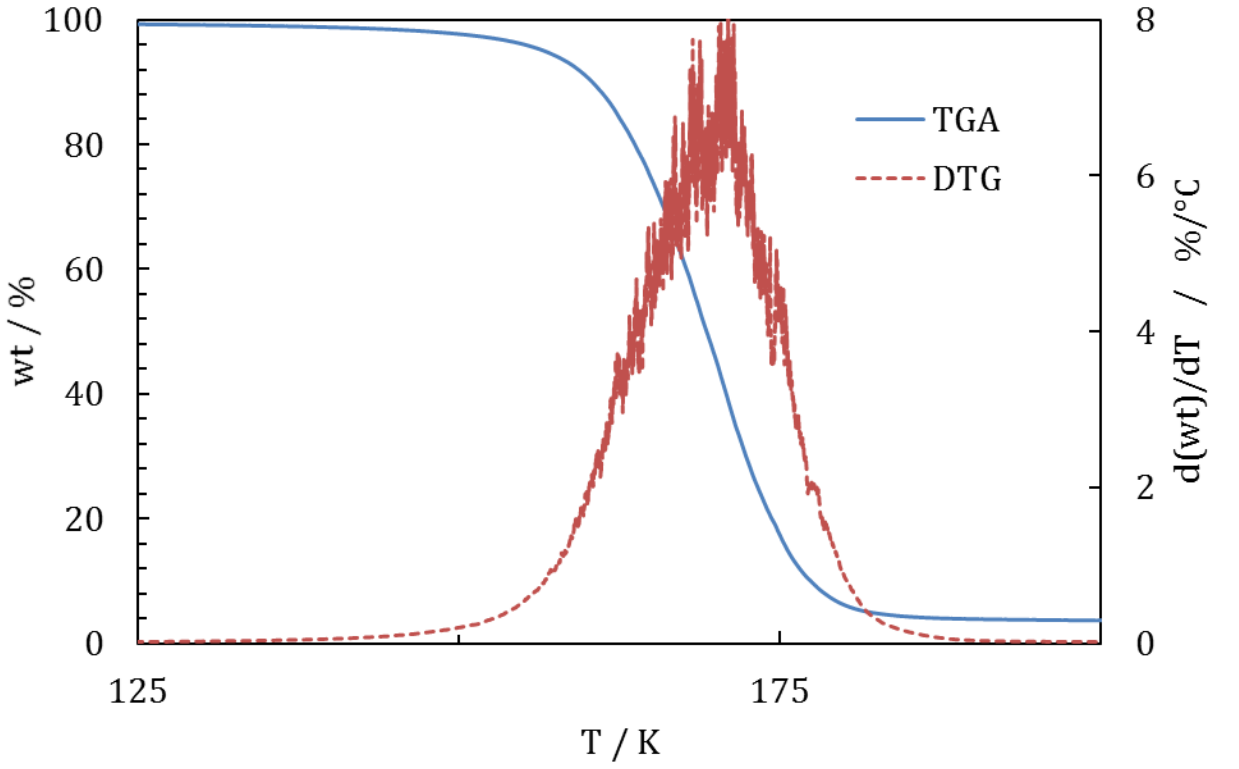

Figure 59: TGA-DTG spectrum for Gd[fod]$_3$.

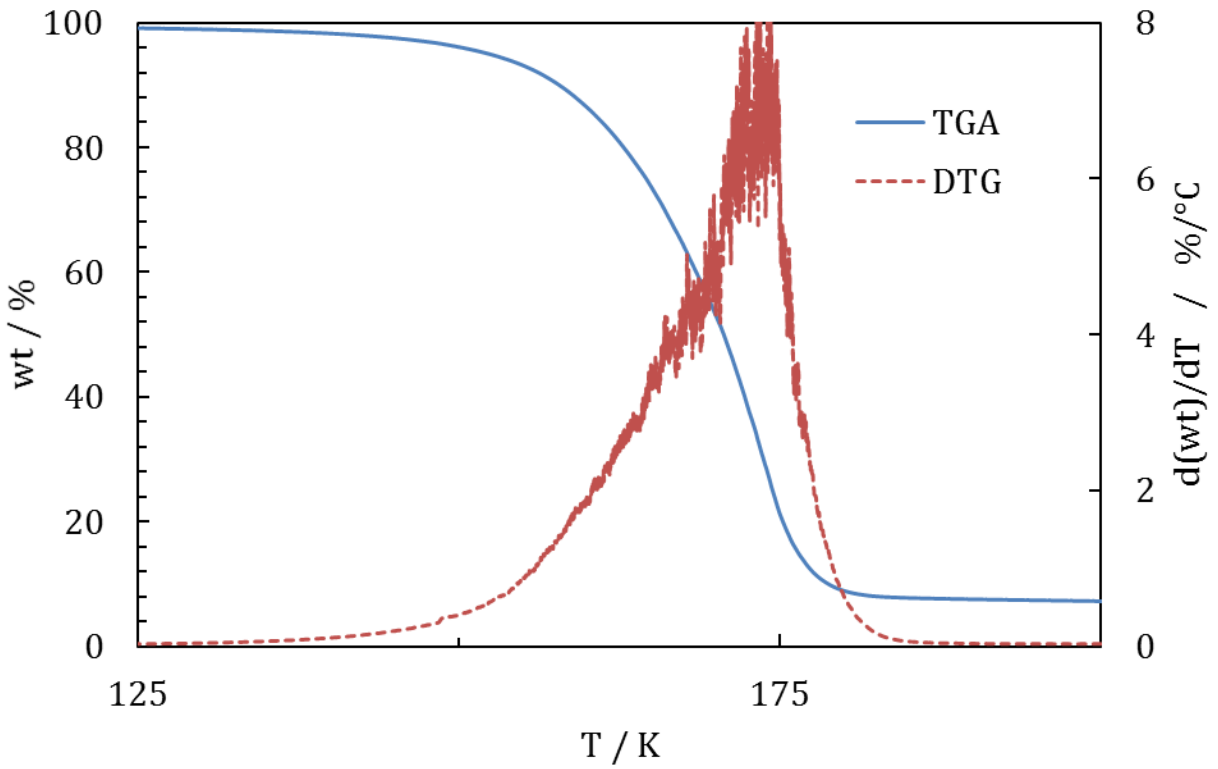

Figure 60: TGA-DTG spectrum for $Tb[fod]_3$.

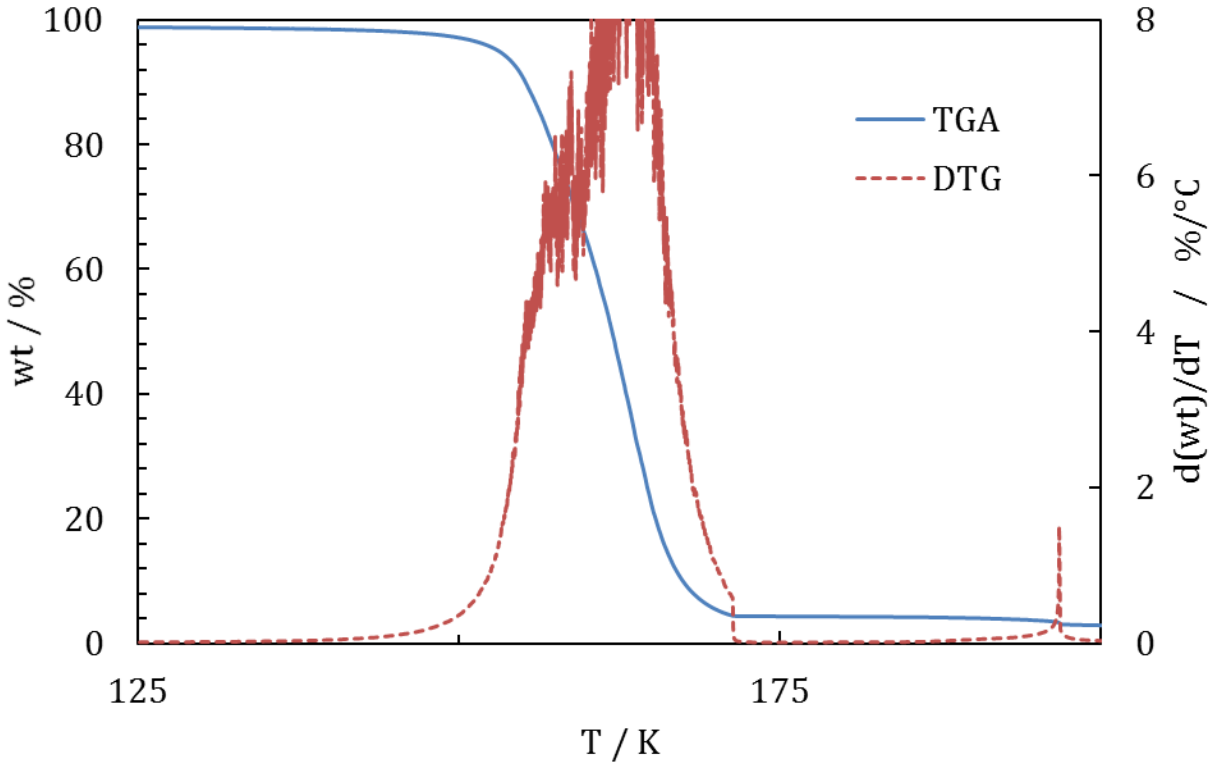

Figure 61: TGA-DTG spectrum for $Dy[fod]_3$.

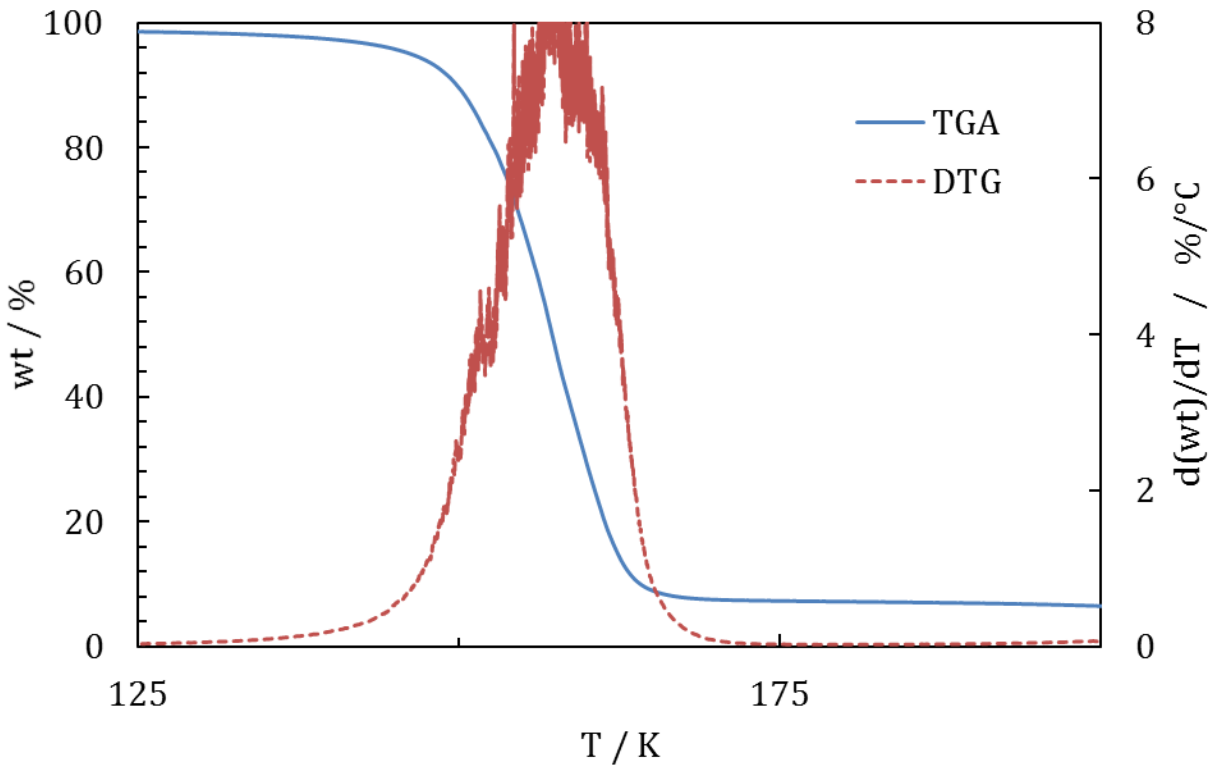

Figure 62: TGA-DTG spectrum for Ho[fod]$_3$.

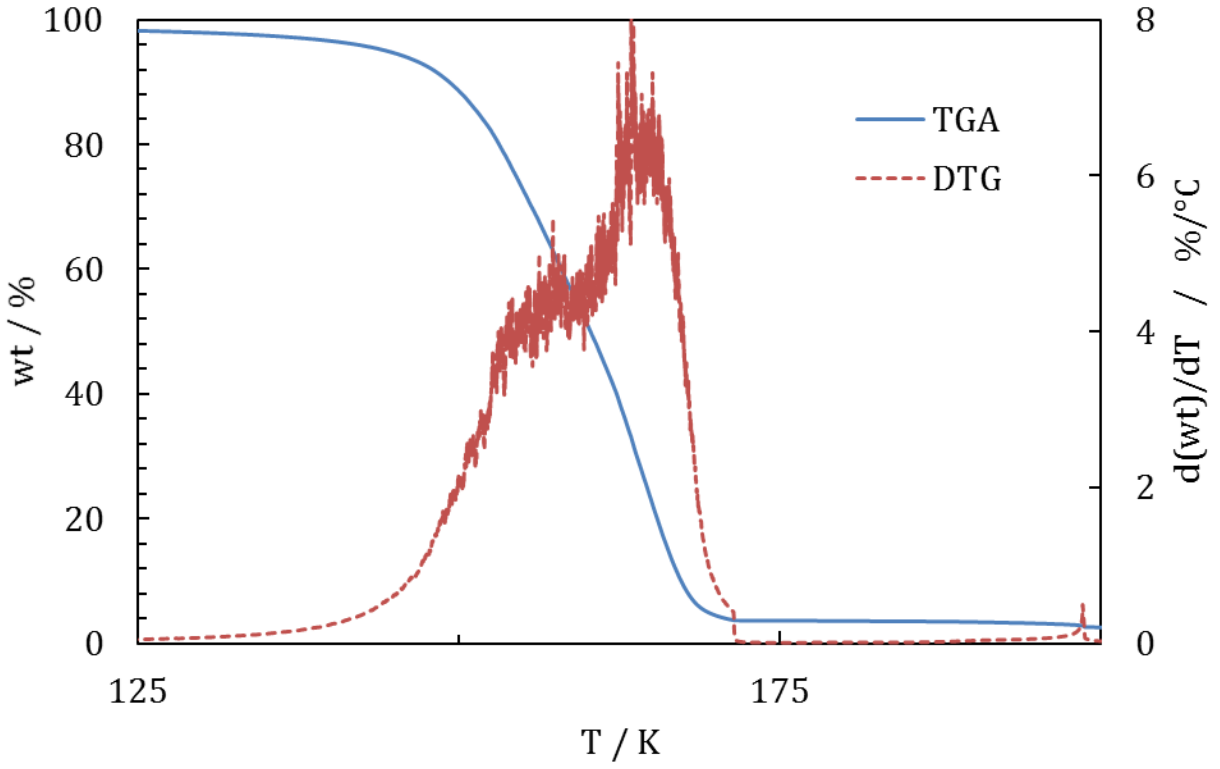

Figure 63: TGA-DTG spectrum for Er[fod]$_3$.

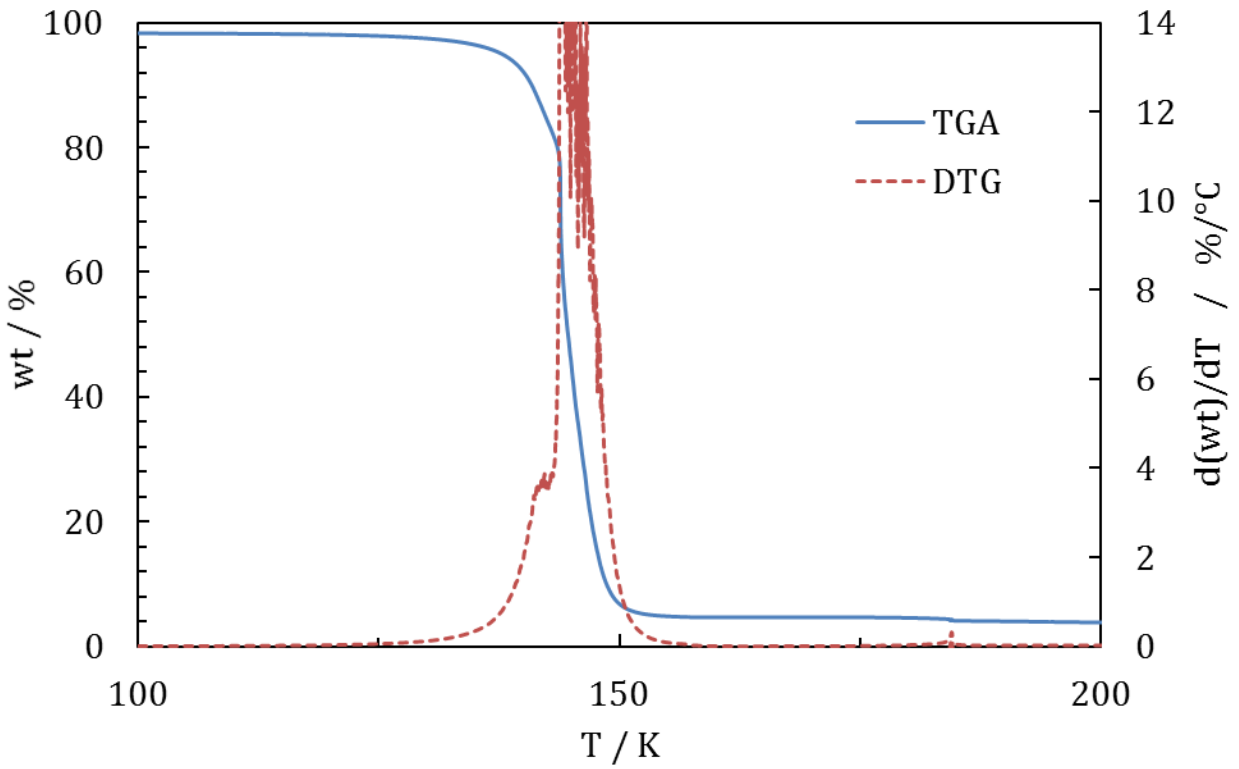

Figure 64: TGA-DTG spectrum for $Tm[fod]_3$.

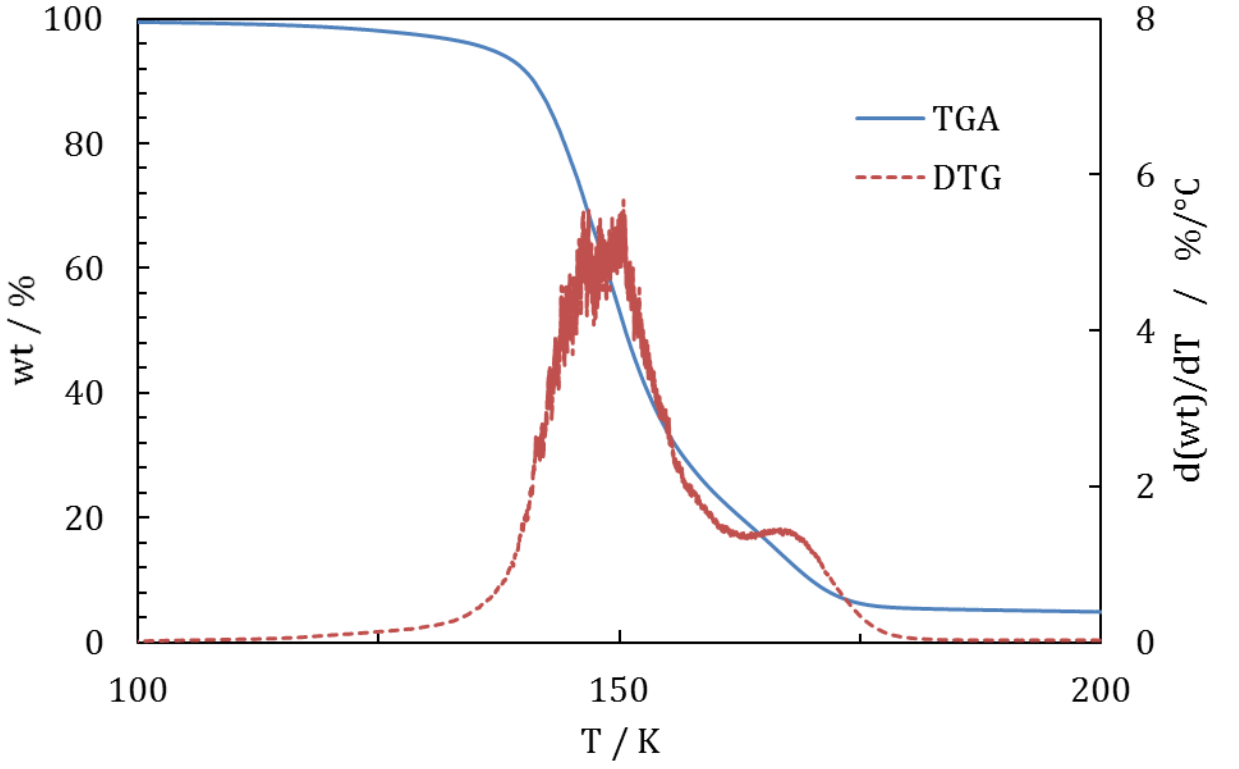

Figure 65: TGA-DTG spectrum for $Yb[fod]_3$.

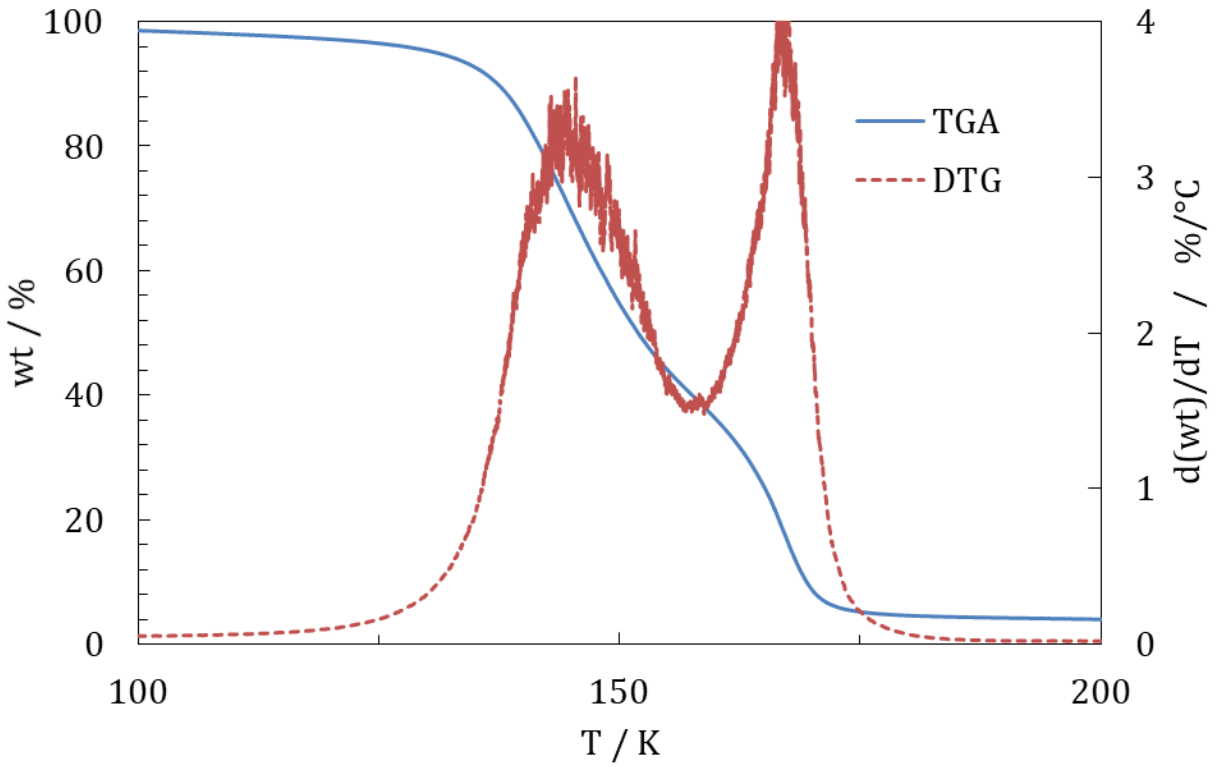

Figure 66: TGA-DTG spectrum for $Lu[fod]_3$.

Vita

Shayan Shahbazi earned his B.S. in Chemical Engineering from the University of California in Irvine, CA in the spring of 2014, with minors in Mathematics and Materials Science Engineering. He spent the last two years of his undergraduate studies conducting experiments in chemical separations, radiochemistry and radiation detection under Professor Mikael Nilsson. After completing his M.S. and PhD in Nuclear Engineering under Dr. Howard Hall, Shayan hopes to pursue continued research in the nuclear science fields including nuclear fuel cycle, new reactor types and radioactive waste management, as well as nuclear security and forensics. Mr. Shahbazi hopes for a future in the nuclear industry, spreading the peaceful uses of nuclear science to the world.